

Air Force Institute of Technology

**AFIT Scholar**

---

Theses and Dissertations

Student Graduate Works

---

12-6-2005

## Multiple Channel Laser Beam Combination and Phasing Using Stimulated Brillouin Scattering in Optical Fibers

Brent W. Grime

Follow this and additional works at: <https://scholar.afit.edu/etd>



Part of the [Plasma and Beam Physics Commons](#), and the [Semiconductor and Optical Materials Commons](#)

---

### Recommended Citation

Grime, Brent W., "Multiple Channel Laser Beam Combination and Phasing Using Stimulated Brillouin Scattering in Optical Fibers" (2005). *Theses and Dissertations*. 3341.  
<https://scholar.afit.edu/etd/3341>

This Dissertation is brought to you for free and open access by the Student Graduate Works at AFIT Scholar. It has been accepted for inclusion in Theses and Dissertations by an authorized administrator of AFIT Scholar. For more information, please contact [AFIT.ENWL.Repository@us.af.mil](mailto:AFIT.ENWL.Repository@us.af.mil).



# **MULTIPLE CHANNEL LASER BEAM COMBINATION AND PHASING USING STIMULATED BRILLOUIN SCATTERING IN OPTICAL FIBERS**

DISSERTATION

Brent W. Grime, Captain, USAF  
AFIT/DS/ENP/06-1

DEPARTMENT OF THE AIR FORCE  
AIR UNIVERSITY

## **AIR FORCE INSTITUTE OF TECHNOLOGY**

---

---

Wright-Patterson Air Force Base, Ohio

APPROVED FOR PUBLIC RELEASE; DISTRIBUTION UNLIMITED

The views expressed in this dissertation are those of the author and do not reflect the official policy or position of the United States Air Force, Department of Defense, or the United States Government

**MULTIPLE CHANNEL LASER BEAM COMBINATION  
AND PHASING USING STIMULATED BRILLOUIN  
SCATTERING IN OPTICAL FIBERS**

DISSERTATION

Presented to the Faculty

Graduate School of Engineering and Management

Air Force Institute of Technology

Air University

Air Education and Training Command

In Partial Fulfillment of the Requirements for the

Degree of Doctor of Philosophy

Brent W. Grime, BS, MS

Captain, USAF

December 2005

**MULTIPLE CHANNEL LASER BEAM COMBINATION  
AND PHASING USING STIMULATED BRILLOUIN  
SCATTERING IN OPTICAL FIBERS**

DISSERTATION

Brent W. Grime, BS, MS  
Captain, USAF

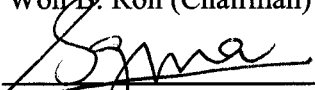
Approved:



Won B. Roh (Chairman)

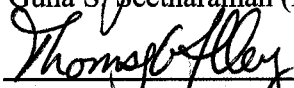
Date

28 Nov 2005



Guna S. Seetharaman (Dean's Representative)

28 NOV 2005



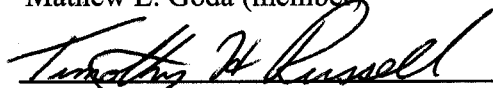
Thomas G. Alley (member)

28 Nov 2005



Mathew E. Goda (member)

1 DEC 2005



Timothy H. Russell (member)

29 Nov 2005

Accepted:



Robert A. Calico, Jr.  
Dean, Graduate School of Engineering and Management

6 Dec 2005

Date

## **Abstract**

Brightness scaling lasers using stimulated Brillouin scattering (SBS) in optical fibers is explored. A multiple-channel amplifier approach is used to increase the total power of a laser system while avoiding a significant burden on a single channel. The work explores two approaches utilizing both SBS beam cleanup and SBS piston error conjugation.

A unique beam combiner that takes advantage of the SBS beam cleanup properties of a long, gradient-index multimode fiber was designed and tested. The beam combiner was developed to combine multiple-channel laser beams simultaneously with high input and output coupling efficiency. The design for the SBS beam combiner is presented along with experimental demonstration of multiple-channel beam combining using the technique.

Using SBS piston error conjugation to phase multiple-channel two-pass amplifiers is also explored. Various system configurations were investigated to demonstrate SBS beam phasing of both passive, unamplified channels and active channels containing fiber amplifiers. Beam phasing of the channels was successfully demonstrated with enough gain and power to merit consideration as a viable approach to multiple-channel laser power scaling. Methods for improving efficiency and scaling to include a greater number of channels were also tested.

## Acknowledgments

I am grateful to the many people who have contributed to this work and my education over the last few years. Prior to arriving at AFIT, someone recommended Dr. Won Roh as a research advisor and I am very thankful for that recommendation. Dr. Roh's guidance has been invaluable during my research. He allowed leeway to plot much of my course while always guiding my direction if I veered too far off path. I hope that I have finally internalized his sage advice to build an experiment one step at a time instead of always reaching immediately for the end goal.

Thank you to LTC Thomas Alley, Maj Timothy Russell, Capt Nathan Terry, and the rest of the nonlinear research group. Our weekly meetings were always a great opportunity to seek advice and share progress. I am also indebted to AFRL/DELO for their financial support and sharing of an even more precious asset, technical expertise. Anthony Sanchez is a master of fiber optical components and always willing to share his knowledge. Thanks also to the 'go-to' men of the Engineering Physics Department, Mike Ranft and Greg Smith.

I am especially grateful to my wife who is a blessing to me every day. She proofread this entire document and probably learned more about stimulated Brillouin scattering than she ever wanted to. Thank you to our daughter who was born during the second year of this effort and whose welcome-home smile could fade away any bad day in the laboratory.

Finally, being one prone to anxiety, I thank God for his huge part in this work and for a continual reminder to “Be anxious for nothing, but in everything, by prayer and petition, with thanksgiving, present your requests to God. And the peace of God, which transcends all understanding, will guard your hearts and your minds in Christ Jesus.”

Philippians 4:6,7

Brent W. Grime



# Table of Contents

Abstract.....	iv
Acknowledgments.....	v
List of Figures .....	x
List of Tables .....	xvi
1 Introduction.....	1
1.1. Motivation.....	1
1.2. Overview.....	5
1.3. Document Organization .....	6
2 Theoretical Background.....	8
2.1. Nonlinear Optics .....	8
2.2. Stimulated Brillouin Process.....	11
2.2.1. Stimulated Brillouin Scattering.....	11
2.2.2. Stimulated Brillouin Scattering Threshold .....	17
2.3. Optical Phase Conjugation.....	20
2.3.1. Overview of Optical Phase Conjugation.....	20
2.3.2. Phase Conjugation through Stimulated Brillouin Scattering .....	22
3 SBS Beam Cleanup and Combining.....	26
3.1. Background.....	26
3.2. 62.5-micron and 100-micron Beam Cleanup.....	28
3.3. Four-Channel Beam Combining .....	34
3.3.1. Design .....	36

3.3.2.	Experiment.....	39
3.3.3.	Discussion.....	46
3.4.	Conclusion .....	48
4	SBS Beam Phasing .....	50
4.1.	Single-Frequency Fiber Amplifier.....	50
4.1.1.	Background.....	50
4.1.2.	Fiber Amplifier Implementation.....	55
4.1.3.	Discussion.....	62
4.2.	SBS Beam Phasing Using Long Multimode Fiber .....	63
4.2.1.	Background.....	63
4.2.2.	Beam Phasing Two Passive Channels .....	70
4.2.3.	Beam Phasing Two Amplified Channels Using a 2:1 Fiber Coupler .....	78
4.2.4.	Beam Phasing Two Amplified Channels Using Polarization Combining.....	84
4.2.5.	Beam Phasing Two Amplified Channels Using a 2:2 Fiber Coupler .....	91
4.2.6.	Discussion.....	105
4.3.	SBS Beam Phasing using a Gain Fiber.....	108
4.3.1.	Background.....	109
4.3.2.	Ytterbium-Doped Multimode Fiber Investigation.....	113
4.3.3.	Discussion.....	128
5	Conclusions.....	136
5.1.	Significant Contributions.....	136
5.2.	Recommendations for Future Work.....	137

5.2.1.	Multiple Channel SBS Beam Combiner .....	137
5.2.2.	SBS Beam Phasing .....	139
Appendix A: Glossary of Symbols .....		147
Bibliography .....		150

## List of Figures

Figure	Page
1. Acousto-optic effect.....	12
2. Stimulated Brillouin scattering .....	13
3. Stimulated Brillouin scattering phase matching condition for backward scattering .....	14
4. Plane wave propagating through random media-- Solid lines indicate the incident wave and the dotted lines indicated the reflected wave of (a) a conventional mirror and (b) a phase conjugate mirror.....	21
5. Schematic diagram to examine beam cleanup in 62.5 $\mu\text{m}$ and 100 $\mu\text{m}$ core diameter fibers. ....	29
6. SBS input vs. output characteristics for 8.8 km, 62.5 $\mu\text{m}$ fiber. ....	30
7. Fabry-Perot spectrum analyzer data taken at a pump power of 100 mW. The Fabry-Perot data is used to verify SBS threshold and to observe the frequency shift of the Stokes beam. ....	31
8. Determining SBS frequency shift using a Fabry-Perot spectrum analyzer. ....	32
9. SBS input vs. output characteristics for (a) 2.2 km and (b) 6.6 km, 100 $\mu\text{m}$ fibers .....	32
10. Spatial intensity distributions of the reflected pump and generated Stokes beam for the 62.5 $\mu\text{m}$ (a,b) and the 100 $\mu\text{m}$ (c,d) fibers. The figure demonstrates that an aberrated input beam generates a Gaussian-like Stokes output through SBS beam cleanup. ....	33
11. Schematic diagram (a) and graphical end view (b) of the SBS beam combiner. A picture of the actual beam combiner implemented in this study is shown in (c). ....	35
12. Side view schematic for multiple SBS beam combiner design .....	36
13. Schematic diagram for the four beam SBS combining experiment.....	40

14. Transmitted power for (a) 8.8 km of 62.5 $\mu\text{m}$ core diameter and (b) 6.6 km of 100 $\mu\text{m}$ core diameter fiber. The transmitted power observed when seeding a single beam directly in the center is included for reference. ....	41
15. Schematic diagram for the four beam SBS combining experiment with a center-pumped beam to initiate the Stokes wave.....	43
16. Effect of spherical aberration for off-axis focusing.....	44
17. Laser intensity profiles for the four-beam SBS combiner with center seed. The input to the SBS lens is shown for the (a) center seed alone and (b) the center seed with four-beam input as well as the Stokes wave generated (c) without and (d) with the four-beam input. ....	45
18. Spatial intensity profiles showing (a) collimated output from the SBS beam combiner and (b) the best focal four beam overlap using a 20 cm lens. Dark circular rings are included in (b) to help distinguish the different beams.....	47
19. Mode filtering in 20 $\mu\text{m}$ and 30 $\mu\text{m}$ , 0.06 NA fiber cores. ....	53
20. Large mode area Yb-doped fiber amplifier .....	54
21. Absorption and emission spectrum for Yb-doped fiber.....	54
22. Schematic diagram for master oscillator fiber power amplifier .....	56
23. Profile view of a (a) flat and (b) $\sim 8^\circ$ angle cleave of the 400 $\mu\text{m}$ octagonal-shaped fiber .....	57
24. Current vs. output power for (a) LIMO #1 (S/N 1554) and (b) LIMO #2 (S/N 1555) diode lasers. ....	58
25. (a) Sample spectrum and (b) temperature wavelength tuning of the LIMO fiber coupled diode laser. ....	59
26. Input-output characteristics for the Yb-doped LMA fiber seeded with 500 mW. The amplifier achieved 13.4 W of power with a slope efficiency of 67%. The inset Fabry-Perot spectrum analyzer scan verifies the single-frequency output of the amplifier.....	60
27. (a) Fiber amplifier output showing the single transverse mode operation for the LMA fiber spooled on a 10 cm spool. For comparison, (b) shows the fiber amplifier output when the fiber is coiled on a larger, 17 cm spool. ....	61
28. Basic two-channel SBS beam phasing experimental schematic.....	65

29. Experimental schematic used by Moyer <i>et. al.</i> <sup>16</sup> to investigate SBS piston error correction. ....	67
30. Lateral Shearing Interferometer (LSI). The reflections from the two inner surfaces of the LSI create regions of self interference of the individual laser beams and mutual interference between the two beams. Continuity across the three regions indicates successful piston error correction. ....	68
31. Experimental schematic testing SBS beam phasing for two passive channels. A 2:1 fiber coupler is used to combine the two beams into a single 4-km, 50 $\mu\text{m}$ core diameter gradient index fiber. ....	71
32. Fused fiber coupler .....	72
33. Data from the lateral shearing interferometer (a) before the two reflections from the LSI are brought together and (b) after the reflections are overlapped to form interference fringes.....	73
34. LSI data showing (a) lack of continuity across the fringe zones (unphased) using a flat mirror and (b) continuity across the fringes (phasing) using the SBS multi-mode fiber. ....	74
35. Stokes input-output characteristics for the 2:1 passive fiber phasing test. ....	75
36. Stokes input-output characteristics for (a) channel #1 and (b) channel #2 of the 2:1 fiber coupler individually. The bottom axis is vs. total input power for easy comparison with Figure 35, while the top axis provides the power measured in each channel following the prism wavefront split. ....	76
37. Experimental schematic testing SBS beam phasing for two amplified channels. A 2:1 fiber coupler is used to combine the two beams into a single 4-km, 50 $\mu\text{m}$ core diameter gradient index fiber. ....	79
38. Lateral shearing interferometer data demonstrating two-channel amplified phasing using a 2:1 fiber coupler. (a) Shows both LSI surface reflections of the two Stokes beam traveling side by side. The remaining figures (b-d) show LSI interference fringes of various thickness and spacing. ....	80
39. LSI fringe comparison for the two pass amplifier with (a) a flat mirror and (b) the SBS fiber providing the back reflection for the second pass amplification. ....	81
40. Stokes input-output characteristics for the 2:1 amplifier fiber phasing test. The output powers from both Stokes beams are plotted vs. the total diode pump power for both amplifiers.....	82
41. Experimental schematic for SBS beam phasing of two amplified channels using polarization beam combining.....	85

42. Lateral shearing interferometer data from (a) a flat mirror and (b) the SBS multi-mode fiber. ....	87
43. Fabry-Perot spectrum analyzer scan for Corning 50 $\mu\text{m}$ core diameter fiber. The measured SBS shift is $15.2 \pm 0.2$ GHz. ....	88
44. Lateral shearing interferometer. The data shows the repetition of fringe patterns as the path length for channel #1 is increased via the optical trombone. The relative path length difference is (a) 0 mm, (b) +10 mm, (c) +20 mm, and (d) +30 mm .....	89
45. Input-output characteristics for (a) the double-pass fiber amplifier channels individually and (b) total phased output power from both channels. The inset in (b) shows a typical Fabry-Perot scan demonstrating single-frequency output. ....	90
46. Experimental schematic testing SBS beam phasing for two amplified channels. A 2:2 fiber coupler is used to combine the two beams into two 50 $\mu\text{m}$ core diameter gradient index fibers. ....	93
47. Lateral shearing interferometer data for two-channel amplified phasing using a 2:2 fiber coupler. ....	94
48. Input-output graphs for a two-channel fiber amplifier system using 2:2 fiber couplers. The (a) total output power and the (b and c) individual channel two-pass performance are given. Previous results obtained using 2:1 fiber couplers are included for comparison.....	95
49. Graphs of output power vs. time for a diode pump power level of (a) 7 W and (b) 9.5 W. ....	96
50. Lateral shearing interferometer data displaying fringe fluctuations. ....	97
51. Lateral shearing interferometer data using 2:2 fiber couplers with amplifiers. The data shows the repetition of fringe patterns as the path length for channel 1 is increased via the optical trombone. The relative path length difference is (a) 0 mm, (b) +9.7 mm (c) +19.5 mm and (d) +29.5 mm. ....	98
52. Transmitted power recorded simultaneously through both SBS fibers. The output dynamics when using (a) both or (b) only one of the fiber input couplers are shown. ....	99
53. SBS power measured for both channels at 8W of diode pump power. The power is calibrated from the two surface Fresnel reflection of the beam pick-off. ....	101

54. Input-output graphs for two-channel fiber amplifier system using 2:2 fiber couplers. The total power of the two channels demonstrating 4.4 W is shown in (a) and two LSI interference patterns for the higher power are given in (b) and (c). .....	102
55. Relative error vs. diode pump power for (a) the total two-channel output power in the TFP leg and (b) each channel's SBS beam as collected using beam pick-offs. A linear fit is included for each of the data sets.....	103
56. SBS power measured for both channels at 24 W of diode pump power. The power is calibrated from the two surface Fresnel reflection of the beam pick-off. ....	104
57. Fiber loop seeding configuration .....	110
58. Tapered fiber geometry for SBS threshold reduction .....	111
59. Basic implementation of a phase conjugate fiber amplifier.....	112
60. Ytterbium cross sections for (a) absorption (solid) and emission (dotted) and (b) absorption in the region near 1064 nm. ....	114
61. 915 nm diode pump absorption in Yb-doped multimode fiber. Options for coupling diode pump power into (a) only one side and (b) both sides are shown. ....	115
62. Schematic diagram for investigating 50 $\mu$ m, double-clad, Yb-doped fiber.....	116
63. Current vs. output power for the Polaroid 915 nm fiber-coupled diode laser. ....	117
64. Data for 55m of Yb-doped multimode fiber. The (a) amplifier performance and (b) backreflected power for two different 1064 nm seed powers. ....	118
65. Output spectrum for 55 m, Yb-doped multimode fiber amplifier. The figure illustrates the necessity of angle cleaving the fiber to prevent self-oscillation.....	120
66. Data for 20 m of Yb-doped multimode fiber. The (a) amplifier performance and (b) backreflected power for front end and both end diode pumping. The fiber amplifier output spectrum and Fabry-Perot spectrum for the dual pumping are included in (c) and (d), respectively.....	121
67. Duty cycle plots for chopper testing. The plots are recorded from the optical chopper output monitor and show both (a) 50% and (b) 3 % duty cycle. ....	123
68. Data for 20 m of Yb-doped multimode fiber using an optical chopper. The (a) amplifier performance, (b) backreflected power, output spectrum, and Fabry-Perot scan for duty cycles of (c,d) 50% and (e,f) 3% are recorded. ....	124



69. Data for 11.5 m of Yb-doped multimode fiber. The (a) amplifier performance, (b) backreflected power, (c) output spectrum, and (d) Fabry-Perot scan are recorded.....	126
70. Data for 11.5 m of Yb-doped multimode fiber with three different 1064 nm seed powers. The (a) amplifier performance and output spectrum are provided for seed powers of (b) 0.5 W (c) 1.0 W and (d) 10.0 W. ....	127
71. Data for 11.5 m of Yb-doped multimode fiber varying seed power while keeping diode pump power constant at $P_{\text{pump}} = 26$ W. The (a) amplifier performance and (b) backwards propagating power are presented.....	128
72. Yb-doped multimode fiber amplifier performance comparison for three fiber lengths: 11.5 m, 20 m, and 55 m. ....	129
73. Total exponential Stokes gain ( $G_t$ ) vs. diode pump power for 264 W single-frequency amplifier. A few different value for the convective coefficient are shown. ....	133
74. Total exponential Stokes gain ( $G_t$ ) vs. diode pump power for the Yb-doped multimode fiber presented in this section. A few different value for the convective coefficient are shown. ....	134
75. SBS threshold for 50 $\mu\text{m}$ , 100 $\mu\text{m}$ , and 200 $\mu\text{m}$ fibers. ....	140
76. Potential SBS threshold in for 50 $\mu\text{m}$ , 100 $\mu\text{m}$ , and 200 $\mu\text{m}$ using tellurite-based fibers. ....	142
77. 7:1 multimode fiber combiner. A (a) schematic representation of the device is shown along with (b) an actual picture of the cleaved end facets.....	144
78. SBS beam phasing diagram using a N:1 bidirectional fiber coupler .....	145
79. Multiple channel SBS beam phasing using a fiber bundle .....	146

## List of Tables

Table	Page
1. Nonlinear effects and their associated susceptibility terms .....	10
2. Fiber parameters for SBS threshold calculations .....	20
3. Summary of multiple-channel beam combination (a) design parameters and (b) calculated values. ....	39
4. Comparison of 4-beam combiner and centered-pumped SBS threshold for 62.5 $\mu\text{m}$ and 100 $\mu\text{m}$ core diameter fibers. ....	42
5. Power conversion for the four beam SBS combiner with center seed.....	45
6. Nufern large mode area double clad Yb-doped fiber specifications.....	56
7. Beam parameters for the 13.4 W fiber amplifier output measured using the Coherent Mode-Master. $M^2$ is the beam quality parameter, $\omega_0$ is the spot size, $Z_r$ is the Rayleigh range, and $\theta_{\text{div}}$ is the beam divergence.....	61
8. Summary of work by Heuer using a fiber amplifier for SBS phase conjugation ...	113
9. Specifications for Yb-doped multimode fiber .....	113
10. Optical chopper configuration for 20 m Yb-doped multimode fiber experiment...	123
11. Summary of symbols used in temperature broadened Brillouin gain.....	133

# **MULTIPLE CHANNEL LASER BEAM COMBINATION AND PHASING USING STIMULATED BRILLOUIN SCATTERING IN OPTICAL FIBERS**

## **1 Introduction**

### ***1.1. Motivation***

The laser was first demonstrated in 1960 and has since proven useful in numerous applications. The applications are quite varied and the range includes data storage, communication systems, surgical tools, and high power welding devices.<sup>1</sup> It would not be an exaggeration to say that the average American uses some form of a laser every day and that the technology has changed our way of life.

The United States Department of Defense (DoD) also recognizes the utility of employing lasers in its weapon systems. The Gulf War unveiled the U.S. capabilities of precision laser guided munitions and their uses have transformed the strategies of war.<sup>2,3</sup> In addition to providing guidance to weapons systems, research continues in using the laser itself as a weapon.

The advantages of a weapon system capable of traveling at the speed of light and engaging the target before it has a chance to respond has obvious merit and the DoD is working to develop such technology.<sup>4</sup> Perhaps the most notable programs are the Airborne Laser Program (ABL) designed to intercept missiles in their boost phase<sup>5,6</sup> and a new type of precision gunship, the Advanced Tactical Laser (ATL).<sup>7</sup> Two of the

primary technical difficulties in creating operational systems lie in the development of the high power laser itself and the propagation of the energy through the turbulent atmosphere. This work will not focus on the propagation of the laser through the turbulent atmosphere, but it should be stressed that development of a high power laser alone does not guarantee success of a laser weapon system. A significant design effort is also required to develop systems to accurately deliver the laser beam through the turbulent atmosphere and provide enough power on the target.<sup>8</sup>

High power lasers for the DoD historically have been chemical lasers. The Chemical Oxygen Iodine Laser (COIL) is a proven workhorse generating Megawatt class average power output and is the design platform for the ABL program.<sup>4,9</sup> Although chemical lasers provide the high power required for directed energy applications, they do have some unattractive features. Currently, the singlet delta oxygen  $\{O_2(^1\Delta)\}$  required for creating the population inversion in iodine is generated by a chemical process involving  $Cl_2$  and basic  $H_2O_2$ .<sup>10</sup> Transporting and working with the chemicals are logistically challenging and potentially dangerous. While work continues to generate the required  $O_2(^1\Delta)$  electrically,<sup>11,12,13</sup> the DoD has emphasized the need for parallel development of solid-state lasers.

High power solid-state lasers are an attractive complement to chemical lasers. The solid-state medium reduces the logistical burden required by the chemical lasers and could provide a more compact platform. However, solid-state lasers have not reached the same power class as chemical lasers. The DoD recognizes the need to develop higher power solid-state lasers and is currently funding the Joint High Power Solid-State Laser (JHPSSL) program with a goal of a 100 kW average power solid-state laser by 2010.

The initial phase of the JHPSSL program granted contracts to several different companies, each with their own distinct technical approach.<sup>14</sup> The program hopes to address some of the difficulties in power scaling solid-state lasers.

One approach for power scaling is to use an external amplifier to increase the energy in a master oscillator power amplifier (MOPA) configuration. While passing the beam once through the amplifying medium provides some gain, a double pass configuration is often used to increase the MOPA output. A limitation of a basic MOPA system is that in order to create sufficient gain in the amplifying medium, intense pumping of the medium is required and can lead to aberrations in the laser beam output. Fortunately, it is possible to use a phase conjugate mirror (PCM) in a two-pass MOPA to reduce the effects of the aberrations induced by the amplifier.<sup>15</sup> For this case, the first pass through the amplifier induces aberrations to the laser beam. The reflection from the phase conjugate mirror reverses the wavefront so that a second pass through the amplifier corrects the aberrations. Although this method is successful for reducing amplifier distortions, there is a limitation to the power amplification achievable in a single channel.

In an attempt to improve upon the single-channel, double pass MOPA design, the master oscillator laser beam is split into several channels through wavefront splitting. Splitting the master oscillator beam allows separate amplifiers to be used, leading to total powers not accessible with a single amplifier. The drawback of this method is that as the master beam is split, each of the channels has its own optical path and results in a relative phase delay (piston error) between the channels. For a double pass MOPA, a reflection from a regular mirror will only lead to increased phased difference as the beams make the second pass and recombine. However, if a single phase conjugate mirror is used for all of

the channels, the second pass eliminates the phase difference as each channel retraces its path.<sup>16</sup>

The phase difference between the channels becomes important when focusing the total output beam as required in a laser weapon system. If the channels are not phased together, the maximum intensity in the far-field spot is  $N$  times the intensity of a single beam, where  $N$  is the number of channels. For the case when all the beams are phased together, the maximum intensity is  $N^2$  times that of a single channel. It is therefore desirable to accurately phase a multiple channel MOPA laser system using a single phase conjugate mirror as described above. This method of laser beam phasing has been investigated with<sup>17,18</sup> and without<sup>16,19</sup> an amplifier in each channel.

One mechanism for creating a phase conjugate mirror is through stimulated Brillouin scattering (SBS). While many of the early investigations used a liquid or gas in an optical cell as the SBS medium,<sup>20</sup> optical fiber has also proven to be a good source for generation of SBS.<sup>21</sup> Using optical fiber as the SBS medium allows for longer interaction lengths and a simpler implementation than is possible with an optical cell. Investigations of SBS using optical fiber have shown that the properties of the SBS (Stokes) beam generated in the fiber are dependent on the length of the fiber. For long multimode fibers (a few km), the SBS beam is generated in the Gaussian-like  $LP_{01}$  mode of the fiber and is useful for cleaning up an aberrated laser beam.<sup>22,23</sup> For the case of short fibers ( $<10$  m), a phase conjugate beam is generated<sup>24</sup> and can be used in a single-channel phase conjugate MOPA<sup>25</sup> or for multiple channel beam phasing.<sup>19</sup>

## 1.2. Overview

The focus of this research effort is developing stimulated Brillouin scattering for laser power scaling using a multiple channel approach. There are two categories for multiple channel power scaling using SBS in optical fibers. The first method exploits the long fiber beam cleanup properties to combine multiple laser beams. The second approach uses SBS piston error correction to phase multiple laser beams in a two-pass master oscillator power amplifier. Both methods are explored in this research.

The first investigation examines multiple channel beam combining using the SBS beam cleanup properties of long gradient index multimode fibers. For SBS beam cleanup, the output Stokes beam is generated in the Gaussian-like fundamental fiber mode ( $LP_{01}$ ) irrespective of the pump intensity profile. This property has been used to cleanup aberrated laser beams as well as to combine two beams using optical fibers up to 50  $\mu\text{m}$  in core diameter.<sup>22,23</sup> One necessary step for power scaling is using larger fibers to accommodate higher power beams. In this work, the beam cleanup property is first extended to larger core diameter fibers of both 62.5  $\mu\text{m}$  and 100  $\mu\text{m}$ . Following this demonstration, a unique SBS beam combining device was designed, fabricated, and tested using four input channels. The device was designed such that the Stokes beam generated in the fundamental mode of the fiber is efficiently coupled through a center hole in the device.

The second emphasis of this work is SBS beam phasing multiple channel amplifiers. In this effort, a series of experiments were performed demonstrating the phasing of two channels using an optical fiber. An initial test was performed without amplifiers in each channel and a series of experiments including fiber amplifiers in each leg was conducted.

Additionally, the SBS properties and amplifier characteristics of a rare-earth doped multimode gain fiber was tested for use in a beam phasing system.

A few of the significant accomplishments presented in this dissertation are:

1. SBS beam cleanup using 62.5  $\mu\text{m}$  and 100  $\mu\text{m}$  gradient index, multimode fiber.
2. Four-channel SBS beam combining using a custom-designed beam combiner.
3. SBS beam phasing of two passive (unamplified) channels using a 2:1 fiber optic coupler.
4. SBS beam phasing of two active (amplified) channels using a 2:1 fiber optic coupler.
5. SBS beam phasing of two active (amplified) channels using polarization beam combining.
6. SBS beam phasing of two active (amplified) channels using a 2:2 fiber optic coupler.
7. Characterization of SBS properties and fiber amplifier performance of ytterbium-doped multimode gain fiber.

### ***1.3. Document Organization***

The theoretical background necessary for the experimental work is described in Chapter 2. This chapter provides the framework for nonlinear optics, stimulated Brillouin scattering, and optical phase conjugation. Chapter 3 documents the investigations using SBS beam combination in long multimode fibers. Beam cleanup is first demonstrated using both 62.5  $\mu\text{m}$  and 100  $\mu\text{m}$  fibers and is followed by the design, experiment, and discussion of a four-channel SBS beam combiner. Chapter 4 describes



the investigations of SBS beam phasing using optical fibers. It first provides details of the single-frequency fiber amplifiers developed as a necessary component in the phasing system. A variety of configurations using a long multimode fiber for SBS beam phasing are presented followed by experiments testing the SBS properties and amplifier performance of a gain fiber for beam phasing applications. Finally, chapter 5 summarizes the technical achievements of this dissertation effort and discusses some directions for future work.

## 2 Theoretical Background

This chapter provides the theoretical background necessary for the experimental investigations described in this dissertation. The basic aspects of nonlinear optics are first reviewed followed by a presentation of stimulated Brillouin scattering (SBS) and optical phase conjugation. This background lays the foundation required for the subsequent experiments using SBS.

### 2.1. *Nonlinear Optics*

In order to investigate SBS, it is necessary to first develop some of the basic equations used in nonlinear optics. The starting point for this development is Maxwell's equations (given here in differential form),

$$\nabla \times \mathbf{E} = -\frac{\partial \mathbf{B}}{\partial t} \quad (2-1)$$

$$\nabla \times \mathbf{H} = \mathbf{J} + \frac{\partial \mathbf{D}}{\partial t} \quad (2-2)$$

$$\nabla \cdot \mathbf{D} = \rho_c \quad (2-3)$$

$$\nabla \cdot \mathbf{B} = 0 \quad (2-4)$$

where  $\mathbf{E}$  is electric field,  $\mathbf{B}$  is magnetic induction,  $\mathbf{H}$  is magnetic field,  $\mathbf{J}$  is current density,  $\mathbf{D}$  is electric displacement, and  $\rho_c$  is charge density.<sup>26</sup> In this work, we are concerned with dielectric materials which have no free charge or currents ( $\rho = 0$ ,  $\mathbf{J} = 0$ ).

The electric displacement and magnetic induction are defined by

$$\begin{aligned}
\mathbf{D} &= \varepsilon \mathbf{E} \\
&= \varepsilon_0 \mathbf{E} + \mathbf{P} \\
\mathbf{B} &= \mu \mathbf{H}
\end{aligned} \tag{2-5}$$

where  $\varepsilon$  is the permittivity,  $\mu$  is the permeability, and  $\mathbf{P}$  is the polarization vector. The Polarization vector can be written as

$$\mathbf{P} = \varepsilon_0 \chi \mathbf{E}, \tag{2-6}$$

where  $\chi$  is the susceptibility of the medium. The susceptibility is an inherent parameter of the material and is formally defined as the “susceptibility for inducing a dipole moment. The susceptibility is, in general, a function of the electric field applied to the medium and can be approximated by a power series expansion of the electric field,

$$\begin{aligned}
\mathbf{P} &= \varepsilon_0 \chi(\mathbf{E}) \mathbf{E} \\
&\cong \varepsilon_0 [\chi^{(1)} + \chi^{(2)} \mathbf{E} + \chi^{(3)} \mathbf{E}^2 + \dots] \mathbf{E}.
\end{aligned} \tag{2-7}$$

The electric displacement is now written as

$$\mathbf{D} = \varepsilon_0 [1 + \chi^{(1)} + \chi^{(2)} \mathbf{E} + \chi^{(3)} \mathbf{E}^2] \mathbf{E}, \tag{2-8}$$

where the higher orders terms are excluded since their contribution for nonlinear processes of this research effort are negligible. In component form, the polarization and displacement are written as<sup>20,27,28</sup>

$$\begin{aligned}
P_i &= \varepsilon_0 [\chi_{ij}^{(1)} E_j + \chi_{ijk}^{(2)} E_j E_k + \chi_{ijkl}^{(3)} E_j E_k E_l] \\
D_i &= \varepsilon_0 [E_i + \chi_{ij}^{(1)} E_j + \chi_{ijk}^{(2)} E_j E_k + \chi_{ijkl}^{(3)} E_j E_k E_l]
\end{aligned} \tag{2-9}$$

where,  $\chi_{ij}^{(1)}$ ,  $\chi_{ijk}^{(2)}$  and  $\chi_{ijkl}^{(3)}$  are the tensor elements of the 1<sup>st</sup>, 2<sup>nd</sup>, and 3<sup>rd</sup> order susceptibilities, respectively. In this tensor notation, summations over repeated indices are assumed. As an example, the product of the electric field with the  $i^{\text{th}}$  component of

the third order susceptibility is given as  $\chi_{ijkl}^{(3)} E_j E_k E_l = \sum_{j,k,l} \chi_{ijkl}^{(3)} E_j E_k E_l$ . In this case, each of the i, j, k, and l indices take on the direction of the Cartesian coordinates, x, y, and z. A sample of nonlinear effects and their associated susceptibility terms are presented in Table 1.<sup>29</sup>

Table 1: Nonlinear effects and their associated susceptibility terms

Nonlinear Term	Effect
$\chi^{(1)}$ 1st order	index of refraction absorption birefringence
$\chi^{(2)}$ 2 <sup>nd</sup> order	second harmonic generation parametric mixing Pockels effect
$\chi^{(3)}$ 3 <sup>rd</sup> order	third harmonic generation four wave mixing stimulated Brillouin scattering

Distributing the above expression and separating the linear and nonlinear components leads to

$$\mathbf{D} = \underbrace{\varepsilon_0 \mathbf{E} + \varepsilon_0 \chi^{(1)} \mathbf{E}}_{\varepsilon_0 \mathbf{E} + \mathbf{P}_L} + \underbrace{\varepsilon_0 [\chi^{(2)} \mathbf{E} + \chi^{(3)} \mathbf{E}^2]}_{\mathbf{P}_{NL}} \mathbf{E}$$

or

$$\mathbf{D} = \varepsilon \mathbf{E} + \mathbf{P}_{NL} \quad , \quad (2-10)$$

where  $\mathbf{P}_{NL}$  is the nonlinear component of the polarization.

Developing the wave equation for the electric field begins with taking the curl of Equation 2-1. The vector identity  $\nabla \times (\nabla \times \mathbf{E}) = \nabla(\nabla \cdot \mathbf{E}) - \nabla^2 \mathbf{E}$  is used along with substitution of Equation 2-2, Equation 2-3, and the defining relationships (2-5) to obtain the equation in the form

$$\nabla^2 \mathbf{E} - \mu_0 \frac{\partial^2}{\partial t^2} \mathbf{D} = 0. \quad (2-11)$$

While this is a general form for the wave equation, the equation is rewritten in a form that separates the linear and nonlinear effects of the electric field. Substituting the displacement of Equation 2-10 which has separated the linear and nonlinear components into the wave equation (2-11) yields<sup>29</sup>

$$\nabla^2 \mathbf{E} - \mu_0 \varepsilon \frac{\partial^2 \mathbf{E}}{\partial t^2} = \mu_0 \frac{\partial^2 \mathbf{P}_{NL}}{\partial t^2}. \quad (2-12)$$

In this equation, the nonlinear polarization serves to drive the electric field.

At this point, the necessary fields for a particular nonlinear process are used in Equation 2-12 to develop coupled wave equations. The specific process of interest to this research, stimulated Brillouin scattering, is examined in the following section (2.2).

## **2.2. *Stimulated Brillouin Process***

Stimulated Brillouin scattering (SBS) is a nonlinear interaction between the input pump beam and an acoustic wave generated in the medium by the pump.<sup>20</sup> This section first presents a basic description of the SBS process followed by a discussion of the SBS coupled wave equations and SBS threshold.

### **2.2.1. *Stimulated Brillouin Scattering***

Because SBS is an interaction between an optical pump beam incident in a medium and an acoustic wave generated in the medium, it is helpful to describe first the acousto-optic effect portrayed in Figure 1.

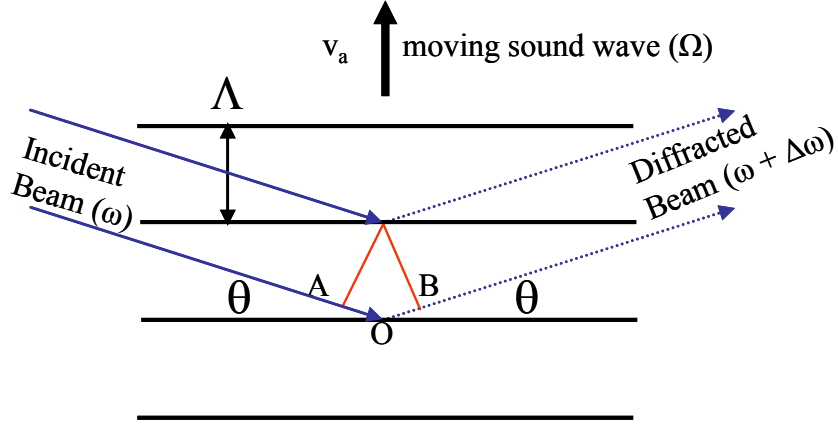


Figure 1: Acousto-optic effect

The acoustic wave propagating in a medium creates a strain field and results in a periodic modulation of the index of refraction (index grating). As the incident pump beam encounters the index grating, the light is diffracted by the grating and the pump frequency ( $\omega$ ) is shifted through the Doppler effect by an amount<sup>30</sup>

$$\Delta\omega = 2\omega \frac{v_a \sin \theta}{c/n}, \quad (2-13)$$

where  $v_a$  is the acoustic velocity. For purely sinusoidal acoustic waves, only the first order diffraction will occur and the acousto-optic interaction is described by the Bragg diffraction equation,<sup>30</sup>

$$2\Lambda \sin \theta = \frac{\lambda}{n}, \quad (2-14)$$

where  $\Lambda$  is the acoustic wavelength and  $\theta$  is the incident angle as shown in Figure 1. In this case, Equation 2-14 is combined with Equation 2-13 to yield the Doppler frequency shift as<sup>30</sup>

$$\Delta\omega = \frac{2\pi v_a}{\Lambda} = \Omega, \quad (2-15)$$

where  $\Omega$  is the acoustic wave frequency.

Stimulated Brillouin scattering is a self-induced acousto-optic effect and a basic experiment is shown in Figure 2. As the incident pump light ( $\omega_p$ ) propagates through the medium, it encounters an acoustic wave traveling in the same direction at the Brillouin frequency,  $\Omega_B$ . As with the acousto-optic effect discussed above, the acoustic wave in the medium generates an index grating which diffracts the incident pump beam to generate a Stokes wave ( $\omega_s$ ). As a result of the acoustic wave moving away from the incident radiation, the frequency of the scattered light is downshifted by an amount equal to the acoustic frequency ( $\Omega_B$ ).

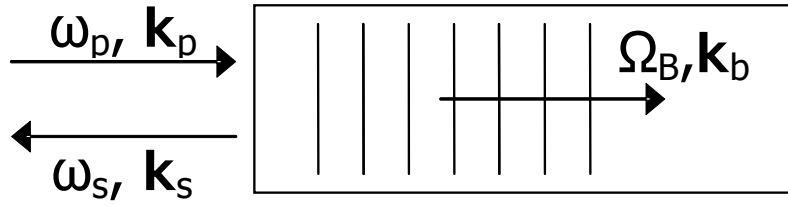


Figure 2: Stimulated Brillouin scattering

The process begins with *spontaneous* Brillouin scattering that occurs when the incident pump light scatters from acoustic waves naturally present at thermal equilibrium. Once the process starts, the created Stokes field interferes with the incident pump laser and reinforces the acoustic wave. There are, in general, two methods in which this interference can drive the acoustic wave: optical absorption and electrostriction. Electrostriction, the more common process, is the tendency of materials to become compressed in the presence of an optical beam.<sup>20</sup>

As the Stokes wave grows, the two processes mentioned serve to reinforce each other. As the incident light scatters from the growing acoustic wave, the Stokes beam increases. As this Stokes beam grows in intensity, it continues to interfere with the input field and drive the acoustic wave via electrostriction. The process continues and can lead to exponential growth of the Stokes wave. Although SBS leads to Stokes amplification in all directions except that of incident beam, it is typically observed in the backward direction (as shown in Figure 2) as it provides the maximum spatial overlap of the laser pump and Stokes beams.<sup>20</sup>

When examining SBS in terms of the particle nature of light, the Stokes scattering is described as annihilation of an incident pump photon while a Stokes photon and acoustic phonon are created. The conservation of energy and momentum requires

$$\begin{aligned}\omega_p &= \omega_s + \Omega_B \\ \mathbf{k}_p &= \mathbf{k}_s + \mathbf{k}_B\end{aligned}, \quad (2-16)$$

where  $\omega_p$ ,  $\omega_s$ , and  $\Omega_B$  are the frequencies and  $\mathbf{k}_p$ ,  $\mathbf{k}_s$ , and  $\mathbf{k}_B$  are the wave vectors of the pump, Stokes, and acoustic wave, respectively. The most general vector phase matching for the backward scattering case is shown in Figure 3. The case in which  $\theta = \pi$  is the same as portrayed in Figure 2 above.<sup>28</sup>

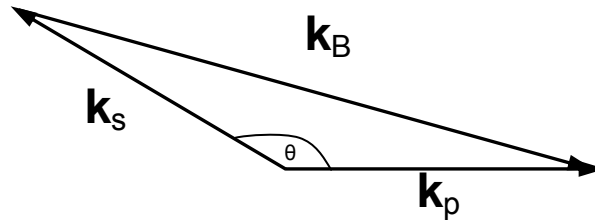


Figure 3: Stimulated Brillouin scattering phase matching condition for backward scattering



Solving Equation 2-16 for the Stokes frequency reveals the previously mentioned downshift,

$$\omega_s = \omega_p - \Omega_B \quad (2-17)$$

The frequency of the acoustic wave is given in terms of the velocity of sound,  $v_a$ , as

$$\Omega_B = |\mathbf{k}_B| v_a \quad (2-18)$$

We shall see shortly that typical acoustic frequencies are approximately  $10^9$  Hz. Because the optical frequencies ( $\omega_p$  and  $\omega_s$ ) are  $\sim 10^{15}$  Hz, it is a fair approximation to allow  $|\mathbf{k}_s| \approx |\mathbf{k}_p|$  yielding  $|\mathbf{k}_B| \approx 2|\mathbf{k}_p|$ . Using this relation with  $|\mathbf{k}_i| = n\omega_i/c$  yields the equation for Brillouin frequency<sup>20</sup>

$$\Omega_B = \frac{2n v_a}{c} \omega_p . \quad (2-19)$$

Stimulated Brillouin scattering can be achieved in a variety of mediums. Many early investigations used a liquid or gas contained in an optical cell. Tables of values for  $\Omega_B$  are given on both page 337 of Boyd<sup>20</sup> and page 189 of Shen,<sup>31</sup> but the former is a more comprehensive list. SBS also occurs in optical fibers and is the focus of this research effort. For silica fiber, the acoustic velocity is  $v_a = 5.96$  km/s and the index of refraction is  $n = 1.45$ .<sup>21</sup> At a pump wavelength of 1064 nm, this results in a frequency shift of  $\Omega_B = 1.02 \times 10^{11}$  rad/sec or  $\nu_B = 16$  GHz. These values justify the approximation mentioned above in the formulation of Equation 2-19.

To develop the coupled wave equations, we begin by considering an ensemble of molecules in the presence of an electromagnetic field. In this case, the molecules are pulled into the regions of the highest field resulting in density changes in the medium.

The density changes in the material produce a corresponding alteration to the permittivity ( $\epsilon$ ) through the elasto-optic effect. The change in permittivity is given by

$$\Delta\epsilon = \frac{\partial\epsilon}{\partial\rho}\Delta\rho, \quad (2-20)$$

where  $\Delta\rho$  is the incremental change in mass density. The nonlinear polarization is then given by

$$\mathbf{P}_{NL} = \Delta\epsilon \mathbf{E} = \frac{\partial\epsilon}{\partial\rho}\Delta\rho \mathbf{E} \quad (2-21)$$

This nonlinear polarization describes the coupling between the electric field and acoustic wave and serves as the driving term in the nonlinear wave Equation 2-12. The coupled wave equations for the pump beam, Stokes beam, and the acoustic wave induced by electrostriction are.<sup>28,32</sup>

$$\begin{aligned} \nabla^2 \mathbf{E}_i - \mu_0 \epsilon \frac{\partial^2 \mathbf{E}_i}{\partial t^2} &= \mu_0 \frac{\partial^2 \mathbf{P}_{NL_i}}{\partial t^2} \\ \frac{\partial^2 \rho}{\partial t^2} - \Gamma' \nabla^2 \frac{\partial \rho}{\partial t} - v_a^2 \nabla^2 \rho &= -\frac{\rho_0}{2} \frac{\partial \epsilon}{\partial \rho} \nabla^2 (\mathbf{E}^2) \end{aligned} \quad (2-22)$$

The subscripted notation (i's) serves to represent either the pump (p) or Stokes (s) component. In the acoustic wave equation,  $\Gamma'$  is the damping parameter,  $v_a$  is the sound velocity, and  $\rho_0$  is the mean density of the medium.

The fields for the pump beam and Stokes beam assuming a plane wave propagating along the z-axis are defined as  $\mathbf{E}_i = A_i e^{i(\pm k_i z - \omega_i t)} + c.c.$ , where  $A_i$  is the field amplitude and c.c. denotes the complex conjugate of the previous terms. Using these fields, taking the appropriate derivatives and applying the slowly varying envelope approximation (SVEA i.e.  $|\partial^2 A / \partial z^2| \ll |k \partial A / \partial z| \rightarrow \partial^2 A / \partial z^2 \approx 0$ ) yields<sup>20</sup>

$$\begin{aligned}\frac{\partial A_p}{\partial z} &= \frac{i\omega_p \rho_o k_B^2}{8nc\varepsilon_0 \Omega_B} \left( \frac{\partial \varepsilon}{\partial \rho} \right)^2 \frac{|A_s|^2 A_p}{\Omega_B - \Omega + i\Gamma_B} \\ \frac{\partial A_s}{\partial z} &= -\frac{i\omega_s \rho_o k_B^2}{8nc\varepsilon_0 \Omega_B} \left( \frac{\partial \varepsilon}{\partial \rho} \right)^2 \frac{|A_p|^2 A_s}{\Omega_B - \Omega - i\Gamma_B}\end{aligned}\quad (2-23)$$

where  $\Gamma_B = k_B^2 \Gamma$  is the Brillouin linewidth,  $\Omega_B$  is the Brillouin frequency previously discussed, and  $\Omega = \omega_p - \omega_s$  is the frequency of the driven acoustic wave. The reciprocal of the Brillouin linewidth is the phonon lifetime,  $\tau_p = (\Gamma_B)^{-1}$ .

By multiplying by  $A_p^*$  and  $A_s^*$ , respectively, the above equations can be converted to their intensity form and for the case of fibers, a loss term is included.<sup>20,21,33</sup>

$$\begin{aligned}\frac{\partial I_p}{\partial z} &= -g_B I_p I_s - \alpha I_p \\ \frac{\partial I_s}{\partial z} &= -g_B I_s I_p + \alpha I_s\end{aligned}\quad (2-24)$$

Here the constant terms have been lumped into the Brillouin gain factor, approximated by<sup>20</sup>

$$g_B(\Omega) = \frac{\omega^2 \rho_o}{2nv_a c^3 \Gamma_B} \left( \frac{\partial \varepsilon}{\partial \rho} \right)^2 \frac{\Gamma_B^2}{(\Omega_B - \Omega)^2 + \Gamma_B^2} \quad (2-25)$$

A list of symbols has been added as Appendix A to help maintain clarity. One solution to the above coupled equations (2-24) is presented in the next section as part of the discussion on SBS threshold.

### 2.2.2. Stimulated Brillouin Scattering Threshold

In order to utilize the SBS process for applications such as beam cleanup, beam combining, phase conjugation, or beam phasing, it is necessary to pump the nonlinear medium with sufficient power to reach SBS threshold. This research effort will use a

continuous wave (cw) pump laser for generating SBS in the nonlinear medium. Because cw lasers do not have the high peak powers available with a Q-switched laser, understanding the requirements for generating SBS is especially important. Numerous techniques have been developed for decreasing the SBS threshold and these ideas will be discussed later in the document (see Section 4.3.1). In this section, the theoretical basis and an approximation formula for the SBS threshold is established.

For estimating the SBS threshold, it is necessary to solve the Stokes differential equation of 2-24. In this case, pump depletion is neglected and the pump intensity used is  $I_p(z) = I_p(0)e^{-\alpha z}$ . Rearranging the terms, the Stokes differential equation (2-24) becomes

$$\frac{\partial I_s}{\partial z} + [g_B I_p(0)e^{-\alpha z} - \alpha] I_s = 0 \quad (2-26)$$

Solving this first order linear differential equation and using the initial conditions leads to

$$I_s(0) = I_s(L) \exp \left[ \frac{g_B I_p(0)}{\alpha} [1 - \exp(-\alpha L)] \right] e^{-\alpha L}, \quad (2-27)$$

where L is the fiber length. This equation is commonly displayed using the effective length of the fiber defined by  $L_{eff} = [1 - \exp(-\alpha L)]/\alpha$  and in terms of input power,

$P_0 = I_p(0) \cdot A_{eff}$ , where  $A_{eff}$  is the effective area of the fiber. In this form the equation becomes<sup>21</sup>

$$\begin{aligned} I_s(0) &= I_s(L) \exp [g_B P_0 L_{eff} / A_{eff} - \alpha L] \\ &\quad \text{or} \\ P_s(0) &= P_s(L) \exp [g_B P_0 L_{eff} / A_{eff} - \alpha L] \end{aligned} \quad (2-28)$$

The introduction of the effective area,  $A_{eff}$ , requires the definition of a few fundamental fiber terms. For a Gaussian beam,  $A_{eff} = \pi \omega_{f0}^2$ , where  $\omega_{f0}$  is the mode field radius. It is possible to approximate the mode radius in terms of the fiber core radius,  $a$ . This approximation has better than 99 % accuracy for single mode fibers and remains a fair approximation in the case of multimode fibers. It is given by

$$\omega_0 \approx a \left( 0.65 + \frac{1.619}{V^{3/2}} + \frac{2.879}{V^6} \right). \quad (2-29)$$

This equation utilizes the fiber normalized frequency parameter,  $V$ . It is defined as

$$\begin{aligned} V &= ak_0 \left( n_{core}^2 - n_{clad}^2 \right)^{1/2}, \\ &= ak_0 NA \end{aligned} \quad (2-30)$$

where  $a$  is the fiber core radius,  $NA = \left( n_{core}^2 - n_{clad}^2 \right)^{1/2}$  is the numerical aperture of the fiber, and  $n_i$  is the respective index of refraction for the core and cladding of the single-clad fiber. The normalized frequency parameter for a given fiber is used to provide bounds for the number of modes allowed to propagate in the fiber.<sup>34</sup>

Smith<sup>35</sup> arbitrarily assigned the critical (or threshold) power to be the input power for which the Stokes power equals the input power at  $z = 0$ . Applying this to Equation 2-28 and assuming a Lorentzian distribution for the SBS gain, the threshold is estimated as

$$P_{th} \approx \frac{21 A_{eff}}{g_B L_{eff}}. \quad (2-31)$$

Although this approximation was developed for single-mode fibers, it still provides a usable benchmark for multimode fiber applications.

To conclude the SBS threshold discussion, a few numerical examples are explored using the fiber parameters given in Table 2.

Table 2: Fiber parameters for SBS threshold calculations

Core Diameter	50 $\mu\text{m}$
Loss, $\alpha$	1.0 dB/km
Pump Wavelength, $\lambda_p$	1064 nm
Brillouin Gain, $g_B$	$5 \times 10^{-11}$ m/W
Brillouin Frequency, $\nu_B$	16 GHz
$n_{\text{core}}$	1.47
$n_{\text{clad}}$	1.45
Brillouin Linewidth	<100 MHz

For a long fiber case with  $L = 4$  km, Equation 2-31 requires a threshold of  $P_{\text{th}} = 140$  mW. A short fiber of  $L = 10$  m with the same parameters requires an estimated power of  $P_{\text{th}} = 36$  W to reach SBS threshold.

### 2.3. *Optical Phase Conjugation*

Optical phase conjugation, as implemented through stimulated Brillouin scattering, is investigated as part of this work. This section provides an introduction to phase conjugation and the required theoretical background. The basic properties of phase conjugation are first discussed, followed by an explanation of phase conjugate generation through SBS.

#### 2.3.1. **Overview of Optical Phase Conjugation**

Optical phase conjugation is a process implemented through nonlinear optics that reverses the sign of the spatial portion of the phase and causes the wave to backtrack along its original path. The process of phase conjugation is best explained with a simple example. A plane wave travels through an aberrating medium as shown in Figure 4.<sup>36</sup> Here, the aberration is represented as a random modulation in index of refraction and distorts the wavefront due to the varying path length of the medium. After traveling

through the medium, the distorted wavefront encounters either a normal reflecting mirror (case a) or a phase conjugate reflecting mirror (Case b). For the normal mirror, the reflection flips the wavefront as shown in Figure 4a and a second pass through the aberrating medium increases the wavefront error. On the other hand, Figure 4b shows the reflection from a phase conjugate mirror. In this case, the reflected wave is the “phase conjugate” and a second pass results in a cancellation of media's effect (reflected wave in Figure 4b). The phase conjugation process is also known as wavefront reversal since it produces the same incident wavefront, but travels in the opposite direction.<sup>20</sup>

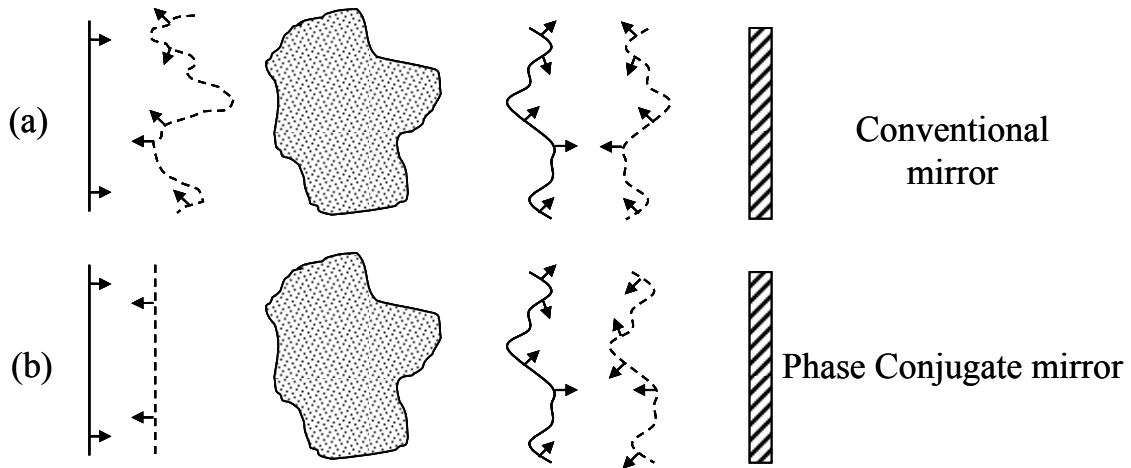


Figure 4: Plane wave propagating through random media-- Solid lines indicate the incident wave and the dotted lines indicated the reflected wave of (a) a conventional mirror and (b) a phase conjugate mirror.

To see the phase conjugation aspect of the process, it is helpful to introduce the equations describing the process. The incident plane wave propagating along the forward  $z$  direction can be written as<sup>37,38</sup>

$$\mathbf{E} = \mathbf{A}(\mathbf{r})e^{i(kz - \omega t)}, \quad (2-32)$$

where  $\mathbf{A}(\mathbf{r})$  represents the complex field amplitude. Taking the complex conjugate of only the spatial portion of this wave produces

$$\begin{aligned}\mathbf{E}_C &= \mathbf{A}(\mathbf{r})^* e^{-i(kz + \omega t)} \\ &\text{or} \\ \mathbf{E}_C &= \mathbf{A}(\mathbf{r})^* e^{i(kz + \omega t)}\end{aligned}\tag{2-33}$$

where the two statements are equivalent when taking the real part of the complex representation. The two waves of Equations 2-32 and 2-33 have the same wavefronts at any point along their propagation, but they propagate in opposite directions. For this reason, the phase-conjugated wave is often referred to as time-reversed wave and the process in general is called wavefront reversal as mentioned above.<sup>37,39</sup>

### 2.3.2. Phase Conjugation through Stimulated Brillouin Scattering

Stimulated Brillouin Scattering was first demonstrated to produce a phase conjugate reflection by Zel'dovich, *et al.* in 1972.<sup>40</sup> In this experiment, a single longitudinal mode ruby laser was transmitted through a piece of etched glass into a waveguide containing methane gas (the SBS medium). The experiment compared the reflection from the SBS cell with that of a mirror. In the SBS case, the distortions induced were corrected on the second pass through the medium. For the mirror, the aberrations were made worse in the second pass as explained above in section 2.3.1. This observation has led to a long series of papers investigating the theoretical development of phase conjugation through stimulated Brillouin scattering.

The initial report of phase conjugation through stimulated Brillouin scattering by Zel'dovich, *et al.*<sup>40</sup> suggested that the production of the phase conjugate wave was a result of a preferential gain for the phase conjugate term. In this analysis, the aberrations



in the source laser produce a nonuniform intensity distribution in the medium (speckle pattern in the Russian literature). This requires that the solutions for the backreflected Stokes waves be broken into a sum of modes.<sup>41</sup> The modes for the Stokes wave will have different gain and Zel'dovich suggested that the phase conjugate mode would have a gain two times that of other modes and would dominate the backscattering process.<sup>40</sup> For the case of perfect phase conjugation, the result is the Stokes wave proportional to the conjugate of the pump wave,  $\mathbf{E}_s(\mathbf{r}) \propto \mathbf{E}_p^*(\mathbf{r})$ .<sup>32</sup> A more detailed outline of the initial work by Zel'dovich *et al.* is available in a review paper by Pepper.<sup>38</sup>

Optical fibers have also been used to produce a phase conjugate mirror through stimulated Brillouin scattering.<sup>24,42,43</sup> To utilize fibers for phase conjugation, it is necessary to use a multimode fiber because a single mode fiber does not provide the nonuniform intensity distribution as described above. It is also necessary to use short fibers (< 10 m) in order to maintain the spatial phase conjugate properties. If the nonlinear medium becomes too long, the difference between the Stokes frequency ( $\omega_s$ ) and the pump frequency ( $\omega_p$ ) leads to a non-conjugated portion of the Stokes beam. The maximum possible length for the fiber is given by<sup>37</sup>

$$L \leq \frac{6r_0^{1/2}c\pi^2}{\Omega_B(NA)^2}, \quad (2-34)$$

where  $r_0$  is the allowable non-conjugated fraction of Stokes beam,  $\Omega_B$  is the Brillouin frequency defined in Equation 2-19, and NA is the numerical aperture of the fiber. For 90% phase conjugation ( $r_0 = 0.1$ ), NA = 0.2, and using  $\Omega_B = 1.02 \times 10^{11}$  rad/sec as previously calculated for  $\lambda_p = 1064$  nm, the maximum length is 1.4 m. Authors differ in their definition for maximum allowable length to achieve phase conjugation and resultant

lengths can vary by as much as 10 times.<sup>37,44</sup> Phase conjugation has been experimentally demonstrated using fibers  $\leq 10$  m.<sup>24</sup>

A second major approach to investigating the phase conjugation aspects of stimulated Brillouin scattering is through use of numerical analysis. The analytical solutions above (along with other work) lead to solutions to the coupled equations only under the plane-wave approximation and with negligible pump depletion. As described in section 2.2.2, specific examples such as threshold can be calculated. Numerical solutions can provide more insight through their calculation of the complete Stokes wave. For example, the well cited two-dimensional BOUNCE code of the Naval Research Laboratory numerically solves the coupled wave equations for the case where the waves are no longer plane waves, but a function of  $x$  ( $I_p(x, z)$  &  $I_s(x, z)$ ).<sup>45</sup> The coupled equations solved in this paper take the parabolic form (in two-dimensional Cartesian geometry)

$$\begin{aligned} \left( \frac{\partial}{\partial z} + \frac{i}{2k} \frac{\partial^2}{\partial x^2} \right) I_p &= g_B I_p I_s \\ \left( \frac{\partial}{\partial z} - \frac{i}{2k} \frac{\partial^2}{\partial x^2} \right) I_s &= g_B I_s I_p \end{aligned} \tag{2-35}$$

These equations are similar to Equation 2-24 on page 17, but the loss term has again been neglected and, since the plane wave assumption is no longer used, the spatial derivative is not simplified.

Subsequent papers on the BOUNCE code also added the effects of pump depletion<sup>46</sup> and optical waveguide effects.<sup>47</sup> The findings of the numerical simulations compared well with the analytical results. One item of interest is that, as expected, the code showed that conjugated light passing twice through an aberrating medium did closely match that of the incident beam in the far field.<sup>46</sup>

In an attempt to model the full 3-dimensional SBS phase conjugation process, Hu, *et al.*,<sup>48</sup> adopted a new approach to numerically solving the complex differential coupled equations. The approach adapted the equations into a form that allowed solution by a perturbative method. The work included the effects of pump depletion and diffraction and demonstrated that the previous analytical solutions, indeed, provide adequate solutions for the conditions in which they are solvable.

A fortunate aspect of the phase conjugation process is that while the theory is continually developed, the experimental reports and applications have been quite extensive. The previous investigations that are critical to this experiment are presented in the respective sections.

### 3 SBS Beam Cleanup and Combining

The first method for power scaling multiple channels is based upon the beam cleanup properties present when exciting an SBS beam in a long ( $> 1$  km) gradient index, multimode fiber. This chapter investigates the background information related to beam cleanup and combining, the results achieved in extending the technology to larger diameter fibers, and an investigation in four-channel SBS beam combining.

#### 3.1. Background

The first method for power scaling lasers using a multiple channel approach exploits the long fiber beam cleanup properties to combine multiple laser beams. Long fiber beam combining is based upon the observation by Bruesselbach<sup>49</sup> that long fibers create an SBS beam in which the Stokes beam has an intensity distribution corresponding to the fundamental fiber mode,  $LP_{01}$ , irrespective of the pump intensity profile. It is possible to exploit this property and ‘clean up’ a distorted pump beam.

The beam cleanup properties of long optical fibers have traditionally been attributed to the preferential gain of the fundamental mode of the Stokes beam (compared to higher-order modes) because of its better overlap with the multimode pump beam. A recent investigation by Murray *et al.*<sup>50</sup> proposes that beam cleanup observed in stimulated Raman scattering (SRS) is related to the statistical central limit theorem. The theorem states that a large number ( $n \geq 30$  for most applications) of sufficiently well-behaved distributions may be approximated by a Gaussian distribution.<sup>51</sup> If the input pump and Stokes beams are examined in terms of their plane wave components, the nonlinear

polarization for SRS may be expressed as a two-dimensional convolution and autoconvolution of the plane wave components. In this case, the convolutions converge towards a Gaussian distribution by the central limit theorem. The result is that the Raman gain distribution from a multimode pump approaches that of a Gaussian and favors amplification of the Stokes beam in the fundamental fiber mode. While this work in beam cleanup was developed for SRS, it is equally valid for beam cleanup observed using SBS.<sup>52</sup>

SBS beam cleanup was verified by Rodgers *et. al.*<sup>22</sup> and their work furthered the investigation to provide a means for beam combination. The group focused two beams into an optical fiber and allowed the beams to combine using the cleanup properties. There are two basic methods of SBS beam combining, coherent beam combining and incoherent beam combining. The difference between the two is in the spectral separation of the input pump beams. If the beams are separated by less than a Brillouin gain bandwidth, in this case  $< 100$  MHz, the pumps drive a common SBS wave that draws energy from both beams. This is demonstrated in cases when a single source is split into two beams and combined into the fiber or when two different sources are used but kept within 100 MHz of each other. Slope efficiencies as high as 67% were observed.

For incoherent beam combining, two laser sources separated by more than 100 MHz are required. A later paper by Russell<sup>23</sup> investigated incoherent beam combining in more detail and demonstrated that in this case, separate SBS waves are excited by the two laser beams. While spectrally different, both beams produced the LP<sub>01</sub> providing excellent spatial overlap. This method of beam combining can be advantageous in attempting to develop high power lasers. In the case of coherent combining, the SBS threshold is

dependent on the combined power of the beams. This can lead to problems with stimulation of the second order Stokes component as powers increase.<sup>53</sup> In incoherent beam combining, each pump beam excites a separate Stokes beams and the thresholds for each Stokes order is only dependent on the individual laser beams, not the combined power.

Part of this research effort was to extend the SBS beam combining work of Rodgers<sup>22</sup> and Russell<sup>23</sup> to include more input channels. The details of the investigation are recorded in this chapter.

### ***3.2. 62.5-micron and 100-micron Beam Cleanup***

One of the first approaches for scaling SBS beam combination to higher power levels is to increase the core size of the fiber. In previous work, the largest fiber used was a 50  $\mu\text{m}$  core diameter gradient index fiber.<sup>54</sup> As the number of combined beams increases, the focusing geometry for coupling the beams into the fiber requires a larger core. Before proceeding with larger fiber beam combination experiments, it was necessary to verify that the larger core still maintains the beam cleanup properties previously mentioned.

The experimental setup used to demonstrate SBS beam cleanup in two larger core gradient index fibers is shown in Figure 5. The laser source is a 1064 nm single-frequency non-planar ring oscillator (NPRO) which was first reported by Kane and Byer<sup>55</sup> and is commercially available from Lightwave Electronics. The NPRO uses a monolithic Nd:YAG cavity in the presence of a magnetic field to generate unidirectional single mode oscillation and delivers a diffraction limited beam with a spectral linewidth  $< 5$  KHz. Our particular model has a maximum power output of 700 mW. The laser is

first isolated from system feedback using a polarizing beam splitter (PBS)/Faraday rotator (FR) combination and is then transmitted into a two-pass amplifier. The gain in this preamplifier is provided by a 3 mm diode-pumped Nd:YAG rod commercially available from Cutting Edge Optronics. The maximum power output available from the two-pass amplifier is  $\sim 2$  W, but the typical operation configuration produced an output power of 1.5W.

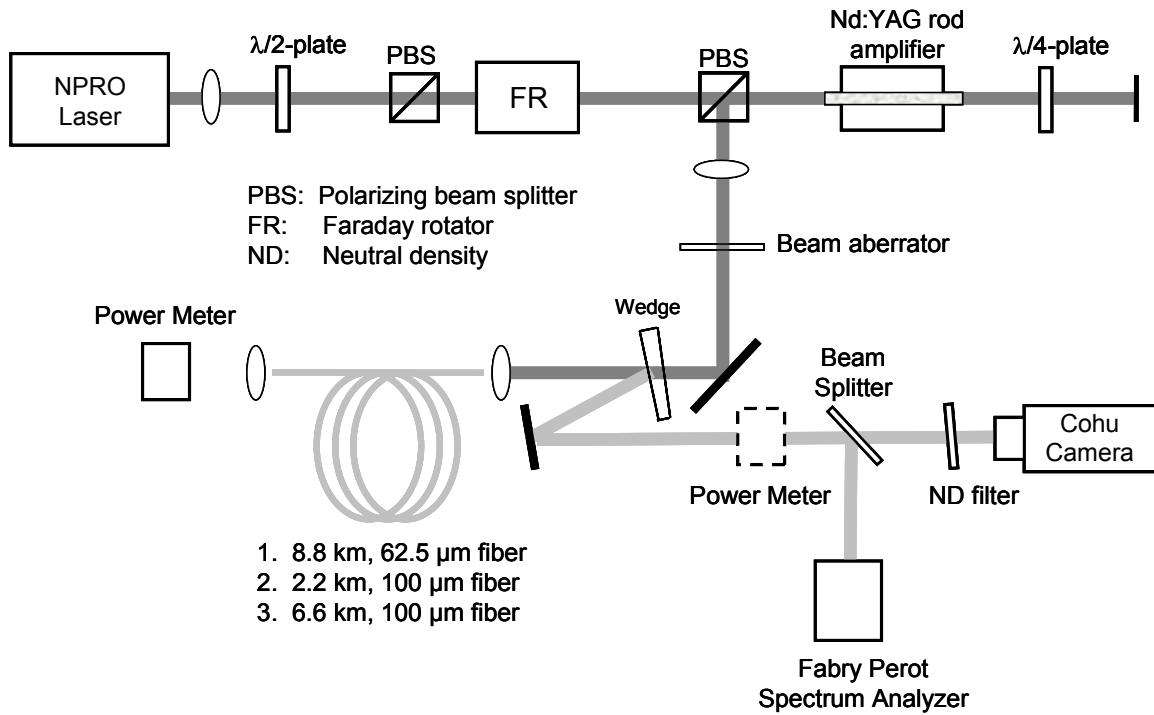


Figure 5: Schematic diagram to examine beam cleanup in 62.5  $\mu\text{m}$  and 100  $\mu\text{m}$  core diameter fibers.

The output from the two-pass amplifier was collimated and passed through a beam aberrator consisting of two pieces of stretched plastic. The stretched plastic was used to distort the phase front to demonstrate that a highly aberrated pump beam is capable of

producing a fundamental mode ( $LP_{01}$ ) through SBS beam cleanup. The pump beam was focused into the fiber using a 20X ( $f = 8\text{mm}$ ) microscope objective.

The Stokes beam traveling in the backwards direction was collimated by the input objective and a portion of beam was reflected from a beam pickoff. The pickoff is an optical wedge that is AR coated for 1064 nm on one side. The pickoff was calibrated to calculate the total power generated in the Stokes beam. The beam pickoff was also used to look at the spectrum using the Fabry-Perot optical spectrum analyzer and to record images with the Cohu CCD camera.

The input-output characteristics for 8.8 km of 62.5  $\mu\text{m}$  core gradient index fiber without the beam aberrator are shown in Figure 6. The inset is included to add more detail to the lower power regime. The SBS threshold in this experiment was 75 mW and the slope efficiency was 65%.

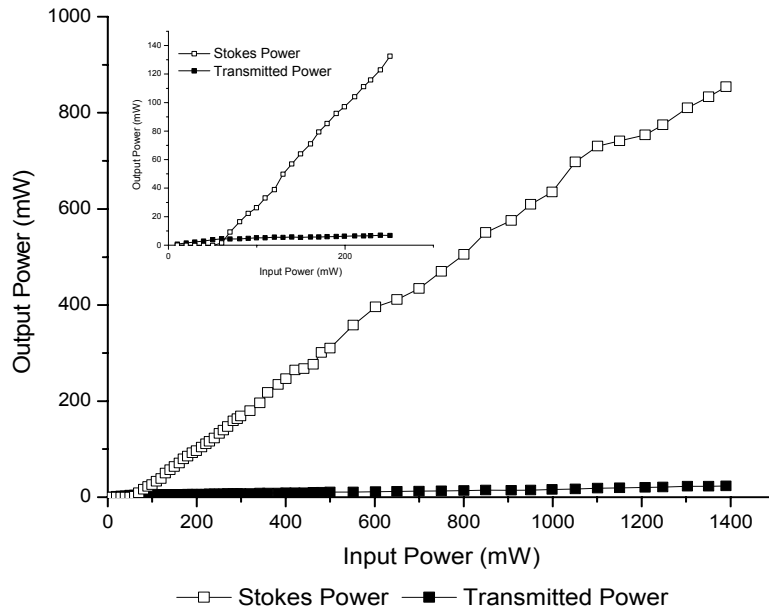


Figure 6: SBS input vs. output characteristics for 8.8 km, 62.5  $\mu\text{m}$  fiber.



The Fabry-Perot spectrum analyzer scan shown in Figure 5 is used to observe the frequency shift of the SBS beam and verify SBS threshold. Figure 7 shows the Fabry-Perot data for a pump power just above threshold (100 mW).

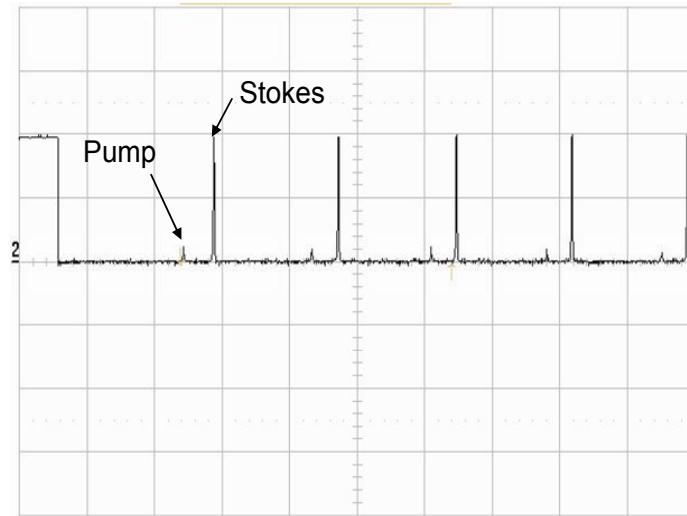


Figure 7: Fabry-Perot spectrum analyzer data taken at a pump power of 100 mW. The Fabry-Perot data is used to verify SBS threshold and to observe the frequency shift of the Stokes beam.

The SBS frequency shift is measured by verifying the direction of the Fabry-Perot scan and calibrating the output using the known free spectral range (FSR) of the device. For the Burleigh Fabry-Perot spectrum analyzer (model # SA-800-A) used in this experiment, the FSR is 8 GHz and a decrease in laser frequency shifts the peaks to the left. As detailed in section 2.2.1, the SBS shift is predicted to be a downshift of  $\sim 16$  GHz. Because this shift is greater than the FSR of the Fabry-Perot, it is necessary to associate the correct pump peak with the corresponding Stokes peak in the multiple free spectral ranges observed in the scan. Figure 8 illustrates this process. In this case, the bold pump1 peak corresponds to the  $\sim 16$  GHz downshifted Stokes 1 as shown in the

figure. To determine the actual frequency shift, the known FSR of 8 GHz is used to calibrate the output and determine the actual value. The frequency shift of the Stokes beam for this experiment with the 62.5  $\mu\text{m}$  core diameter fiber as shown in Figure 7 is  $14.3 \pm 0.2$  GHz.

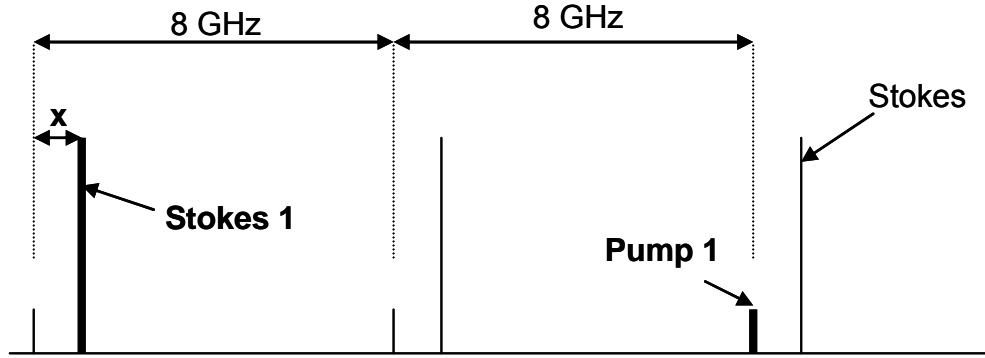


Figure 8: Determining SBS frequency shift using a Fabry-Perot spectrum analyzer.

The unaberrated input-output characteristics for 2.2 km and 6.6 km of 100  $\mu\text{m}$  core gradient index fiber are shown in Figure 6. The SBS thresholds and slope efficiencies for the 2.2 km and 6.6 km length were 300 mW / 82% and 200 mW / 80%, respectively.

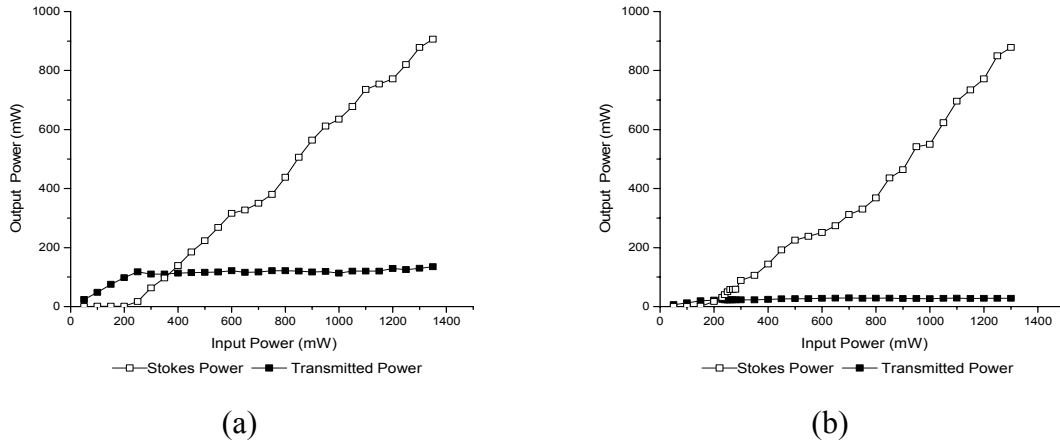


Figure 9: SBS input vs. output characteristics for (a) 2.2 km and (b) 6.6 km, 100  $\mu\text{m}$  fibers

To test the beam cleanup properties of the fibers, the beam aberrator was placed in the beam path and the spatial intensity profiles of both the reflected pump beam and backwards propagating Stokes beams were recorded with the Cohu CCD camera. Figure 10 shows the distorted pump beam for the (a) 62.5  $\mu\text{m}$  and (c) 100  $\mu\text{m}$  fibers (2.2 km) as well as the Stokes output (b) and (d), respectively. It is evident from the figure that although a highly aberrated pump beam is used, the Stokes output is ‘cleaned up’ and generates a high quality beam output as observed in previous experiments.<sup>22,54</sup>

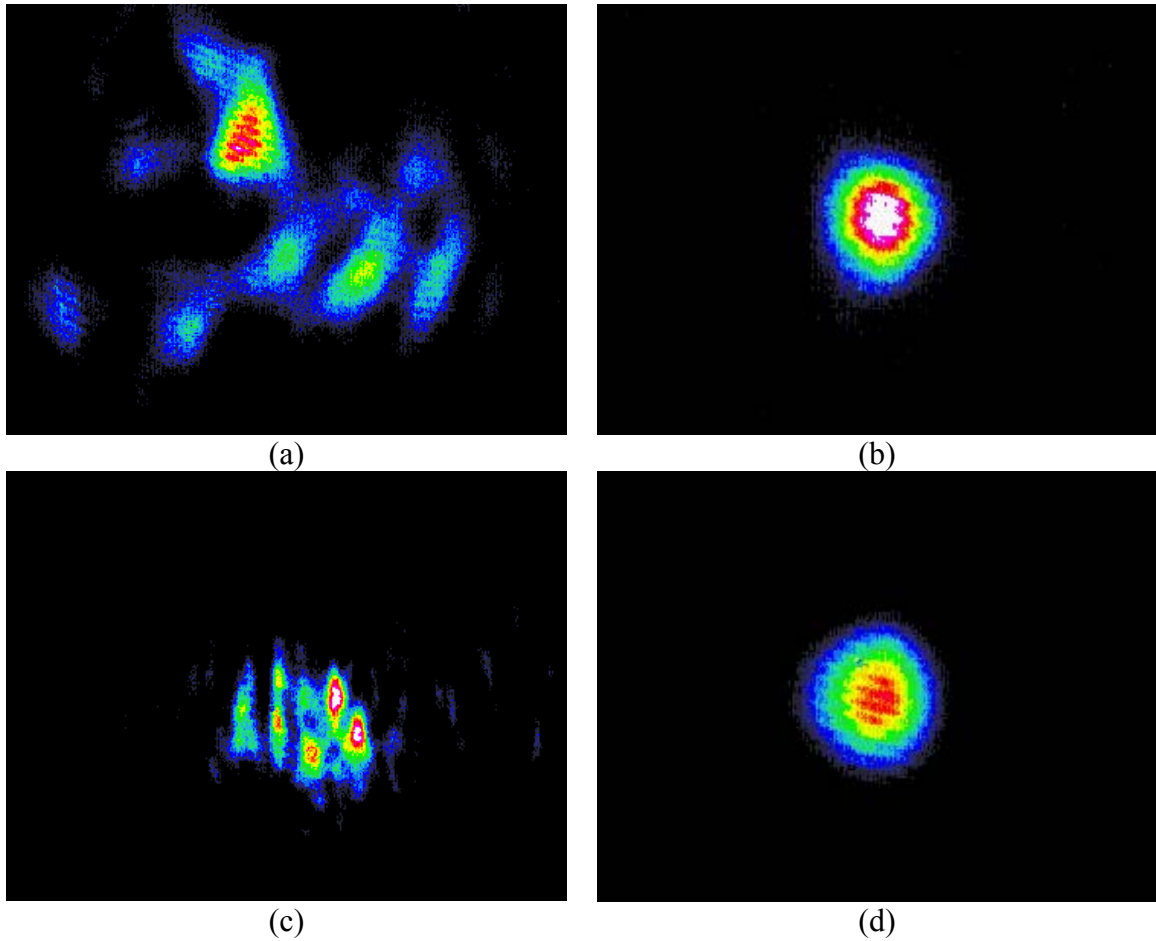


Figure 10: Spatial intensity distributions of the reflected pump and generated Stokes beam for the 62.5  $\mu\text{m}$  (a,b) and the 100  $\mu\text{m}$  (c,d) fibers. The figure demonstrates that an aberrated input beam generates a Gaussian-like Stokes output through SBS beam cleanup.

As previously mentioned, the successful demonstration of beam cleanup with larger core gradient index fibers is an important step in scaling the technology to accommodate higher power levels. The experimental verification of beam cleanup in both the 62.5  $\mu\text{m}$  and 100  $\mu\text{m}$  allows for further investigation in beam combining using stimulated Brillouin scattering and, specifically, allowed investigation of four beam combining as discussed below.

### ***3.3. Four-Channel Beam Combining***

The previous experiments investigating SBS beam combining have established the basis for combining multiple laser beams. There are still, however, challenges to making the technique useful for multiple laser beam combination. One of the problems is the lack of a device that permits efficient coupling of the input and output beams into and out of the SBS fiber. In all previous experiments, a polarizing beam splitter was used for spatially superposing two input beams and an ordinary beam splitter separated the output Stokes beam. Although acceptable for feasibility demonstration, the configuration is not acceptable for practical applications because of the poor output coupling efficiency. Moreover, it permits combining only two beams. In order to make the SBS beam combining technique practical, one needs to develop an optical device that couples multiple input beams and output Stokes beam into and out of the SBS fiber efficiently.<sup>54</sup>

This section investigates a beam combiner for joining multiple pump beams into the SBS fiber and coupling the Stokes beam out of the combining system with high efficiency. Fig. 1 shows a schematic diagram of the multiple-beam combiner investigated.

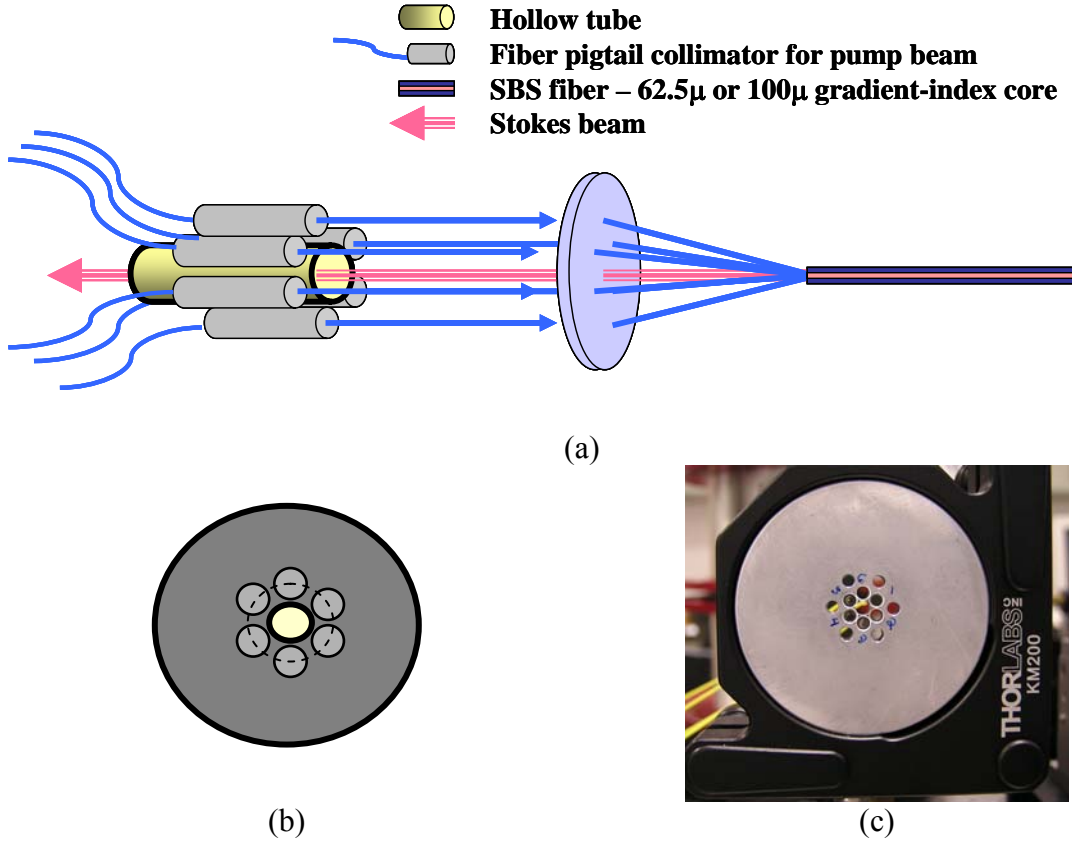


Figure 11: Schematic diagram (a) and graphical end view (b) of the SBS beam combiner. A picture of the actual beam combiner implemented in this study is shown in (c).

The system is designed with a set of six pigtail fiber collimators transporting the pump beams arranged symmetrically around a center hole in a ‘Gatlin gun’ configuration. The pump beams are focused through a lens onto the end facet of a multimode SBS fiber that is, in turn, aligned to make its axis collinear with that of the pigtail collimators. When the total power of the pump beams exceeds the SBS threshold, the fiber will generate a Stokes beam. The Stokes beam should be generated in the fundamental fiber mode due to the SBS beam cleanup property and travel backward through the center hole allowing for efficient coupling of the of the beam combiner output. As shown in Figure

11c, the pigtail collimators are fixed in an aluminum plate which is held in a mirror mount such that the direction of the beams can be adjusted.

### 3.3.1. Design

In developing the SBS beam combiner, there are certain design considerations that must be simultaneously satisfied to achieve efficient input/output coupling. The first consideration is that the size of the center hole must be sufficiently large to pass the collimated Stokes beam without clipping it. Second, the focal spot size of the pump beams must be smaller than the core size of the SBS fiber. Third, the numerical aperture of the pump beams as viewed from the SBS fiber must not exceed that of the fiber. Finally, the pigtail collimators have to be aligned and mounted such that the collimated beams are sufficiently parallel to each other. Figure 11 shows a side view of the beam combiner whose relevant parameters are discussed below.

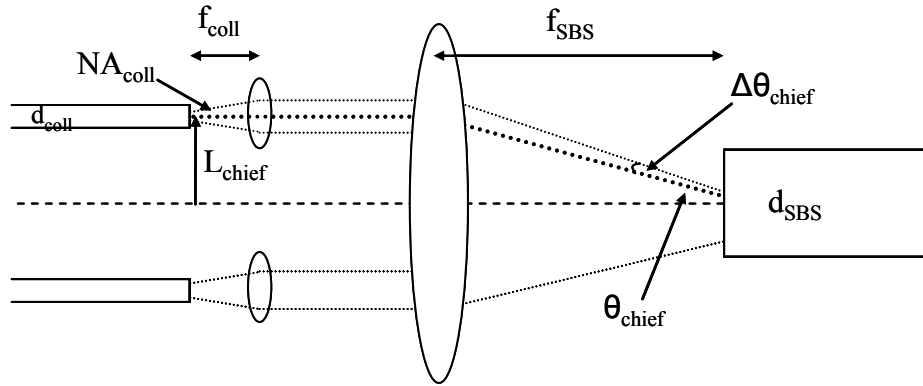


Figure 12: Side view schematic for multiple SBS beam combiner design

In calculating the required center hole size, it is necessary to determine the waist size of the output Stokes beam. This experiment uses a gradient index fiber allowing us to approximate the LP<sub>01</sub> output as a Gaussian beam with spot size<sup>1</sup>

$$\omega_o = \sqrt{\frac{\lambda d_{SBS}}{2\pi NA}}, \quad (3-1)$$

where  $d_{SBS}$  is the diameter of the SBS fiber. This leads to a collimated output SBS waist size of<sup>54</sup>

$$\omega_{SBS} = \sqrt{\frac{2\lambda NA}{\pi d_{SBS}}} f_{SBS} \quad (3-2)$$

for a collimating lens of focal length,  $f_{SBS}$ . In order to insure that 99% of the beam is transmitted through the center hole, the diameter is chosen to be greater than three times that of the expected SBS beam radius. This leads us to a center hole design requirement of

$$d_h > 3 \sqrt{\frac{2\lambda NA}{\pi d_{SBS}}} f_{SBS}, \quad (3-3)$$

where  $d_h$  is the diameter of the center hole.

The next design requirement is that the core size of the SBS fiber must be larger than the focused spot of the beams from the pigtail collimators. In this case, the focal spot size of the beams is essentially a magnified image of the beam at the end facet of the pigtail fiber. Consequently, the diameter of the focused beams ( $d_s$ ) at the SBS fiber facet is given by

$$d_s = \frac{f_{SBS}}{f_{coll}} d_{coll}, \quad (3-4)$$

where  $f_{\text{coll}}$  and  $d_{\text{coll}}$  are the focal length and fiber core diameter of the pigtail collimators, respectively. The requirement for the SBS fiber core diameter ( $d_{\text{SBS}}$ ) then becomes

$$d_{\text{SBS}} > d_s = \frac{f_{\text{SBS}}}{f_{\text{coll}}} d_{\text{coll}} . \quad (3-5)$$

The ray angle of the marginal ray of the pump beams being focused onto the SBS fiber facet is determined by the sum of the ray angle of the chief ray from the individual pigtail collimators and the marginal ray angle of the individual pump beam relative to its chief ray. This maximum ray angle is given by

$$\begin{aligned} \theta_{\text{max}} &= \theta_{\text{chief}} + \Delta\theta_{\text{chief}} \\ &\cong \frac{L_{\text{chief}}}{f_{\text{SBS}}} + \text{NA}_{\text{coll}} \left( \frac{f_{\text{coll}}}{f_{\text{SBS}}} \right), \end{aligned} \quad (3-6)$$

where  $\text{NA}_{\text{coll}}$  is the numerical aperture of the pigtail fiber. The numerical aperture of the SBS fiber must be greater than this maximum ray angle to ensure the entire beam is coupled into the fiber.

In order to capture all of the energy from the pigtail collimators, it is also necessary to align the output of the collimators so that the beams travel parallel with one another. If the beams are not parallel, the focus spot will translate in the focal plane by an amount approximated as  $d_{\text{offset}} \cong f_{\text{SBS}} \theta_{\text{off}}$ . It is then necessary that this offset be kept small enough to accommodate the beams within the diameter of the SBS fiber core, i.e.

$$\begin{aligned} d_{\text{SBS}} &> d_{\text{offset}} + d_s \\ &\rightarrow \theta_{\text{off}} < \frac{d_{\text{SBS}} - d_s}{f_{\text{SBS}}} , \end{aligned} \quad (3-7)$$

Table 3 provides the values used in the subsequent experiment at  $\lambda = 1064$  nm. The numbers for the fiber pigtail collimator ( $f_{\text{coll}}$ ,  $d_{\text{coll}}$ ,  $\text{NA}_{\text{coll}}$ ) are selected using units that are



commercially available. The SBS focusing lens was selected as 15 mm and the center hole was set at 3 mm to be large enough for both the 62.5/100  $\mu\text{m}$  fibers. Four pigtail collimators were mounted around the hole along a 6.0 mm diameter circle ( $L_{\text{chief}} = 3.0$  mm) as shown in Figure 11. With these design parameters, the numerical aperture is large enough to accommodate the largest ray angle and the magnified spot is smaller than the fiber core diameter. As shown in the table, the output beams from the collimator need to be aligned so that they are parallel with a 1 to 3 mrad tolerance.

Table 3: Summary of multiple-channel beam combination (a) design parameters and (b) calculated values.

(a)	(b)	
Design parameters	62.5 $\mu\text{m}$ /0.275 NA fiber	100 $\mu\text{m}$ /0.29 NA fiber
$f_{\text{coll}} = 2.6$ mm	$d_s = 52$ $\mu\text{m}$	$d_s = 52$ $\mu\text{m}$
$d_{\text{coll}} = 9$ $\mu\text{m}$	$\theta_{\text{max}} = 0.22$	$\theta_{\text{max}} = 0.22$
$\text{NA}_{\text{coll}} = 0.12$	$d_h > 2.5$ mm	$d_h > 2.0$ mm
$d_{\text{chief}} = 3$ mm	$\theta_{\text{offmax}} = 1$ mrad	$\theta_{\text{offmax}} = 3$ mrad
$f_{\text{SBS}} = 15$ mm		
$d_h = 3$ mm		

The SBS beam combiner was produced based upon this design and tested as detailed in the following section

### 3.3.2. Experiment

Figure 13 shows the experimental schematic for testing the four-beam SBS combiner. In this configuration, the feasibility of SBS beam combination for fiber amplifier/oscillator applications is simulated by splitting a master oscillator into four separate channels and combining them using the ‘Gatlin gun’ beam combiner.

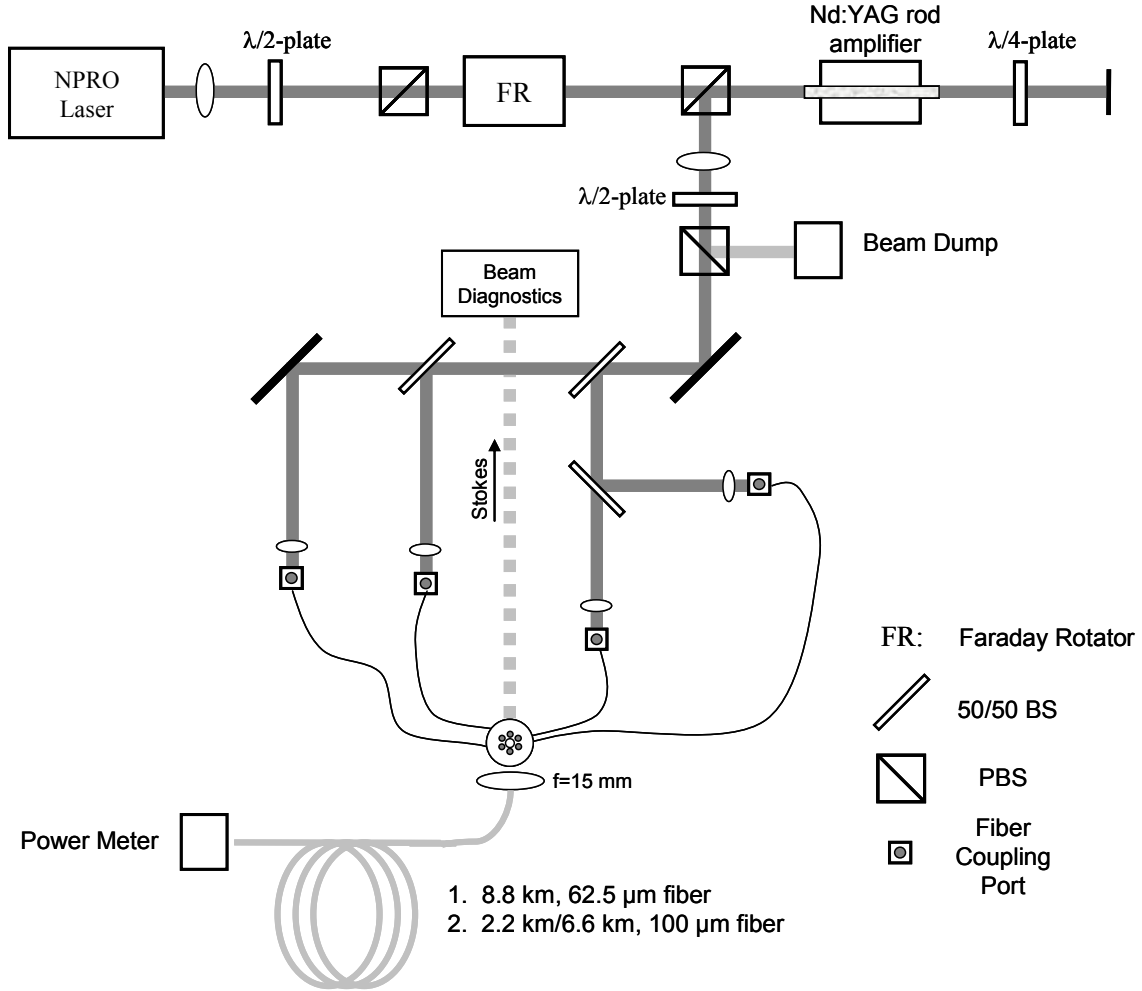


Figure 13: Schematic diagram for the four beam SBS combining experiment

As described in more detail in Section 3.2, the 1064 nm, single-frequency source is isolated and amplified to generate  $\sim 2.0$  W of pump power. The output from the amplifier was collimated and passed through a half wave-plate/polarization beam splitter to control the power entering the beam splitting system. The laser beam was split into four channels using a combination of 50/50 beam splitters with each channel having  $\sim 25\%$  of the power. The beams from each channel were focused into the single-mode (SMF-28 9- $\mu\text{m}$ , 0.12 NA) fiber pigtails using Optics for Research fiber ports (PAF). The

fiber ports incorporate the focusing lens along with a direct connection for the fiber's FC connector in a compact package. The coupling efficiency through the single-mode fiber was typically 60-70%.

The outputs from the beam combiner were focused into the SBS fiber using an  $f = 15$  mm lens. Because a large lens aperture was required to accommodate all of the beams from the 6 mm diameter on which the collimators are mounted, it was not possible to use a microscope objective or aspheric lens. Figure 14 shows the transmitted power through the fiber as the four beam input power was increased. The output from the beam combiner was monitored and no evidence of a Stokes beam was observed. As a comparison, the transmitted power when using a single beam directly in the center of the fiber (see Figure 6 and Figure 9b) is included. In this case, the slope of the transmitted power reduces significantly once SBS threshold is achieved.

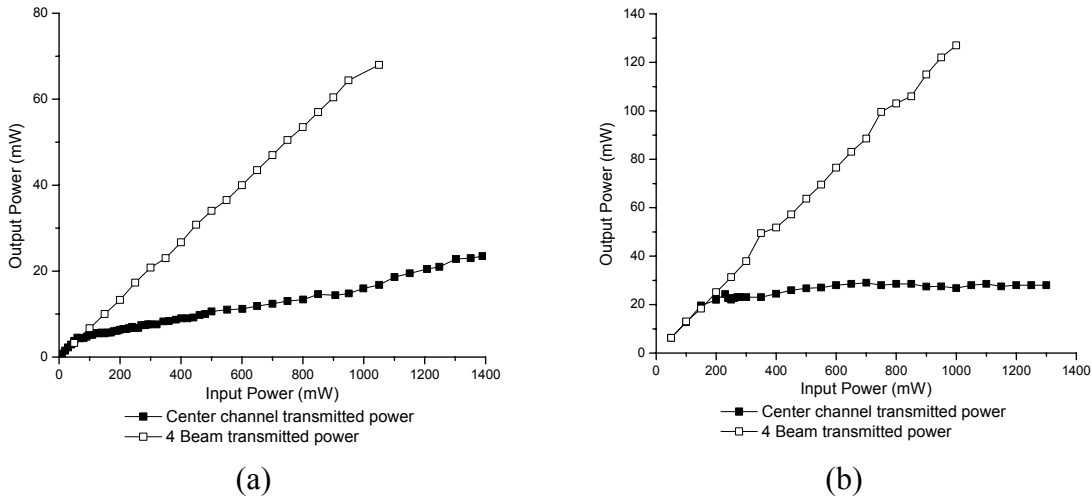


Figure 14: Transmitted power for (a) 8.8 km of 62.5 μm core diameter and (b) 6.6 km of 100 μm core diameter fiber. The transmitted power observed when seeding a single beam directly in the center is included for reference.

Although the total input power of the 4 beams from the pigtail collimators far exceeded the center-pumped SBS threshold, no Stokes output was observed. In order to compare the 4-beam data with the center channel input, the 4-beam fiber coupling efficiency was determined using a short fiber. Table 4 summarizes the results and quantifies the maximum power coupled using the 4-beam combiner as compared with direct center-pumping.

Table 4: Comparison of 4-beam combiner and centered-pumped SBS threshold for 62.5  $\mu\text{m}$  and 100  $\mu\text{m}$  core diameter fibers.

Fiber	Max transmission	Measured coupling	Max 4-beam coupled power	Center-pumped SBS Threshold
62.5 $\mu\text{m}$ , 8.8 km	58 mW	60%	600 mW	75 mW
100 $\mu\text{m}$ , 6.6 km	127 mW	84%	840 mW	200 mW

Because there was not enough laser power available from the SBS beam combiner to excite the Stokes wave by itself, a subsequent experiment was designed using a seed coupled directly into the center of the fiber. In this case, the center-pumped beam generated the SBS Stokes wave and the power from the beam combiner channels were added to determine how much is converted to the Stokes wave. Figure 15 is the system schematic for this test. The set-up is very similar to that described above. For this experiment, a portion of the amplifier output was split at the polarizing beam splitting cube and used as the seed. This beam was sent through a PBS/Faraday rotator combination so that the returning Stokes wave was separated to the system diagnostics.

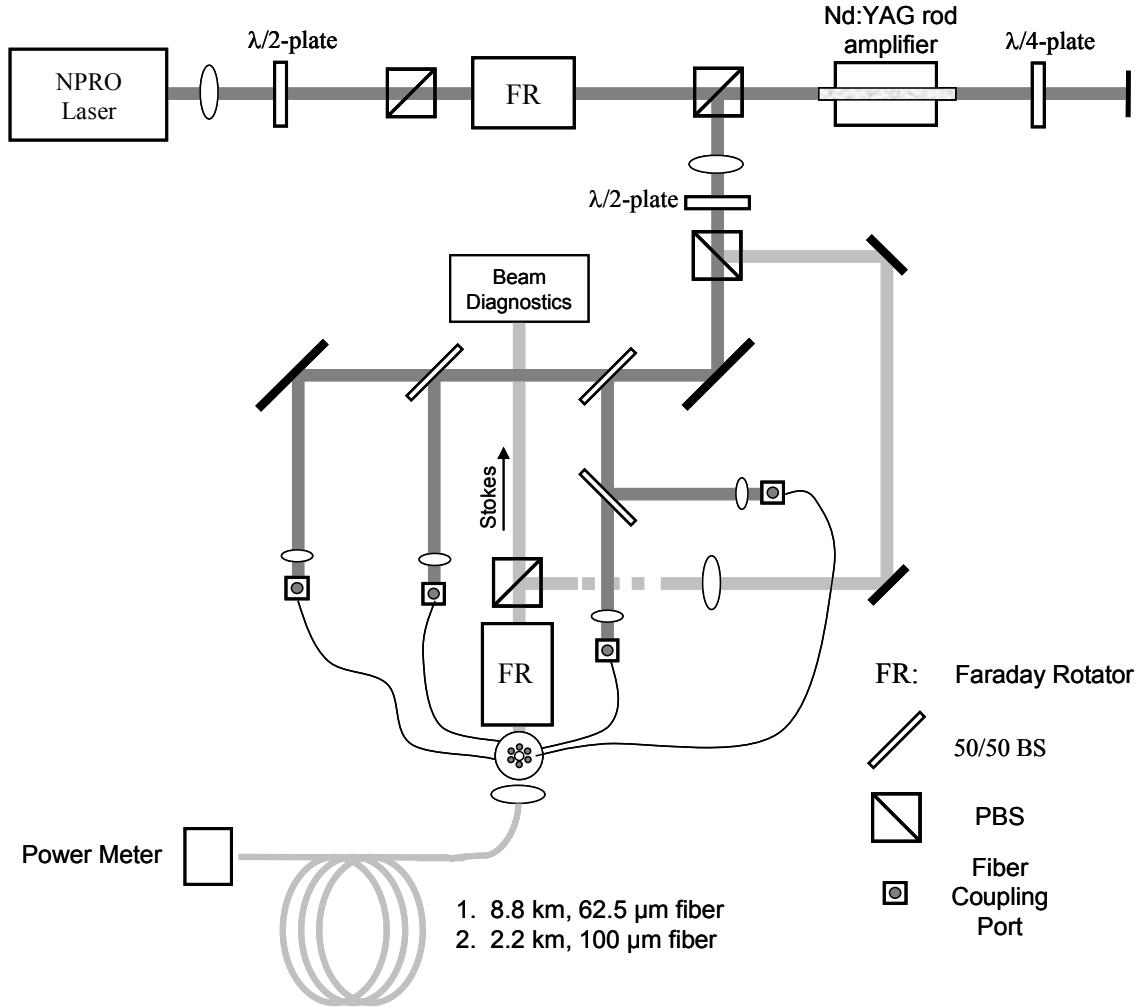


Figure 15: Schematic diagram for the four beam SBS combining experiment with a center-pumped beam to initiate the Stokes wave.

The additional lens in the path of the center seed was included to create a two-lens system for focusing the seed. This was necessary to allow the seed focal point to overlap with that of the 4-beam combiner. Because the fiber pigtail beams mounted in the beam combiner are 3 mm off-axis, the spherical aberration is significant enough to offset the focal point by  $\sim 2$  mm from that of a center pumped channel. This effect was tested and demonstrated by observing the transmitted power (well below SBS threshold) of a laser beam focused through the center of the 15 mm SBS lens and at two off-axis positions as

shown in Figure 16. For each of the on/off-axis positions, the fiber was translated and aligned to the various z positions. The figure shows the best focus spot for a beam 3 mm off-axis is  $\sim 2$  mm closer than that of a beam going through the center of the lens. By using a two-lens system, it is possible to shift the focal position of the seed beam to better overlap with the 4-beam SBS combiner.

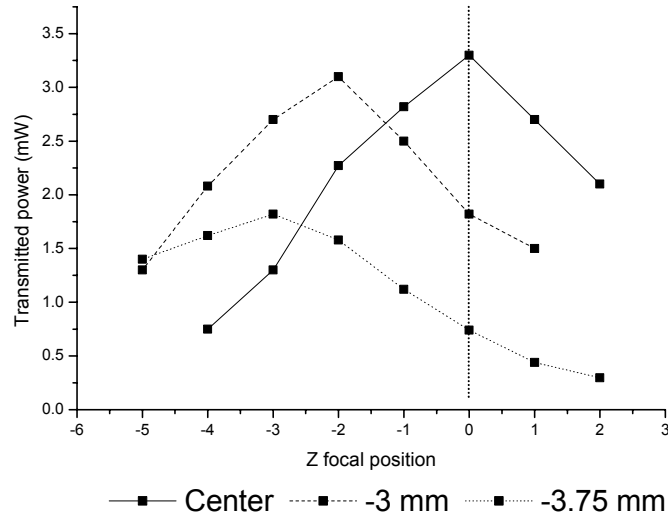


Figure 16: Effect of spherical aberration for off-axis focusing

Using the set-up in Figure 15, the center seed was used to initiate the Stokes beam and the Stokes power conversion from the 4 fiber pigtail beams was observed. Figure 17 first shows the input to the fiber focusing lens with (a) the center seed alone and (b) the center seed with the four off-axis beams from the Gatlin gun beam combiner. The generated Stokes beams for both configurations are given in (c) and (d). In this configuration, a portion of the power from the SBS beam combiner was successfully transferred to energy in the Stokes beam. The measured power conversion is given in Table 5.

Table 5: Power conversion for the four beam SBS combiner with center seed.

	Center channel	4 beams from Gatlin gun	Both	4 beam efficiency
Power Input	490 mW	470 mW	960 mW	
SBS Power	200 mW	0 mW	275 mW	16%
Power Transmitted	28 mW	68.5 mW	89.1 mW	

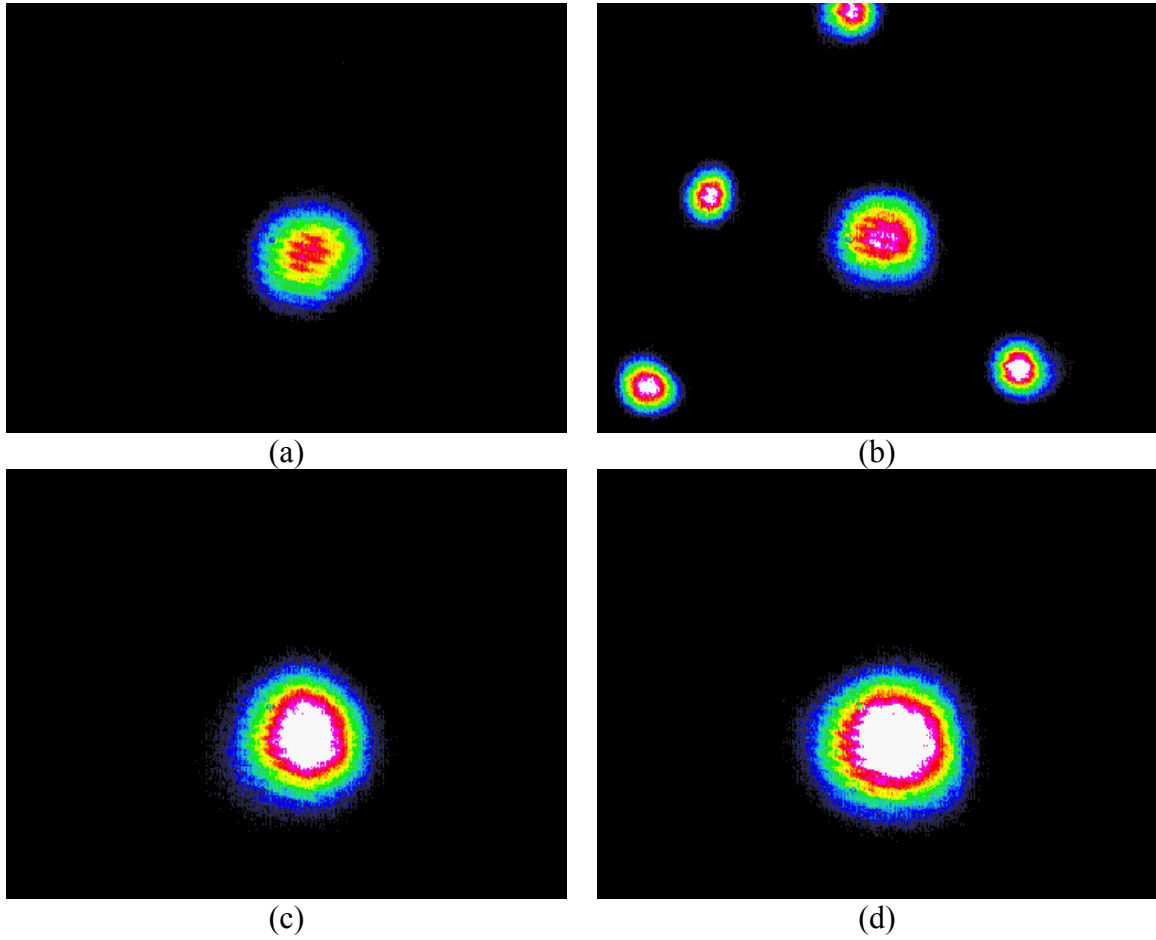


Figure 17: Laser intensity profiles for the four-beam SBS combiner with center seed. The input to the SBS lens is shown for the (a) center seed alone and (b) the center seed with four-beam input as well as the Stokes wave generated (c) without and (d) with the four-beam input.

### 3.3.3. Discussion

The work presented in the previous section is the first successful conversion of pump to Stokes power using four-channel SBS beam combination. As shown in Figure 17d, the output is single-mode as expected due to the beam cleanup properties of the long gradient index fiber. It is, however, desirable to improve upon the efficiency of the Stokes generation for the four-channel beam combination and eventually generate the Stokes beam without a center seed channel. This section explores some of the issues in pursuing this goal.

The primary limitation in accurately building the SBS beam combiner from the design parameters is the ability to make the beams parallel with one another. As discussed in Section 3.2, to focus all of the beams into the fiber, it is necessary to keep them mutually parallel with only a 1-3 mrad tolerance. This proved to be difficult. The pigtail fibers are collimated using a gradient index lens that is pre-mounted when purchased. Unfortunately, the alignment of the GRIN lenses was poor which was evident by a strong steering of the output beam. From a purchase of 10 fiber pigtail collimators, only half of the units were usable for manufacturing the SBS beam combiner. Great care was taken to optically align the collimators while gluing them in the beam combiner. However, some shift occurred during the curing process.

Figure 18 shows (a) the collimated output of the SBS beam combiner and (b) the best focal overlap using an  $f = 20$  cm lens. The relatively long focal length lens (compared to  $f = 15$  mm used for focusing into the fiber) was used to capture the intensity profiles using a CCD camera. Although the misalignment appears severe using the 20 cm lens, 60% and 84% coupling efficiency was achieved in the 62.5  $\mu\text{m}$  and 100  $\mu\text{m}$  fibers,



respectively. It is desirable, however, to completely overlap the beams in the focal plane. Future investigations may explore new techniques to improve the pigtail collimator alignment when assembling the SBS beam combiner. For example, it may be necessary to investigate alignment techniques and also to use a shrink-free epoxy

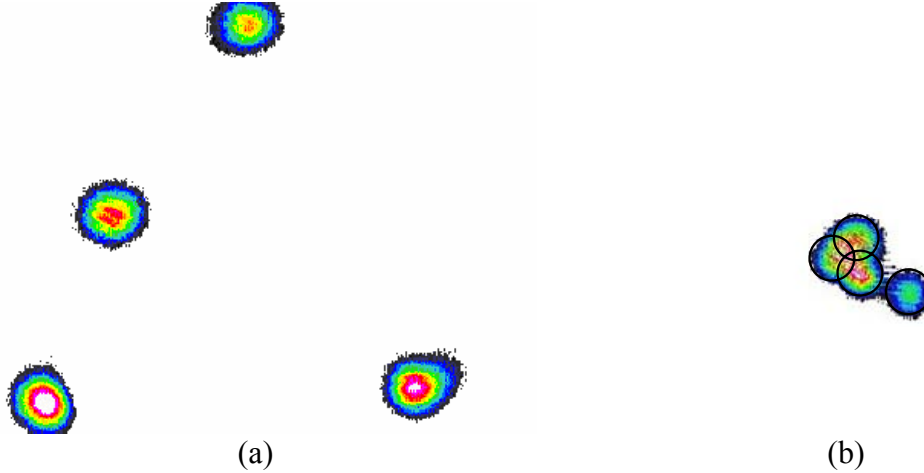


Figure 18: Spatial intensity profiles showing (a) collimated output from the SBS beam combiner and (b) the best focal four beam overlap using a 20 cm lens. Dark circular rings are included in (b) to help distinguish the different beams.

Another limiting factor for the experiment was the amount of power available for the 1064 nm, single-frequency source. For this experiment, the four-channel SBS beam combination was tested with a maximum of  $\sim 2$  W. Future experiments may use a fiber amplifier such as described in Section 4.1 to increase the available power and further this beam combining investigation.

Although having more power will be of great benefit, there still may be some limitation in the efficiency of the Gatlin gun SBS combiner scheme. The SBS efficiency is proportional to the overlap of the coupled pump beam with the center of the optical fiber.<sup>54</sup> When focusing light directly into the center of a fiber, more of the light is

coupled into the fundamental mode ( $LP_{01}$ ). Since long fibers produce a Stokes beam corresponding to this fiber mode, the greater the pump overlap with the Stokes wave, the greater the SBS efficiency. It thus becomes necessary to consider the ability to couple light into the fundamental fiber mode using the SBS beam combiner geometry.

A variety of papers explore the efficiency of exciting lower order fiber modes for various launch conditions.<sup>56,57,58</sup> The primary issue in using the SBS beam combiner is the effect of pumping the fiber with a tilted beam. The chief ray of the fiber collimator beam 3 mm off-axis enters the fiber at an angle of 0.2 rad or 11.4°. The paper by Imai and Hara<sup>56</sup> models, specifically, the excitation of lower-order fiber modes with a tilted Gaussian beam. According to their model, the efficiency for directly exciting the fundamental mode of the fiber with a Gaussian beam tilted at 0.2 rad is < 1%. While this is a theoretical value not accounting for all the conditions for a long multimode fiber, it may present a scaling limitation using the Gatlin gun beam combiner design. Future investigations with higher powers will clarify the effect of pumping the fiber with tilted Gaussian beams and determine its effects for SBS multiple channel beam combination.

### **3.4. Conclusion**

This chapter investigated methods for power scaling SBS beam combining. Scaling SBS beam cleanup to larger core diameter fibers was presented. Although beam cleanup in long multimode gradient index fibers have been explored in detail, the previous work was limited to fibers with core diameters 50  $\mu\text{m}$  and less.<sup>22,23</sup> Power scaling SBS beam combination requires the use of larger fibers. This work successfully demonstrated beam cleanup for both 62.5  $\mu\text{m}$  and 100  $\mu\text{m}$  core diameter fibers. For multiple beam

combining, a technique for efficiently coupling the SBS beam was designed and tested.

The SBS beam combiner provided the first successful demonstration of pump to Stokes power conversion from four-channel SBS beam combination.

## 4 SBS Beam Phasing

One of the key areas of investigation for this research is that of phasing multiple laser beams. As mentioned in the introduction, independently amplifying a master oscillator in separate channels and phasing the channels together is one major research effort in laser power scaling. This chapter first provides the development of single-frequency fiber amplifiers necessary for the investigations and is followed by a series of experiments demonstrating and utilizing beam phasing using a long multimode fiber. The final section of this chapter explores the use of a short ( $< 10$  m) gain fiber as the SBS medium.

### ***4.1. Single-Frequency Fiber Amplifier***

One of the essential elements addressed in this research effort was developing a higher power single-frequency laser source. The power available from the two-pass Nd:YAG rod amplifier discussed in chapter 3 was not sufficient for the remaining SBS investigations. This section presents the development of a single-frequency fiber amplifier used in the subsequent experiments. The work presented increased the available single-frequency radiation by almost an order of magnitude and allowed further investigations in multiple channel beam combining and phasing.

#### **4.1.1. Background**

Developing high power single-frequency laser radiation is of great interest in the optics community. There are a wide variety of laser applications requiring a low-noise, diffraction limited, single-frequency laser source. Some of the applications for these laser systems include gravitational wave detection at the Laser Interferometer and

Gravitational Wave Observatory (LIGO),<sup>59</sup> generation of an adaptive optics sodium guidestar beacon,<sup>60</sup> and coherent laser beam combination.<sup>61</sup> For this research effort, the relatively narrow gain bandwidth of SBS ( $< 100$  MHz) requires a single-frequency source.

A few different approaches have been used to develop high power single-frequency laser radiation. Most of the techniques are based in some way on a seed from a monolithic, nonplanar ring cavity (NPRO) as described previously.<sup>55</sup> Although the NPRO provides excellent beam quality and frequency stability, the maximum reported power is  $\sim 2$  W.<sup>62</sup>

One approach for higher power is to amplify the NPRO output using an external Nd:YAG rod amplifier in a single-pass or two-pass geometry. One amplifier system was developed by Lightwave Electronics for use in the LIGO system.<sup>63</sup> In their configuration, four Nd:YAG rods, each pumped by two 20 W diode bars, were used for two-pass amplification. The system, which was seeded with 500 mW from an NPRO, produced 20 W of output when pumped with a total of 144 W of diode power. The 20 W output from the two-pass amplifier was later amplified to 100 W using a combination of Nd:YAG slabs and a total pump power of 500 W.<sup>64</sup> Overall, the low optical efficiency in the amplifiers is one of the drawbacks in using this system for a high power single-frequency source.

Another method for generating high power, single-frequency radiation is injection-locking a slave laser to an NPRO master oscillator. A wide variety of papers demonstrating this technique are available and power levels greater than 100 W of single-frequency, 1064 nm output have been demonstrated.<sup>65,66,67</sup> The difficulty with injection-

locking systems is that they require complex electrical control. Such a system makes it difficult to maintain long-term, reliable performance.

In this work, a master oscillator fiber power amplifier was used to obtain the required high power, single-frequency source. The experiment used a double-clad, large mode area (LMA) fiber, which has become a standard for high power fiber oscillators and amplifiers.

LMA fibers typically have a core diameter between 20 and 30  $\mu\text{m}$ . For standard fibers of this size, the core allows multiple spatial modes to propagate through the fiber. In this case, however, the numerical aperture of the fiber is small. Recall from section 2.2.2 that the V-number is used as a reference for the number of modes that can propagate in the optical fiber. From Equation 2-30,  $V = ak_0 NA$ . Keeping the NA small results in a lower V-number, and thus, a lower number of propagating modes.

While typical LMA fibers allow a few modes to propagate through the fiber, Koplow *et al.* demonstrated that bend loss induced by coiling LMA fibers was sufficient to suppress the higher order modes to produce a single transverse mode output.<sup>68</sup> Figure 19 illustrates mode filtering for both 20  $\mu\text{m}$  and 30  $\mu\text{m}$  core diameter, 0.06 NA fibers.<sup>69</sup> As the figure shows, the larger core diameter fiber requires a tighter bend to suppress the  $LP_{11}$  mode. For example, with a bend radius of 5 cm, the modal loss for the  $LP_{11}$  mode is  $\sim 10$  dB/m and  $> 100$  dB/m for the 30  $\mu\text{m}$  fiber and 20  $\mu\text{m}$  fibers, respectively.

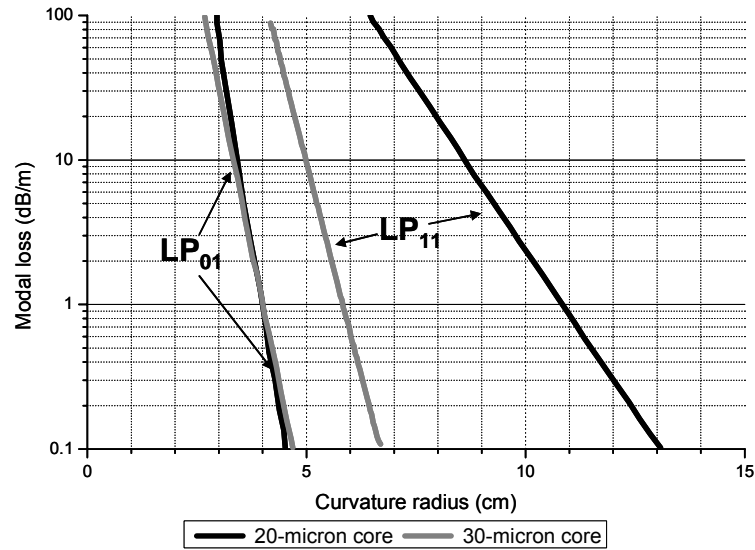


Figure 19: Mode filtering in 20  $\mu\text{m}$  and 30  $\mu\text{m}$ , 0.06 NA fiber cores.

As mentioned above, LMA fibers typically use a double cladding. In this configuration, the inner cladding is coated with a low-index polymer so that it is also guides light through the fiber. The inner cladding is designed with a much larger core diameter ( $\sim 200\text{--}400\ \mu\text{m}$ ) and high numerical aperture ( $\sim 0.46$ ) to accommodate pumping from fiber-coupled diode lasers. This inner cladding is often given a non-round shape to prevent helical mode propagation, which prevents absorption of the pump light into the fiber core.

Figure 20 shows a basic geometry for implementing a ytterbium-doped LMA fiber amplifier. While fiber amplifiers are often pumped from only one side of the fiber, a more comprehensive case of launching a diode pump from both ends of the fiber is shown in the figure.

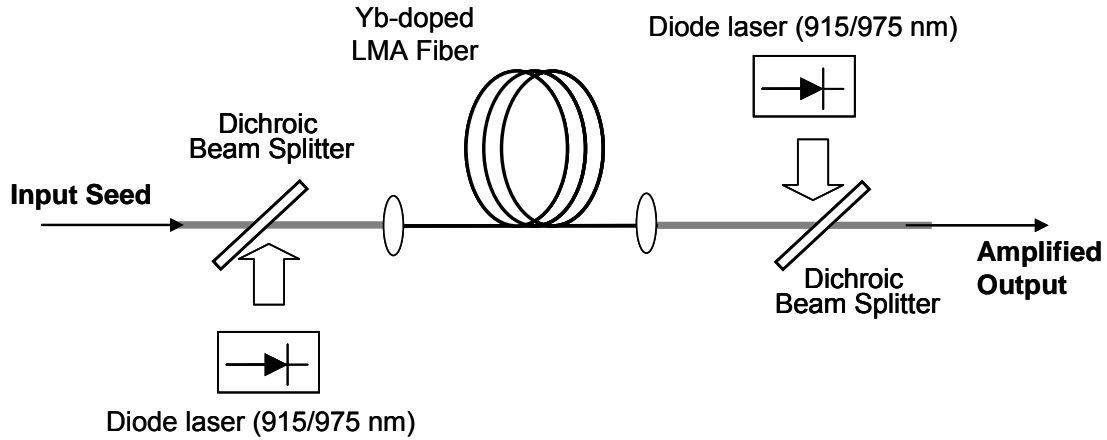


Figure 20: Large mode area Yb-doped fiber amplifier

The dual wavelength notation indicates two typical wavelengths used for pumping Yb-doped fiber, 915 nm and 975 nm. The absorption and emission spectrum for Yb is shown in Figure 21.<sup>70</sup>

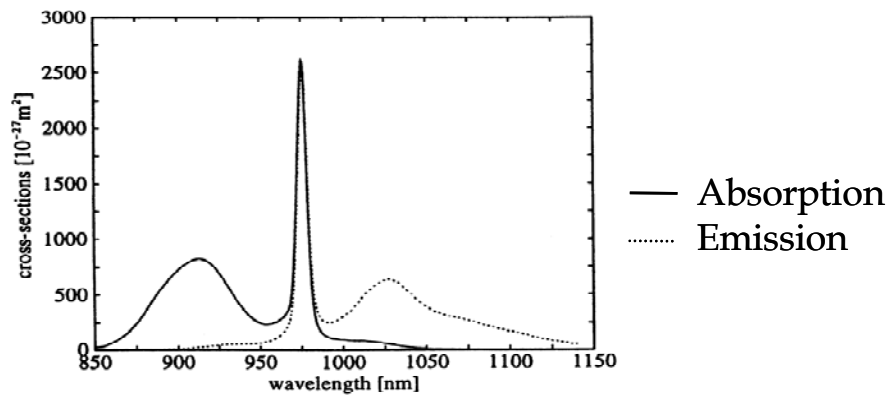


Figure 21: Absorption and emission spectrum for Yb-doped fiber

Although the absorption centered near 915 nm is weaker than the peak at 975 nm, it is also much broader spectrally. The broad spectrum reduces the constraints on wavelength



control, which can lead to simpler implementation. For the strong absorption peak at 975 nm, the narrow spectrum requires precise diode wavelength monitoring through active temperature control. Thus, pumping with a 975 nm diode is more complex, but may be preferred for the stronger absorption.

Large mode area gain fiber has been very successful in amplifying single-frequency lasers. Höfer *et al.* used a 9 m Yb-doped LMA fiber amplifier to generate 20.1 W of single-frequency, single-transverse mode operation.<sup>71</sup> In their work, 500 mW of 1064 nm NPRO light seeded the amplifier which was pumped with up to 60W at 915 nm. The reported slope efficiency for the experiment was 38%. A later investigation from the same group used 9.4 m of Yb-doped LMA fiber with an 800 mW NPRO seed and 180 W of diode pump power at 976 nm to yield over 100 W of single-frequency radiation.<sup>72</sup> Most recently, 264 W of single-frequency output was achieved with an LMA fiber pumped by 390 W at 975 nm.<sup>73</sup>

#### **4.1.2. Fiber Amplifier Implementation**

Figure 13 shows the experimental schematic for the master oscillator fiber power amplifier implemented in this work. The primary components are the master oscillator, LMA double clad fiber, and a fiber-coupled diode laser. The master oscillator is a 1064 nm single-frequency NPRO that is pre-amplified as described in Section 3.2.

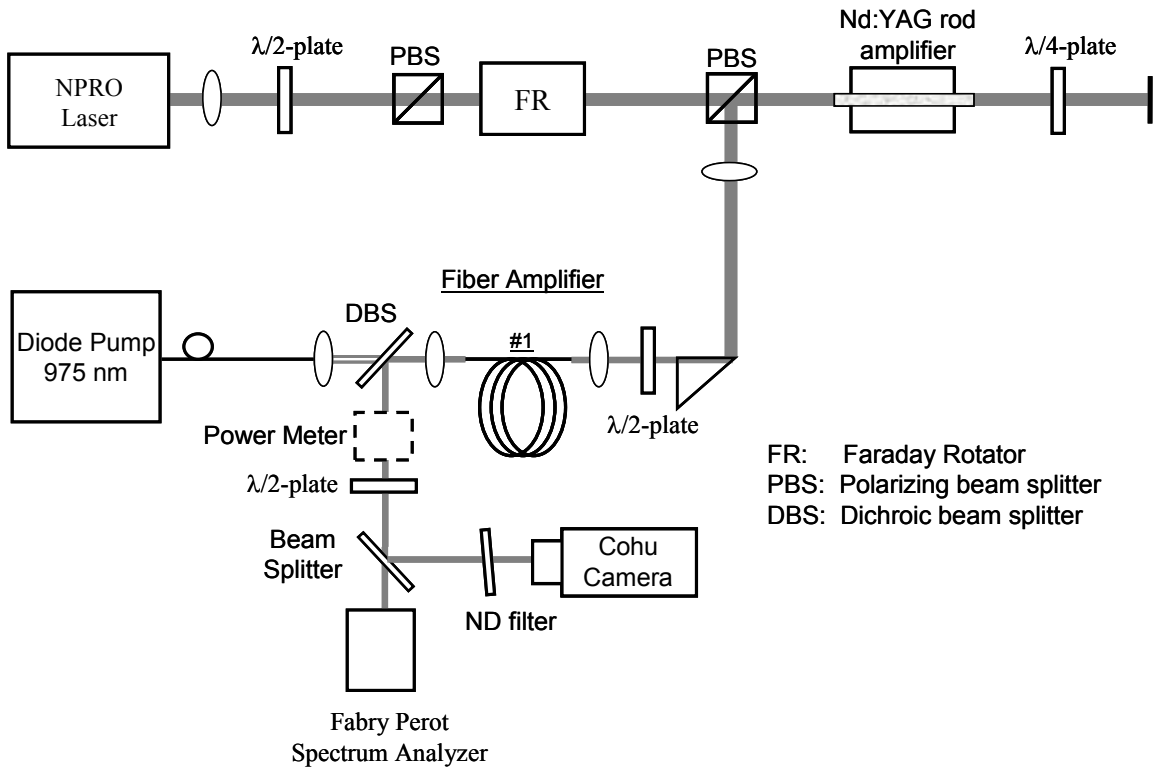



Figure 22: Schematic diagram for master oscillator fiber power amplifier

The Yb-doped LMA fiber used for this experiment is available commercially from Nufern (LMA-YDF-20/400). Table 6 displays the specifications for the fiber.

Table 6: Nufern large mode area double clad Yb-doped fiber specifications

Core Diameter	20 $\mu\text{m}$
Inner Clad Diameter	400 $\mu\text{m}$
Coating Diameter	550 $\mu\text{m}$
Absorption 915nm/975 nm	0.6 dB/m / 2.0 dB/m
Core NA	0.06
Cladding NA	0.46
Octagonal shape	

As described above, the 20  $\mu\text{m}$ /0.06 NA fiber core can maintain a single mode output by inducing bend loss to the higher order modes. The model shown in Figure 19 indicates

that a 5 cm bend radius should induce sufficient bend loss to the  $LP_{11}$  mode. Using this model, a 10 cm diameter Al spool was manufactured and 10 m of the fiber was precisely wrapped onto the spool. In addition to providing the necessary bend loss, the Al spool also serves as a heat sink. Thus, the fiber is spooled in only a single layer with sufficient separation between each wrap. Ten meters of fiber is sufficient length to absorb 99% of the 975 nm diode pump that is coupled into the inner cladding and is absorbed at 2.0 dB/m.

One end of the fiber is angle cleaved to prevent self-oscillation in the amplifier. If both ends of the fiber are perfectly flat, the Fresnel reflection from the fiber ends may provide sufficient feedback to lase. The angle cleave was around  $8^\circ$ , although small angles ( $\sim 4^\circ$ ) were sufficient to suppress oscillation with the available pump power.

Figure 23 shows sample side profile views for a relatively flat and an angle cleave of the 400  $\mu\text{m}$  octagonal shaped fiber .

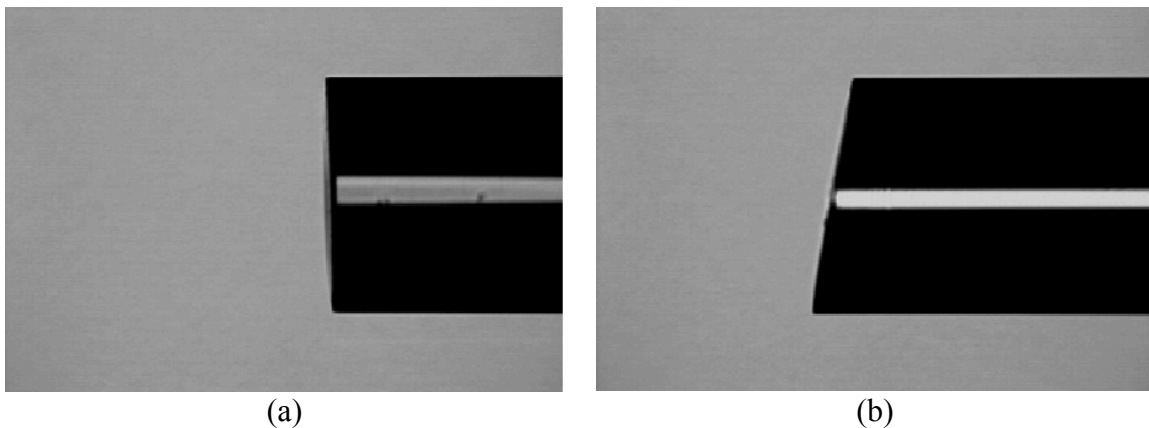


Figure 23: Profile view of a (a) flat and (b)  $\sim 8^\circ$  angle cleave of the 400  $\mu\text{m}$  octagonal-shaped fiber

As pump power increases, it may be necessary to angle cleave both the input and output to prevent oscillation. In this experiment, however, the seed input end was kept flat to facilitate seed laser coupling.

The seed light is coupled into the LMA fiber core using a 10X ( $f=15.4$  mm) aspheric fiber coupling lens (New Focus 5726-H-B). The small core diameter and low NA of the LMA fiber makes the input coupling difficult and the maximum coupling efficiency achieved into the core was  $\sim 60\%$ . The total input power was typically  $\sim 500$  mW and the  $\sim 300$  mW coupled into the core was sufficient for the amplifier. The light missing the core is guided via the inner cladding and passed out the back end.

The Yb-doped fiber amplifier is pumped from the back end using a 975 nm fiber-coupled diode laser. Two 25 W diode lasers were used in this experiment and Figure 24 shows the power output vs. current for the two devices.

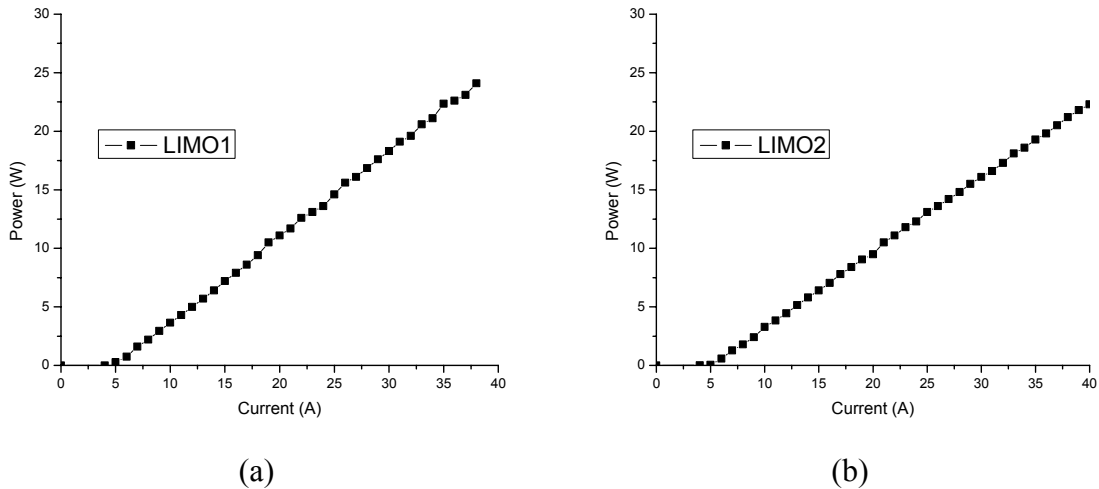


Figure 24: Current vs. output power for (a) LIMO #1 (S/N 1554) and (b) LIMO #2 (S/N 1555) diode lasers.

The diode lasers are actively cooled to ensure spectral overlap with the narrow Yb-absorption spectrum at 975 nm. The diode lasers are nominally 976 nm with a FWHM bandwidth of  $\sim 4$  nm and are wavelength tunable at  $\sim 0.4$  nm/deg C. Figure 25 shows a sample spectrum as well as the effect of temperature tuning the diode wavelength.

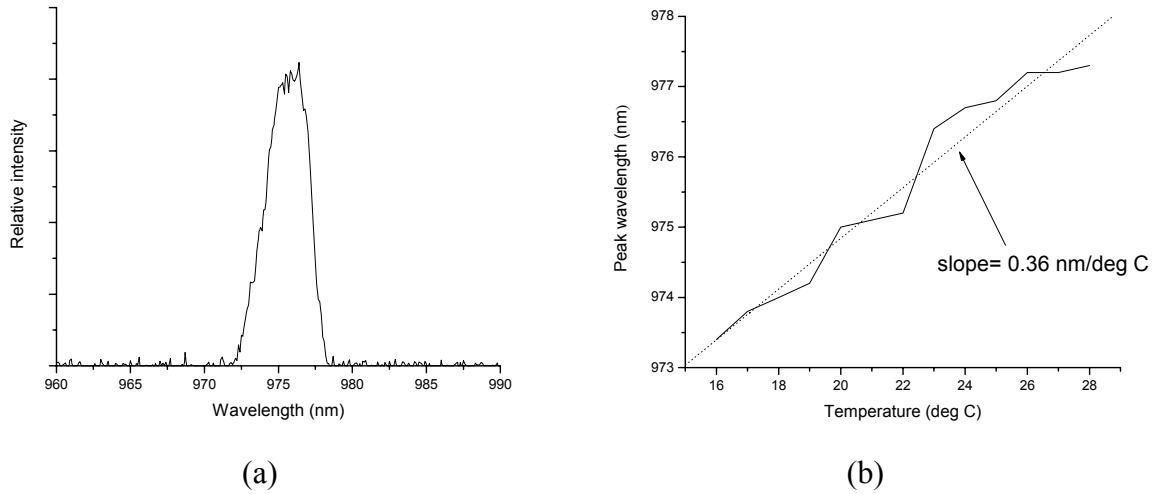


Figure 25: (a) Sample spectrum and (b) temperature wavelength tuning of the LIMO fiber coupled diode laser.

As shown in Figure 22, the output from the 200  $\mu\text{m}/0.2$  NA diode laser fiber is collimated, transmitted through a dichroic beam splitter, and coupled into the inner cladding (400  $\mu\text{m}/0.46$  NA) of the Yb-doped LMA fiber. The higher brightness of the diode laser fiber (relative to the LMA inner cladding) reduces the difficulty in coupling the diode light. Because the collimated output of the diode laser still diverges rather quickly, the distance between the two fibers is kept as short as possible to ensure all of the light passes through the clear aperture of the LMA fiber objective lens.

Figure 26 shows the input-output characteristics of the fiber amplifier when seeded with  $\sim 500$  mW. The inset in the figure is a scan from the Fabry-Perot analyzer verifying single-frequency operation at the maximum output power.

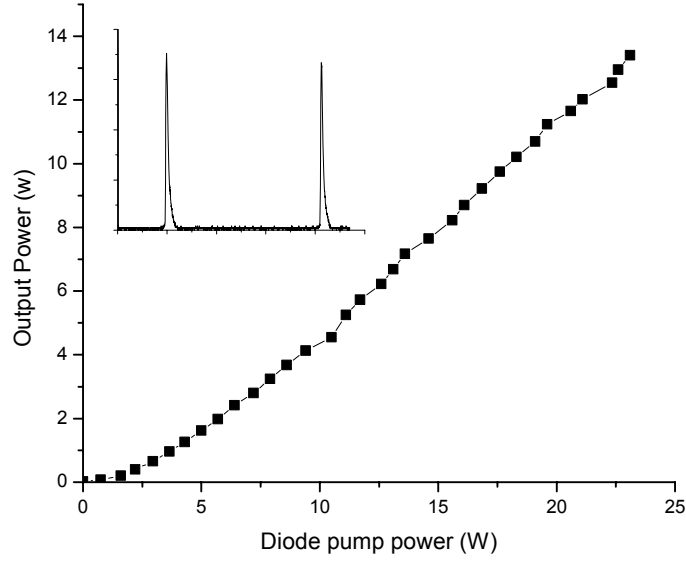


Figure 26: Input-output characteristics for the Yb-doped LMA fiber seeded with 500 mW. The amplifier achieved 13.4 W of power with a slope efficiency of 67%. The inset Fabry-Perot spectrum analyzer scan verifies the single-frequency output of the amplifier.

The coiling of the LMA fiber on the 10 cm diameter aluminum spool was sufficient to ensure single mode operations as shown in Figure 27a . As a comparison, Figure 27b shows the amplifier output with the fiber coiled on a 17 cm diameter spool. In this case, the bending loss for higher order modes is not as high (see Figure 19) and the output resembles more of the  $LP_{11}$  mode.

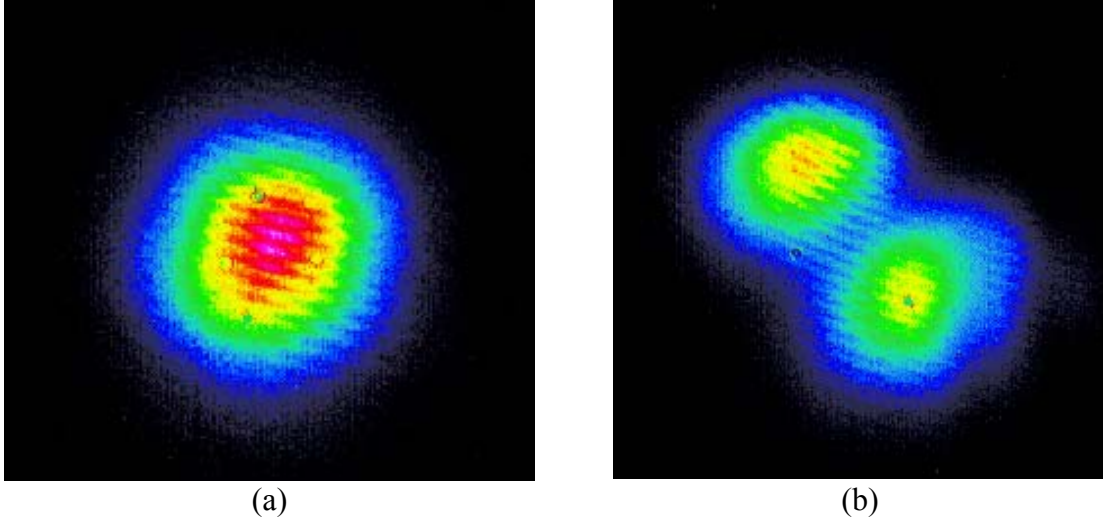


Figure 27: (a) Fiber amplifier output showing the single transverse mode operation for the LMA fiber spoiled on a 10 cm spool. For comparison, (b) shows the fiber amplifier output when the fiber is coiled on a larger, 17 cm spool.

To quantify the beam quality of the fiber amplifier, the output was measured using a Coherent ModeMaster. The ModeMaster uses a scanning lens and a rotating knife edge to determine the  $M^2$  along with the beam propagation characteristics.<sup>74</sup> Table 7 lists the beam parameters determined from the ModeMaster scan taken at full output power (13.4W). The  $M^2$  is less than 1.1 confirming diffraction limited performance.

Table 7: Beam parameters for the 13.4 W fiber amplifier output measured using the Coherent ModeMaster.  $M^2$  is the beam quality parameter,  $\omega_0$  is the spot size,  $Z_r$  is the Rayleigh range, and  $\theta_{div}$  is the beam divergence.

Beam Parameter	X	Y	R
$M^2$	0.97*	1.0	1.0
$2\omega_0$	680 $\mu\text{m}$	585 $\mu\text{m}$	636 $\mu\text{m}$
$Z_r$	0.353 m	0.252 m	0.290 m
$\theta_{div}$	1.93 mrad	2.32 mrad	2.13 mrad

---

\* The  $M^2$  accuracy of the Coherent ModeMaster is  $\pm 5\%$ .

Although the LMA fiber is not polarization maintaining, the stress-induced birefringence induced by coiling on the 10-cm diameter spools was sufficient to produce a polarized output. The polarization axis changes slowly as the fiber reaches thermal equilibrium, but after sufficient warm-up, a polarization ratio greater than 500:1 could be maintained. The half-wave plates on both ends of the fiber amplifiers shown in Figure 22 are used to align the input polarization to that of the fiber as well as to control the output polarization.

#### **4.1.3. Discussion**

The single-frequency amplifier presented in this section was developed to further the investigations of SBS in optical fibers. The work increased the available power by almost an order of magnitude, allowing for new SBS investigations previously not accessible. Additionally, having fiber-based amplifiers is advantageous for exploring multiple channel SBS beam combining and phasing. The double-clad, Yb-doped LMA fiber provides over 13 W of single-frequency radiation with a slope efficiency of 67%. The output beam is diffraction limited and can provide a polarized output.



## ***4.2. SBS Beam Phasing Using Long Multimode Fiber***

This section describes investigations of beam phasing using a long multimode fiber as the SBS medium. The background for SBS beam phasing is provided, followed by experimental results for a variety of configurations. The work presented is the first demonstration of the technique and the significant progress achieved in phasing two-channel power amplifiers justifies consideration for future high power applications.

### **4.2.1. Background**

As mentioned previously, one method for power scaling lasers is to split a master oscillator into multiple channels and amplify each one separately. The total power from all of the amplified channels is then used to propagate to the target. One problem that becomes evident in this approach is that each of the amplifier channels will have different path lengths and will not be in phase. The phase difference between the channels becomes important when focusing the total output beam. In order to achieve the maximum intensity in the far field, it is necessary that the individual beams match in phase, making it desirable to develop a ‘phased’ laser array. Research in phased laser arrays is typically centered on either electro-optically controlling the phase of the laser through a servo interface or beam phasing through nonlinear optical phase conjugation.

A significant effort is taking place for developing an electro-optically controlled optical phased array.<sup>61,75,76</sup> While the specific approach varies among research groups, the basic premise remains the same. In this method, a master oscillator is split into multiple channels and is amplified separately in the individual channels. The signal from

each channel then interferes with a portion of the master oscillator that is split off and frequency shifted via an acousto-optic cell. The interference pattern generates a beat waveform that is used to measure the relative phase of each channel. The phase of each leg is then actively controlled using a phase modulator.<sup>61</sup> This approach has successfully phased multiple elements to generate a phased amplifier array.<sup>61,75,76</sup> The difficulty with this implementation is the complexity associated with the number of optical components and the associated electronics. As the number of amplifier channels increase, the complexity grows. For this reason, it is very attractive to develop an accurate phasing method without the need for complex electronic control.

One passive method for beam phasing employs the nonlinear optics process known as mutual phase conjugation. Figure 28 shows a set-up for a two-channel beam phasing experiment and is used to illustrate the process. In this configuration, a master oscillator is split into two channels. Traveling with its own optical path, each channel is amplified separately and focused into the same SBS medium. The optical path length difference of the channels results in a phase difference (or piston error) for the two beams entering the SBS medium. As the two beams are focused into the SBS medium (in this case, an optical fiber), the multiple beams appear as a single beam that has phase and intensity modulation associated with the piston error. The piston error from the two beams is conjugated and the Stokes beam retraces each channel's respective optical path resulting in a zero phase delay (piston error) between the beams. This process is also referred to as SBS piston error correction or SBS beam phasing.<sup>16,77</sup>

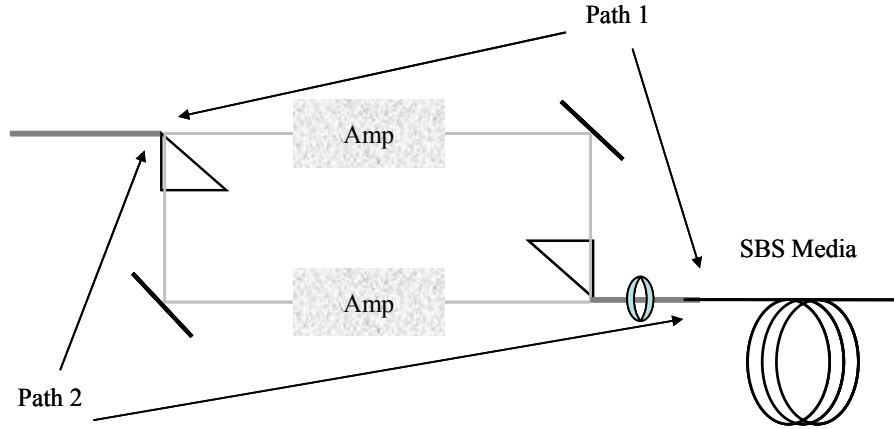


Figure 28: Basic two-channel SBS beam phasing experimental schematic

While the end goal of this type of beam phasing is to amplify each channel, a large group of papers is published using SBS mutual phase conjugation to correct piston errors in unamplified path lengths. Much of the work is well summarized in a review paper by Moyer<sup>77</sup> and a few of the significant results are discussed in detail below.

Basov *et al.*<sup>19</sup> was the first to successfully demonstrate piston correction by separating a laser beam into two channels with a double dove prism and combining them in an SBS cell. Besides demonstrating the concept, the authors also revealed the necessity for focusing the beams into the same portion of the medium. If the lasers are combined in the same portion of the medium, the acoustic field created is common to all beams and proper phase conjugation is possible. On the other hand, if the SBS beams excite a separate acoustic wave, the random nature of SBS generation from thermal noise causes the beams to have a random relative phase. Experimental evidence supports this idea by Basov's demonstration of coherent combination for overlapped beams and incoherent combination when the beams are not overlapped.<sup>19</sup>

The same group reports another discovery related to efficient beam phasing in a later paper.<sup>78</sup> After phase conjugation, the residual piston error ( $\delta$  in waves) resulting from the small frequency difference between the pump and Stokes beams is given by the relation

$$\delta = \Delta_B \Delta_L, \quad (4-1)$$

where  $\Delta_B$  is the SBS shift in wave number and  $\Delta_L$  is the optical path length difference.

The limitation imposed by this equation is that for the desired piston correction accuracy, it is necessary to accurately control the measurable optical path length difference (OPD) between the channels.<sup>16,78</sup> As an example related to this research, a laser wavelength of 1064 nm has an estimated SBS shift of ~16 GHz ( $\Delta_B = 53.3 \text{ m}^{-1}$ , see section 2.2.1) and requiring a maximum piston correction error of 0.1 waves leads to a maximum path length difference of 1.9 mm. Fortunately, the relative piston error cycles with respect to the OPD through multiple waves allowing for a repetition of good phasing positions (i.e.,  $\delta \approx 0, 1, 2$ , etc.). Previous work has demonstrated this cyclic nature with OPD in systems without amplifiers<sup>78</sup> and this research effort investigated the issue for the first time using active amplification as described in the sections below. A final requirement to achieve good beam phasing with this approach is that the total path length difference needs to be a small fraction of the laser coherence length.<sup>16,78</sup>

Moyer *et al.*<sup>16</sup> investigated SBS piston error correction for the specific purpose of coherently combining multiple laser beams. Figure 29 shows the experimental schematic used in their work.

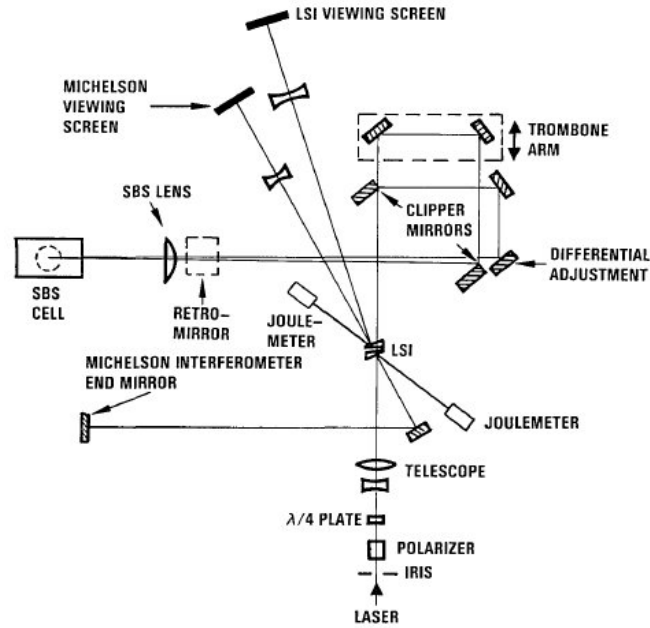


Figure 29: Experimental schematic used by Moyer *et. al.*<sup>16</sup> to investigate SBS piston error correction.

In their experiment, a pulsed single-frequency laser operating at 355 nm was split into two channels using clipper mirrors. The two beams traveled their own passive optical path and were focused into a single SBS cell. A trombone arm was used in one of the channels to control the residual piston error as described above. In their experiment, a lateral shearing interferometer (LSI, see Figure 30) was used to investigate the beam phasing properties and verified successful piston error correction. This same diagnostic was used for this dissertation effort and the details of its operation are described below.

The lateral shearing interferometer (LSI) shown in Figure 30 consists of a pair of uncoated wedges aligned so that the inner surfaces are nearly parallel to each other. The parallel beams entering the system are partially reflected from both of these surfaces. The result is that one of the reflections is laterally displaced from the other so that three different zones of interference are created. The two outer regions are self-interference

from each of the two channels with its laterally displaced self. The center region is mutual interference between the channels. Beam phasing is demonstrated when the fringes are continuous across all three zones.

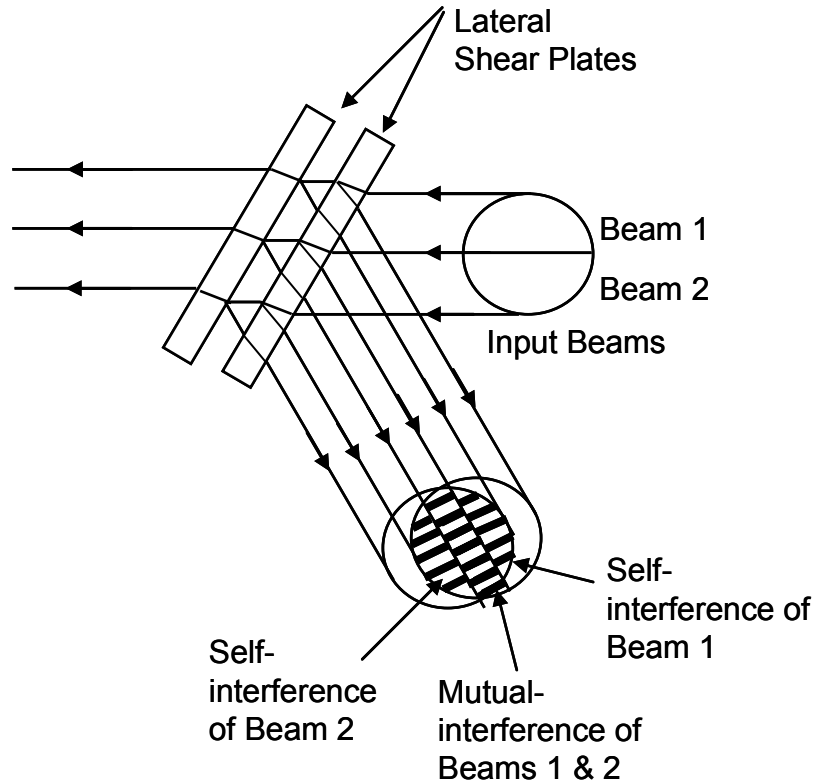


Figure 30: Lateral Shearing Interferometer (LSI). The reflections from the two inner surfaces of the LSI create regions of self interference of the individual laser beams and mutual interference between the two beams. Continuity across the three regions indicates successful piston error correction.

Additional published investigations on SBS beam phasing include effects of back-seeding,<sup>16,79</sup> beam parameter characterization (bandwidth, power ratio, polarization mismatch),<sup>80</sup> and theoretical studies on beam phasing efficiency.<sup>81,82</sup> Some additional experiments furthered this concept for power scaling by demonstrating pulsed laser beam phasing for two channels, each containing a Nd:YAG rod amplifier.<sup>17,18</sup> Perhaps one of the greatest limitations for the early work was the requirement for precise alignment in

the SBS cell.<sup>79,81,83</sup> It is for this reason that a more recent investigation used a multi-mode fiber as the SBS medium to phase a pulsed laser beam traveling in a passive two-channel system.<sup>84</sup> Having the waveguide geometry negates the stringent overlap requirement and leads to simpler implementation. This is the method used in this investigation.

Another limitation to the early experiments in SBS beam phasing is the requirement of using a pulsed laser system. In all previous work, pulsed laser systems were used in order to reach the high peak powers necessary to reach SBS threshold. While a pulsed implementation is satisfactory for some work, for many applications it is desirable to use a cw laser beam. This provided the motivation to investigate cw SBS beam phasing.

One of the advantages of using an optical fiber for the SBS medium is that longer lengths can be used to reduce the SBS threshold. As evident from Equation 2-31 (pg. 19), increasing the length of the fiber decreases the SBS threshold. For long lengths of fiber, the SBS threshold for single-frequency laser sources reduces to levels obtainable with a cw laser source. For example, the work in Section 3.2 reports SBS thresholds of 200-300 mW.

While using a longer fiber reduces the SBS threshold to levels accessible to cw laser sources, the Stokes beam no longer produces a complete phase conjugate of the pump beams. As discussed in Section 2.3.2, to obtain full spatial phase conjugation, a short multi-mode fiber (typically <10m) should be used as the SBS medium. As the fiber length increases, the non-phase conjugate portion of the beam resulting from the difference between the pump and Stokes frequencies increases.<sup>37</sup> Nevertheless, this research effort used a long gradient index fiber (4 km) to lower the SBS threshold to a level attainable with a laboratory cw laser system. In this type of fiber, the Stokes

intensity profile corresponds to the  $LP_{01}$  fiber mode irrespective of the pump profile through the beam cleanup process discussed in Chapter 3.<sup>22</sup> Although it would clearly be better to have full transverse spatial phase conjugation in addition to piston phase correction, this investigation's primary goal is beam phasing and the experiments of this section investigate the phasing properties when using a long multimode fiber for the SBS medium.

This research demonstrates that phase conjugation necessary for beam phasing is achieved even though the long fiber does not produce a full spatial phase conjugate. The critical requirement for phasing multiple channel beams is the generation of a common SBS beam pumped jointly by beams from each channel. To accomplish this, the beams work together to set up a common acoustic phonon field that is unique to the coherent sum of the pump waves and feeds the growth of the Stokes beam. Thus, the SBS beam produced has a phase that is related to that of the combined pump beams and is a phase conjugate of the piston phase difference between the pump beams.

#### **4.2.2. Beam Phasing Two Passive Channels**

An initial experiment was designed to test the feasibility of using a long multimode fiber for SBS beam phasing. The experiment was similar to previous work by Moyer<sup>16</sup> and Willis<sup>84</sup> in that it separated a beam into two passive optical paths and focused the beams into a single SBS medium. However, this experiment used a single-frequency cw laser as the pump for the SBS process and a long multimode fiber for the SBS medium. Figure 31 shows the system diagram used for the test.





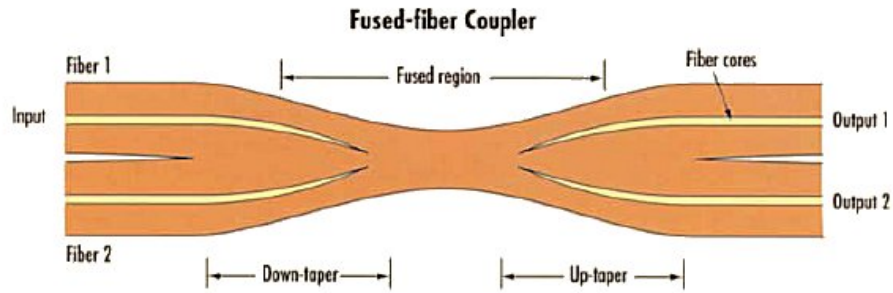


Figure 32: Fused fiber coupler

The light from the two input channels is split into the two output channels and the power splitting ratio can be controlled by the geometry of the device when the fibers are fused. The couplers purchased for this experiment were produced using Corning 50/125 multimode fiber (50  $\mu\text{m}$  core diameter, 0.20 NA) and were specified with a nominal 50% splitting. The standard device produced with this technology is a 2:2 coupler as shown in Figure 32. A 2:1 fiber coupler is achieved by simply terminating one of the fiber output ends and accepting the associated power loss.

The output from the 2:1 fiber coupler was fused to  $\sim 4$  km of matching 50  $\mu\text{m}$  core diameter fiber, which served as the SBS medium. The Stokes wave generated in the fiber travels back through the system where the rotated polarization (now vertical) is reflected from the TFP to the diagnostics.

The Stokes beams from the two channels travel side by side to the LSI and a portion of the beams are reflected from each surface as described above. The light is expanded using a negative lens and the interference pattern formed on the viewing screen is captured by imaging the surface of a viewing screen to a CCD camera.

Examples of observed LSI fringes for this experiment are shown in Figure 33. Here, (a) shows the two reflections from the LSI surfaces before the beams are brought together to form the interference fringes. In Figure 33b, the beams are brought together such that portions of the left and right beams interfere with their laterally displaced selves (self-interference regions). Portions of the left and right beams also interfere with each other to create a region of mutual interference as described above. The continuity of the fringes across all three fringe zones indicates that the two beams are in phase.

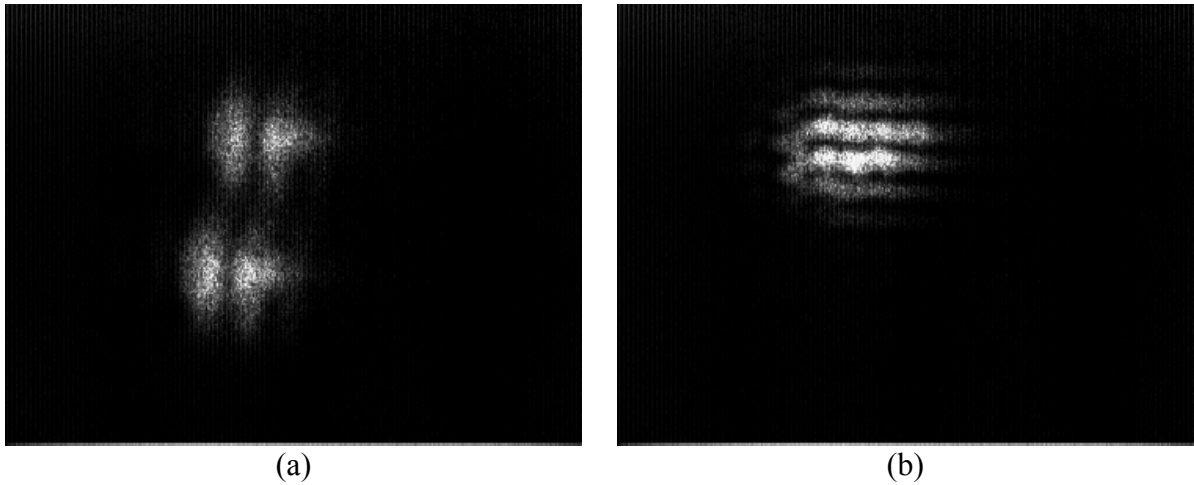


Figure 33: Data from the lateral shearing interferometer (a) before the two reflections from the LSI are brought together and (b) after the reflections are overlapped to form interference fringes.

For comparison, a flat mirror was placed in front of both input ports of the 2:1 fiber coupler as shown in Figure 31. Previous experiments placed a single flat mirror directly in front of the SBS medium,<sup>16,84</sup> but the fusion spliced geometry of this experiment prevented this implementation. Figure 34a shows the fringes formed by the reflection from the flat mirrors. In this case, the piston error between the two beams is not properly compensated and the two beams are not in phase as is evident from the lack of continuity

across the fringe zones. The right frame is another phased example of the fringes formed by the SBS beam with continuity across all three fringe zones.

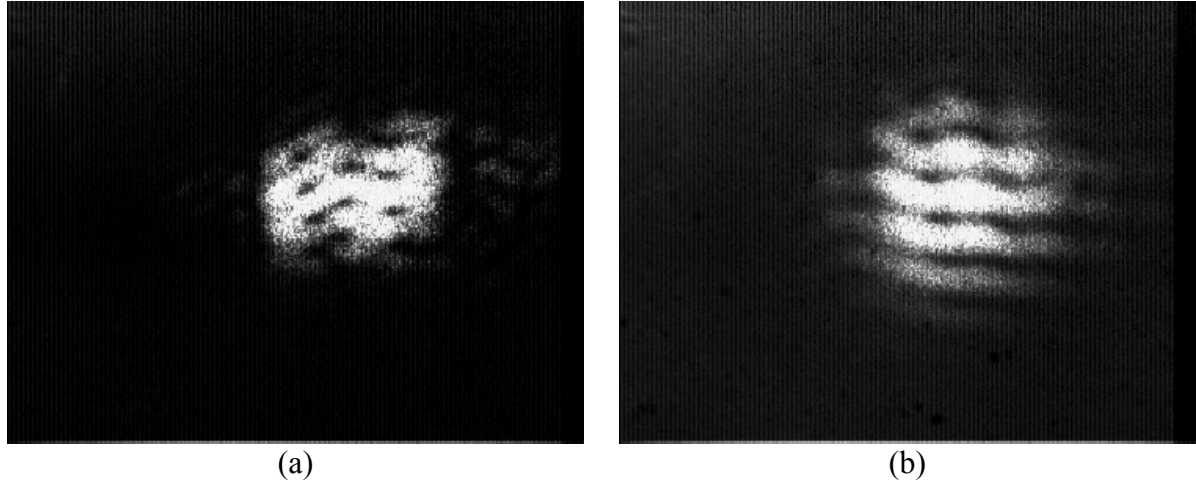


Figure 34: LSI data showing (a) lack of continuity across the fringe zones (unphased) using a flat mirror and (b) continuity across the fringes (phasing) using the SBS multi-mode fiber.

The input-output performance of this passive phasing test is given in Figure 35. The backreflected Stokes and transmitted pump beams are plotted vs. total input power prior to the prism splitting. It should be noted, however, that only  $\sim 40\%$  of this power is coupled into the long multimode fiber due to the losses, primarily in the 2:1 fiber coupler. Recall that when using a 2:1 fiber coupler, half of the power is lost in the unused, terminated end. The figure clearly shows an SBS threshold at  $\sim 500$  mW of total input power and the inset scan from the Fabry-Perot spectrum analyzer displays the smaller pump and larger Stokes peak over multiple free spectral ranges of the Fabry-Perot cavity.

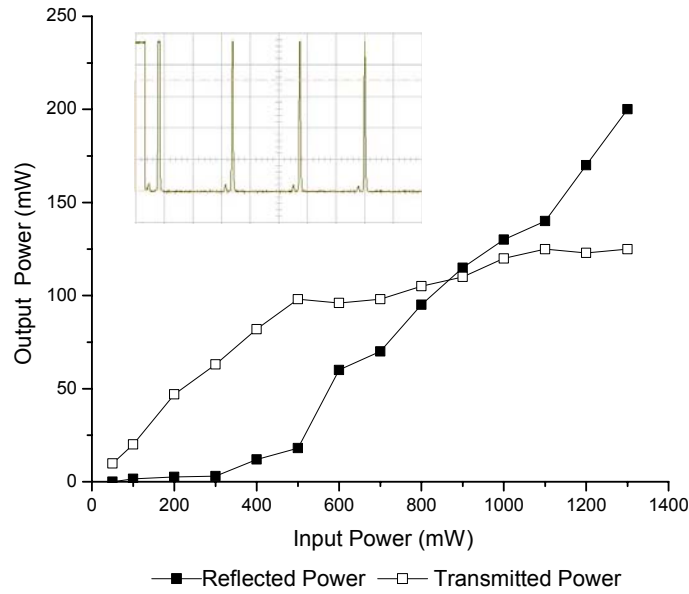
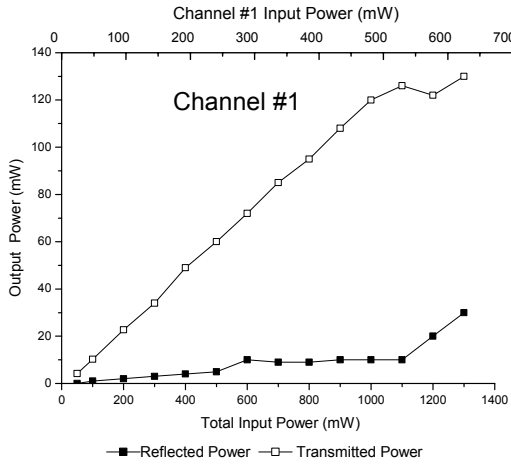


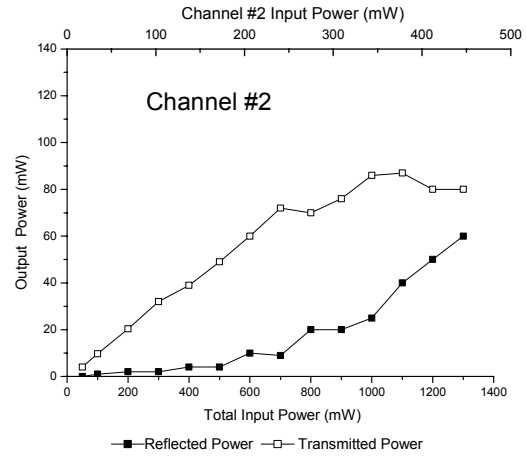
Figure 35: Stokes input-output characteristics for the 2:1 passive fiber phasing test.

This initial test of SBS beam phasing verified the ability of a long fiber to successfully correct for piston error and phase the output beams from a multiple channel system. There were, however, some difficulties in using a 2:1 fiber coupler as part of the implementation. The primary hindrance is output power fluctuations, which are evident in both the power measurements and the LSI fringes. For the LSI data, the fringes flash as the beam intensity changes. The power fluctuations and stability issues associated with using fiber couplers is explored in more detail in Section 4.2.5

Another observation made using the 2:1 fiber couplers is that there is a strong bias to one of the input channels in that it produces an SBS Stokes beam with much greater efficiency and lower threshold. This effect is evident when looking at SBS input-output characteristics for each of the 2:1 channels individually as given in Figure 36.



(a)



(b)

Figure 36: Stokes input-output characteristics for (a) channel #1 and (b) channel #2 of the 2:1 fiber coupler individually. The bottom axis is vs. total input power for easy comparison with Figure 35, while the top axis provides the power measured in each channel following the prism wavefront split.

For the graphs, the data is plotted vs. both the input power to the respective channel (top) and the total system input power (bottom). The individual input power is measured after the prism splitting and does not include the loss in the 2:1 coupler. The actual transmission through the fiber coupler and into the long multimode fiber is  $\sim 45\%$ , where most of the lost power is transferred to the terminated output end of the fiber coupler as previously described. The total input power is provided for direct comparison with Figure 35.

The stronger SBS channel is #2 where the threshold is 200-300 mW. The weaker SBS channel #1 does not reach threshold until  $\sim 500$  mW. For both observations, the Fabry-Perot spectrum analyzer was used to verify the SBS thresholds. In addition, the input fibers were switched to verify that the difference between the two channels is indeed due to the 2:1 fiber coupler and not related to another factor in the configuration.

It is important to note that although channel #1 requires more power to excite the Stokes beam by itself, both channels contribute to the Stokes beam generation when simultaneously pumping the fiber. This is apparent when comparing the two-channel output power (Figure 35) with the individually pumped values (Figure 36) and was confirmed in the laboratory.

Looking back at Figure 32 (pg. 72) helps to explain why one of the channels produces a stronger SBS signal. The most probable explanation is that light coupled into and out of the same side of the fiber coupler has greater overlap with the fundamental mode of the fiber. Since SBS efficiency is dependent on the overlap of the pump beam with the fundamental mode of the fiber,<sup>54</sup> this channel produces a much stronger Stokes output. For example, if the laser is coupled into input fiber # 1 of Figure 32, the light coupled through the same side to output #1 has a better overlap with the fundamental mode than that passing to output #2.

For a 2:1 fiber coupler, one of the outputs is terminated. In this case, one of the input channels passes through with strong fundamental mode overlap and correspondingly strong Stokes generation. The other input channel, which crosses over into the output channel, does not have as good of excitation of the fundamental mode resulting in weaker Stokes output.

The successful SBS beam phasing of the passive channel presented in this section provided the motivation to extend the investigation to include an active amplifier in each channel. Further investigations using a long fiber for SBS beam phasing including more details on the effects of using fiber optics couplers are presented in the remainder of this section.

### **4.2.3. Beam Phasing Two Amplified Channels Using a 2:1 Fiber**

#### **Coupler**

After the initial demonstration of long fiber SBS beam phasing as presented in Section 4.2.2, an experiment was designed to extend the work to include an active amplifier in each channel. Whereas using passive, unamplified, channels is sufficient for initial concept demonstration, the real system utility is in phasing multiple channel amplifiers. Figure 37 shows the system diagram used for the test.

Similar to the experiment above, the single-frequency NPRO was preamplified, collimated, and passed through a thin film polarizer / Faraday Rotator combination. The laser beam was wavefront split using two right angle prisms and was coupled into separate fiber amplifiers. The two fiber amplifiers are built from Yb-doped, double clad, large mode area fibers as developed in Section 4.1. This large mode-area fiber has a core diameter of 20  $\mu\text{m}$  with 0.06 NA and an octagonal-shaped guided inner cladding of 400  $\mu\text{m}$ . The fiber lengths are 1003.6 cm and 994.4 cm for channels #1 and #2, respectively. While keeping such precise track of the fiber length is difficult, it is necessary to accurately control the channels' optical path length (OPL) to help minimize the residual piston error discussed in Section 4.2.1. Both fibers are coiled onto an aluminum spool (10cm diam.) to keep the propagation of the beam in a single mode.<sup>68</sup>



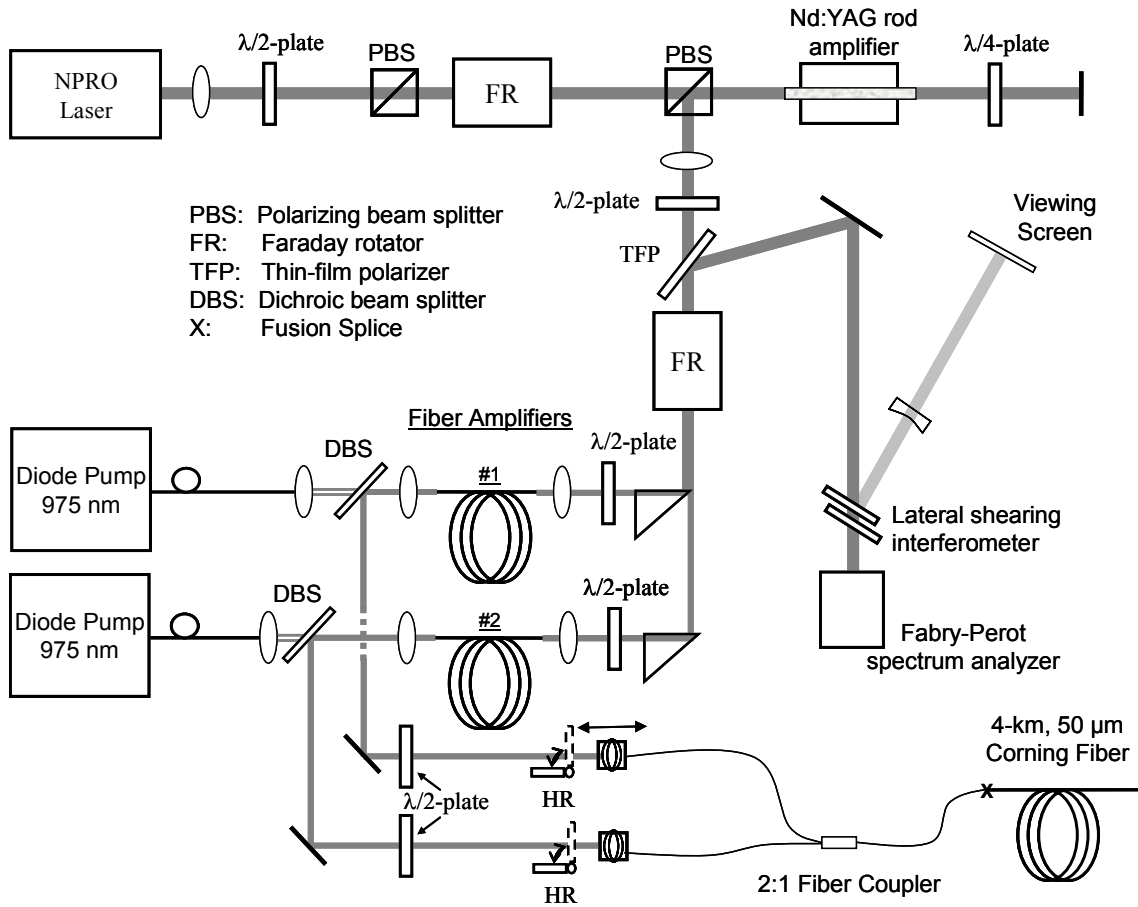


Figure 37: Experimental schematic testing SBS beam phasing for two amplified channels. A 2:1 fiber coupler is used to combine the two beams into a single 4-km, 50  $\mu\text{m}$  core diameter gradient index fiber.

The amplifier fibers are pumped by separate 975 nm diode lasers producing up to 25W and dichroic beam splitters (DBS) are used to couple the diode pump beams into the amplifier fibers. The amplified output beams from both channels were coupled into a commercially available 2:1 fiber optic coupler which was directly fusion-spliced to the long SBS fiber. The input of one of the 2:1 couplers could be translated to change one of the channel's optical path lengths and minimize the residual piston error. The SBS fiber was the same used in the passive phasing experiment of Section 4.2.2, a multi-mode fiber with 50- $\mu\text{m}$  core (Corning LDF-50/125 MMF, 0.20 NA), 4 km in length.

The coherent combination of the two amplified single-frequency beams combine to generate a backwards propagating SBS beam. Although the SBS beam is not a complete spatial phase conjugate, it is possible to properly align that system so that a portion of the SBS beam is coupled into the fiber amplifiers for a second pass. The beams travel back through the system where the rotated polarization is reflected from the TFP to the diagnostics.

A few sample LSI images are presented in Figure 38. The top left figure (Figure 38a)

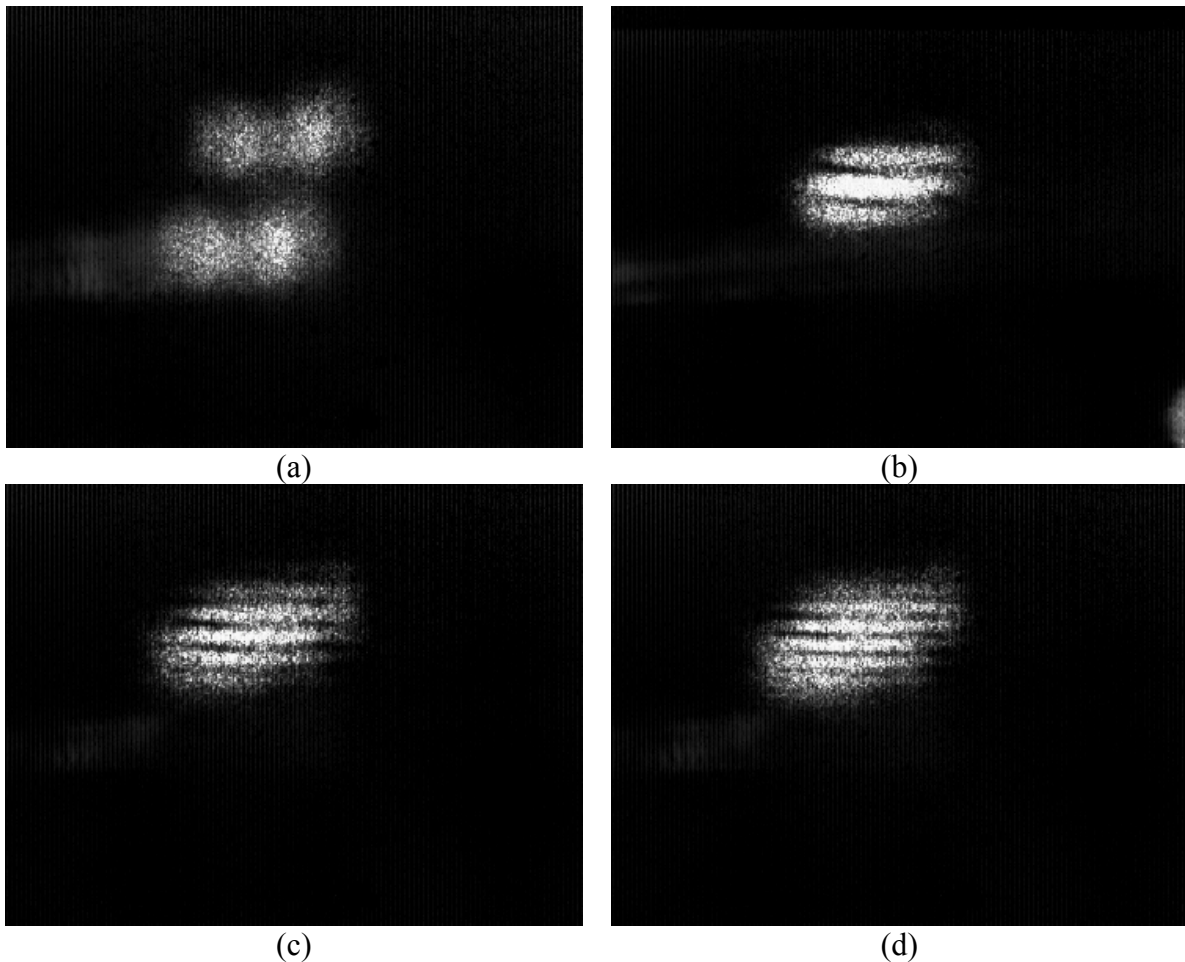


Figure 38: Lateral shearing interferometer data demonstrating two-channel amplified phasing using a 2:1 fiber coupler. (a) Shows both LSI surface reflections of the two Stokes beam traveling side by side. The remaining figures (b-d) show LSI interference fringes of various thickness and spacing.

shows the two sets of reflections from each LSI surface. The right beam is the Stokes beam from channel #1 and the left is from channel #2. The two Stokes beams are brought together so as to create an inner region of mutual-interference of the two Stokes beams that is bounded by regions of self-interference on either side. Three images representing fringes of different sizes are shown in Figure 38b-d. It is possible to vary the size and number of fringes by making slight adjustments to the LSI. All of the figures (b-d) are continuous across all three interference regions indicating that the two Stokes beams are in phase.

A flat mirror was inserted in front of both inputs of the 2:1 fiber coupler to provide a phasing comparison for the Stokes beam. Figure 39 portrays the comparison showing (a) lack of continuity across the fringe zones when a high reflector is used in contrast to (b) the continuity across fringe zones indicating beam phasing when the SBS fiber is used to generate the Stokes beams.

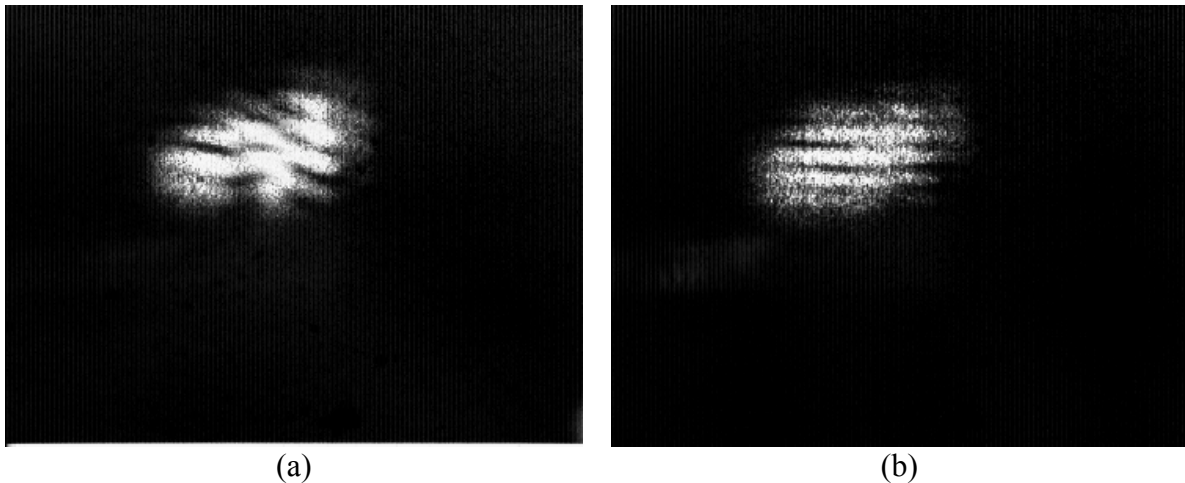


Figure 39: LSI fringe comparison for the two pass amplifier with (a) a flat mirror and (b) the SBS fiber providing the back reflection for the second pass amplification.

For this test, the input power for each fiber amplifier was  $\sim 450$  mW. It is estimated that  $\sim 60\%$  of the seed power is coupled into the LMA fiber core. The light not coupled into the core is simply guided by the inner cladding and passed through the back end of the fiber. The total phased output power from both channels after two-pass amplification is shown in Figure 40. In this experiment, the maximum output power recorded was 560 mW. The experiment did not increase to higher powers because of the maximum power handling capability of the 2:1 fiber couplers. The inset Fabry-Perot scan records the pump and Stokes beam from the experiment.

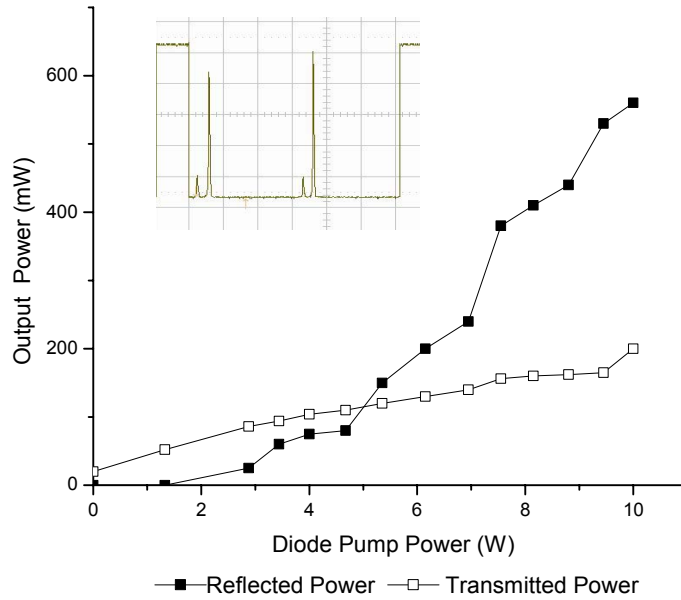


Figure 40: Stokes input-output characteristics for the 2:1 amplifier fiber phasing test. The output powers from both Stokes beams are plotted vs. the total diode pump power for both amplifiers.

This experiment was the first successful cw demonstration of SBS beam phasing for a multiple channel amplifier. The phasing demonstration of this section was a critical step in that it verified the phasing abilities when incorporating fiber amplifiers in SBS piston

error correction. Prior to the successful phasing results, it was unknown whether the complexities of the fiber amplifier implementation (keeping long fiber lengths similar in length to minimize residual piston error, successfully coupling SBS in a second pass through the amplifier, etc.) would prohibit experimental demonstration of the concept. While this demonstration was a successful step, there were still practical limitations.

One main issue is that the overall system efficiency was poor for this implementation. This is not a surprise considering that  $\sim 55\%$  of the power passed through the 2:1 fiber couplers is lost through residual loss and coupling of light to the unused, terminated output. Also, because the SBS beam generated in the fiber is not a true spatial phase conjugate, the beam does not automatically backtrack along its original path and the second amplifier pass is dependent on the optical alignment. These two factors are likely the prime contributors to the low efficiency. The experiment also displayed power fluctuations as observed in the passive experiment of Section 4.2.2. The power fluctuations arise from using fiber optics couplers and are explored in more detail in Section 4.2.5.

The insights developed from this experiment provided two new directions for exploration. One was to investigate a method for coupling the beams into the SBS fiber without the difficulties associated with using fiber couplers. This concept led to the polarization beam combining experiment described in Section 4.2.4. Another was to examine an SBS beam phasing implementation that used both outputs of the 2:2 fiber coupler instead of simply terminating half of the power. This topic is explored in Section 4.2.5.

#### **4.2.4. Beam Phasing Two Amplified Channels Using Polarization Combining**

In developing SBS beam phasing for practical applications, it is necessary to consider the overall system efficiency. While the experiments presented thus far were successful in demonstrating SBS beam phasing using a long multimode fiber, the poor performance limits its functionality. As discussed above, much of the poor performance in the previous section is attributed to the loss incurred at the 2:1 fiber coupler. This section describes an alternative polarization beam combining approach that greatly increased the system efficiency and provided a stable, phased output from a two channel amplifier with power greater than 5 W. The result allows multiple channel SBS beam phasing to be considered as a viable approach for laser power scaling.

The system schematic used in the experiment is provided in Figure 41. The master oscillator is a 700 mW single-frequency Nd:YAG NPRO laser. This source is isolated with a polarizing beam splitter (PBS) / Faraday rotator (FR) combination before being double-pass amplified. The output beam from the preamplifier is collimated and the polarization is rotated to horizontal so that the entire laser beam passes through the thin-film polarizer (TFP). The laser beam is wavefront split using two right angle prisms and is coupled into separate fiber amplifiers. The fiber amplifiers, as described in Section 4.1, use a large mode-area fiber with a core diameter of 20  $\mu\text{m}$  with 0.06 NA and an octagonal-shaped guided inner cladding of 400  $\mu\text{m}$ . The fiber lengths are 981.7 cm and 999.9 cm for channels #1 and #2, respectively. As before, both fibers are coiled onto an aluminum spool (10cm diam.) to keep the propagation of the beam in a single mode.<sup>68</sup>

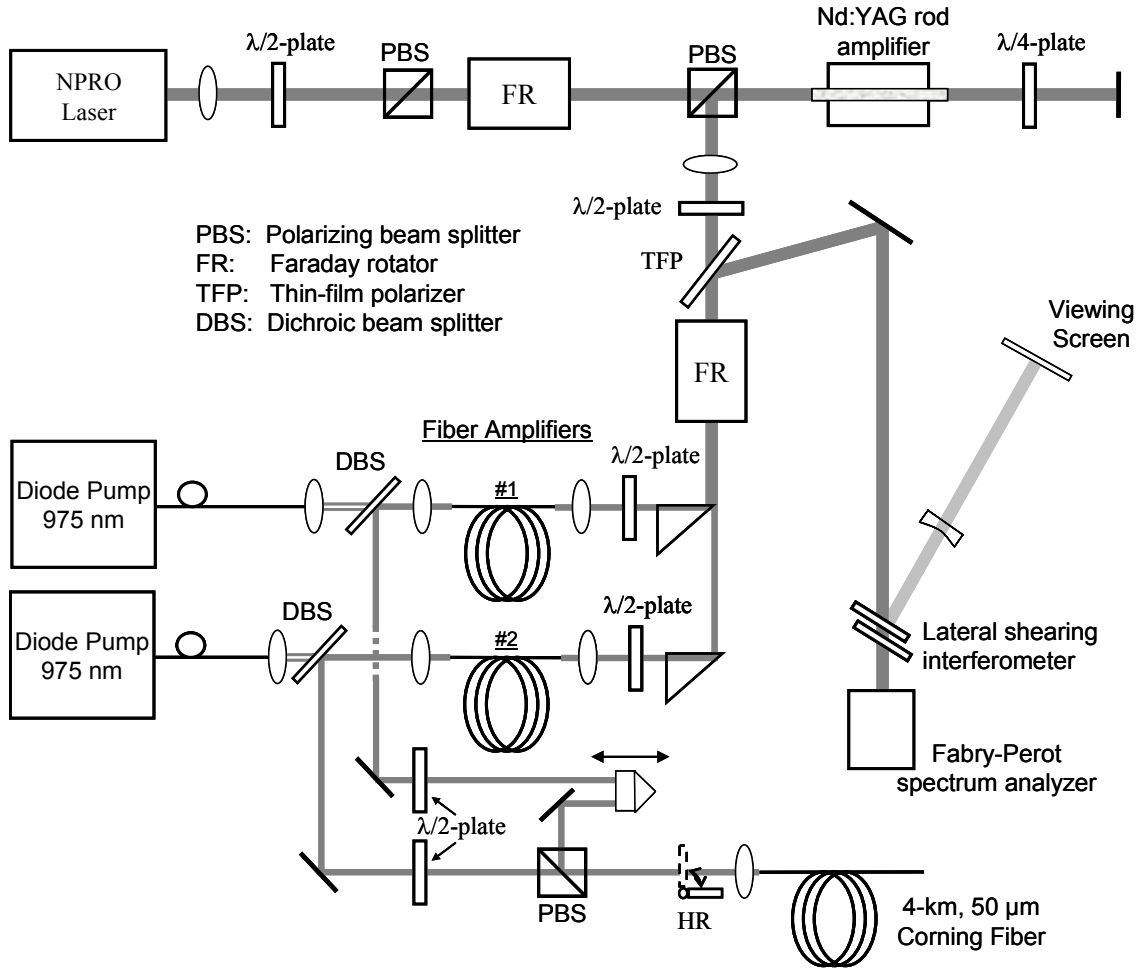


Figure 41: Experimental schematic for SBS beam phasing of two amplified channels using polarization beam combining.

The amplifier fibers are pumped by separate 975 nm diode lasers that are coupled into the LMA fibers via dichroic beam splitters. Although the LMA fiber is not polarization maintaining, the stress-induced birefringence induced by coiling on the 10-cm diameter spools was sufficient to produce a polarized output. The polarization axis changes slowly as the fiber reaches thermal equilibrium, but after sufficient warm-up, a polarization ratio greater than 500:1 could be maintained. The half-wave plates on both ends of the fiber amplifiers are used to align the input polarization to that of the fiber as well as to control

the output polarization. The beams of the fiber amplifiers were overlapped using a PBS cube. Channel #1 includes a corner cube mounted on a translation stage to provide an optical trombone for adjustment of the optical path length. After the two beams are overlapped at the PBS, they are coupled into the SBS fiber where they coherently combine to generate a backwards propagating SBS beam. The SBS fiber was 4 km of Corning multimode fiber with a 50  $\mu\text{m}$ /0.2 NA core.

As described earlier, producing a true phase conjugate of the pump beams requires a short multimode fiber (typically  $< 10$  m) as the SBS medium.<sup>37</sup> In long fibers such as the one used in this experiment, the Stokes intensity profile corresponds to the  $\text{LP}_{01}$  fiber mode irrespective of the pump profile.<sup>22</sup> Although it would clearly be better to have full transverse spatial phase conjugation in addition to piston phase correction, we are pursuing phasing of the channels in this research, so the correction of the piston phase error is the most important goal. This is especially true since our fiber amplifiers are operating in single transverse mode, for which spatial phase conjugation is not critically important. Thanks to the polarization scrambling that occurs in multimode fiber, the two SBS pump beams with orthogonal polarization mix in the fiber and work together to set up a common acoustic phonon field that is unique to the coherent sum of the pump waves so as to feed growth of the Stokes beam. Thus, the SBS beam produced has a phase that is related to that of the combined pump beams. As a result, the Stokes beam is a phase conjugate of the piston phase difference between the pump beams.

As with previous implementations, the phase conjugation necessary for beam phasing is achieved even though the long fiber does not produce a complete spatial phase conjugate. The two beams from each channel provide the joint pumping required to



create the common SBS beam necessary for beam phasing. Although this SBS beam is not an exact spatial phase conjugate, it is possible to properly align that system so that portions of the SBS beam are coupled into the fiber amplifiers for a second pass. The beams travel back through the system where the rotated polarization (now vertical) is reflected from the TFP to the diagnostic system.

Figure 42 shows two LSI interference patterns and demonstrates the phasing of the two amplifier channels. The left frame (a) shows the fringes formed by the reflection from a simple flat mirror placed in front of the SBS fiber as shown in Figure 41. The lack of continuity across the three fringe zones indicates that the beams are not in phase and the piston error is not corrected. The right frame (b) shows fringes from the SBS beam to be continuous across all three fringe zones indicating the piston error is compensated and the beams are in phase.

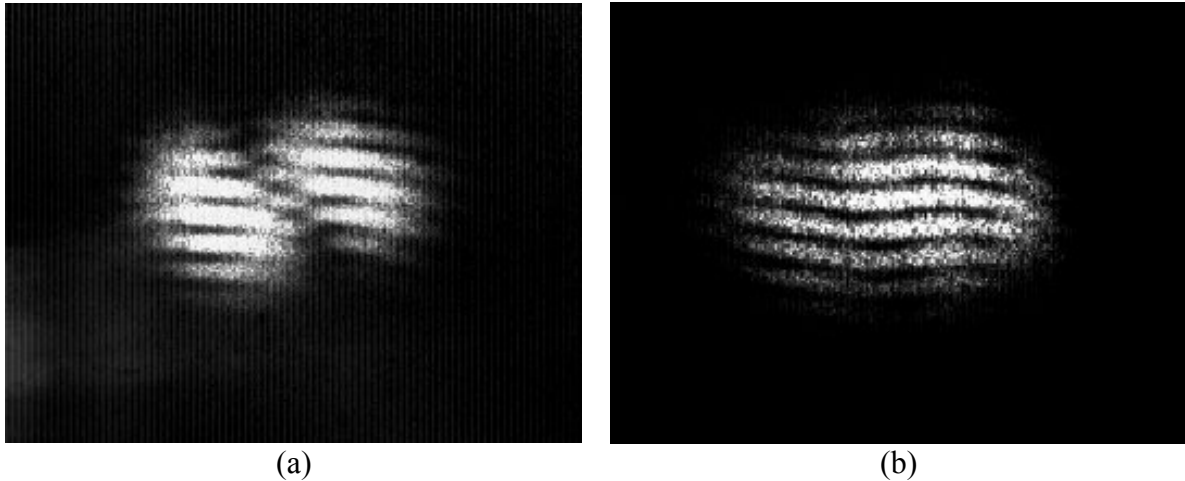


Figure 42: Lateral shearing interferometer data from (a) a flat mirror and (b) the SBS multi-mode fiber.

The addition of the corner cube in this experiment allowed for investigation of the residual piston error. As described above, the residual piston error arises from the difference in frequency between the pump and Stokes waves and is defined in Equation 4-1.<sup>16,78</sup> In order to maintain good SBS beam phasing, it is necessary to minimize the residual piston error. It is for this reason that accurate records were maintained for each of the fiber amplifier channels. It is fortunate that good phasing positions are cyclic over multiple waves<sup>16,78</sup> because it relaxes the need for maintaining absolute path length monitoring.

In order to estimate the change in optical path length required to observe the periodic variation of good phasing positions, it is first necessary to measure the actual SBS frequency shift for the 50  $\mu\text{m}$  fiber used in this experiment. This is accomplished using the scans from a Fabry-Perot spectrum analyzer as described in Section 3.2 (pg. 31).

Figure 43 is a typical Fabry-Perot scan taken during this experiment.

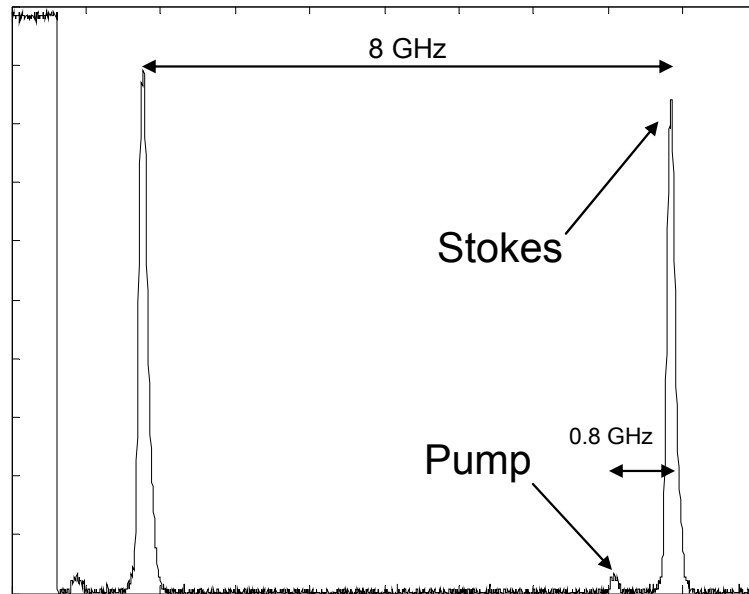


Figure 43: Fabry-Perot spectrum analyzer scan for Corning 50  $\mu\text{m}$  core diameter fiber. The measured SBS shift is  $15.2 \pm 0.2$  GHz.

Using a similar procedure to that described in Section 3.2, the SBS shift is measured to be  $15.2 \pm 0.2$  GHz. Using this value in Equation 4-1, the expected optical path length change for a full period is  $\Delta_L = 19.7 \pm 0.3$  mm.

The optical path length for channel #1 was increased while observing the changes in the LSI interference patterns. In doing this, it was possible to observe the periodic variation of phased fringes (continuity across the three fringe zones) with unphased fringes (lack of fringe continuity) as demonstrated in Figure 44.

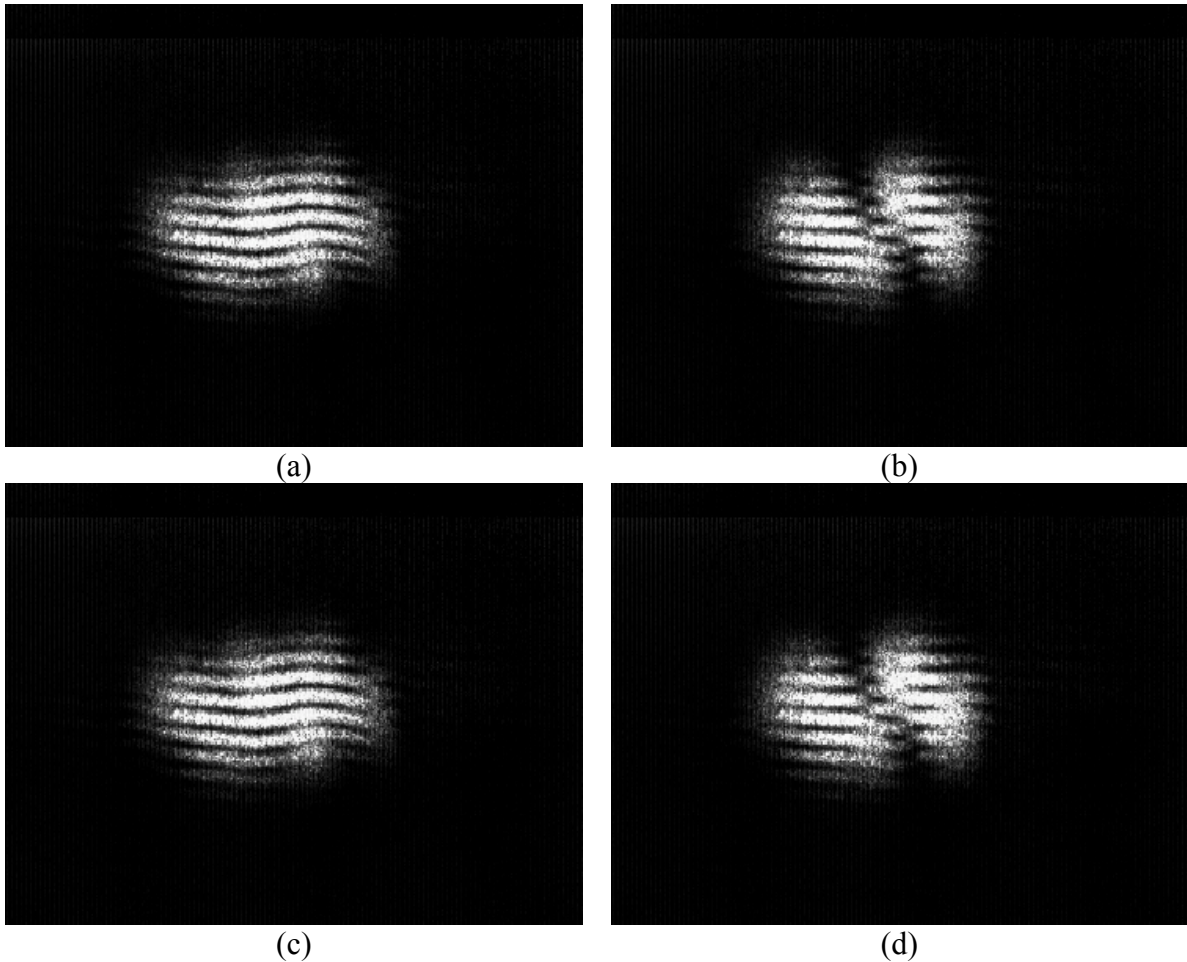


Figure 44: Lateral shearing interferometer. The data shows the repetition of fringe patterns as the path length for channel #1 is increased via the optical trombone. The relative path length difference is (a) 0 mm, (b) +10 mm, (c) +20 mm, and (d) +30 mm.

The figure shows that as the optical path length difference increased, the fringes change from (a) phased to (b) unphased, (c) rephased, and (d) unphased again. A series of these measurements was completed to determine the periodic path length difference as  $\Delta_L = 20 \pm 3$  mm which leads to an SBS frequency shift of  $15 \pm 2$  GHz. The results compare well with the expected values based upon the measured SBS frequency shift.

For the phasing experiment, the measured seed power into the fiber amplifier channels was held constant at 440 mW and 480 mW for channels #1 and #2, respectively. It was estimated that ~60% of the seed power is coupled into the fiber core. Figure 45a shows the double-pass output characteristics of the individual channels as a function of the diode pump power. The total phased output power from both channels after double-pass amplification is shown in Figure 45b.

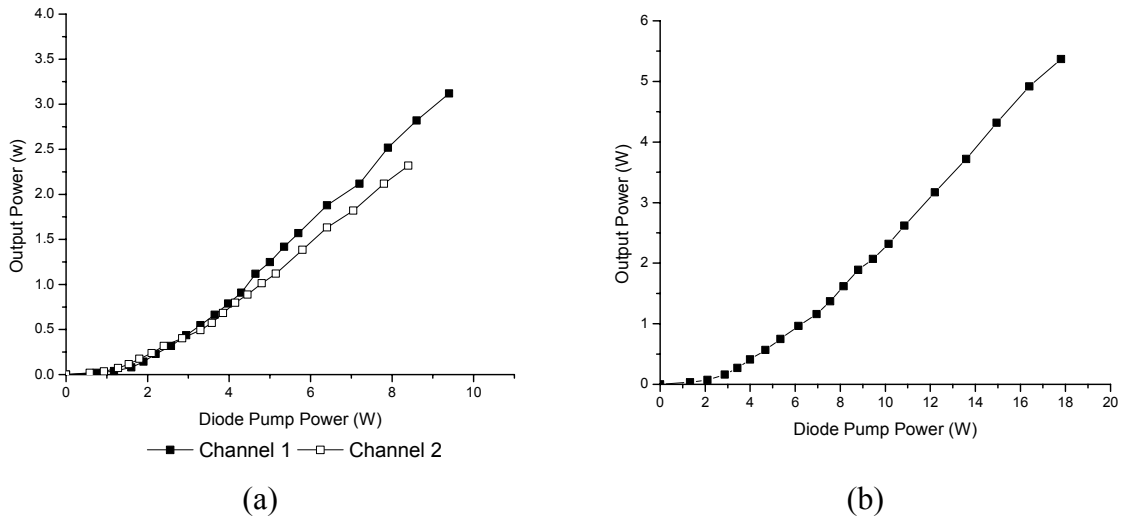


Figure 45: Input-output characteristics for (a) the double-pass fiber amplifier channels individually and (b) total phased output power from both channels. The inset in (b) shows a typical Fabry-Perot scan demonstrating single-frequency output.

A maximum output power of 5.3 W was recorded, representing a gain of over 475% for the total input power of 920 mW. The conversion slope efficiency for the amplifiers

is ~40%. The lower efficiency for the double-pass amplifiers compared to that of single-pass amplifiers, which was ~60%, is believed to be due to the lack of generating a true spatial phase conjugate in the long SBS fiber. As mentioned above, a portion of the Stokes beam is coupled back into the LMA fiber for a second pass, but without the true spatial phase conjugation, the coupling is not perfect.

The greater than 5 W output achieved in this experiment is a significant step for using a passive approach to beam phasing. For the first time, SBS piston error correction for a two-channel fiber amplifier was achieved with significant gain. Because this implementation did not use fiber optic couplers, it avoided the power fluctuations previously reported in Sections 4.2.2 and 4.2.3. The work also verified the periodic variation of phasing due to residual piston error. Although the periodicity of good phasing positions was previously reported,<sup>78</sup> this is the first work reporting the periodicity using a cw beam and a long optical fiber as the SBS medium. The phasing results achieved in this section provide the necessary motivation to continue the investigation to higher power levels, leading towards a fieldable multiple channel beam phasing system.

#### **4.2.5. Beam Phasing Two Amplified Channels Using a 2:2 Fiber Coupler**

Thus far in this section, SBS beam phasing has been demonstrated as a viable option for phasing a multiple channel amplifier system. The demonstration was completed using two channels as a test case for phasing the amplifiers. To approach a weapon class system, it will be necessary to phase more channels in order to achieve the power

required for the applications. It thus becomes necessary to investigate methods for scaling the technology to incorporate more channels.

One method for scaling is to use commercially available fiber optic couplers. This is part of the motivation for the investigation of the 2:1 fiber coupler in Sections 4.2.2 and 4.2.3. While the 2:1 coupler was used to demonstrate two-channel beam phasing, it is possible to purchase 4:1, 8:1, etc. couplers to extend the technology to a higher number of channels. Unfortunately, the loss associated with the terminated end(s) in this type of fiber coupler is quite high. It is for this reason that an exploration into 2:2 fiber couplers, which could be extended to more channels (i.e. N:N), is considered. In this case, both outputs of the fiber coupler are used, greatly reducing the system loss. This section explores SBS beam phasing using a 2:2 fiber coupler. The phasing results for this configuration are presented along with an investigation into the power fluctuations and instabilities observed when using fiber couplers.

The approach in this work uses two separate lengths of long multimode fiber that are fused to the outputs of a commercially available 2:2 fiber coupler. In the previous experiments of this section, a portion of the two beams from each channel coherently combined in a single SBS fiber. The beams work together to set up a common acoustic phonon field that feeds the growth of the Stokes beam and conjugates the piston error of the two channels. When using a 2:2 fiber coupler and two separate optical fibers, both fibers will still receive the coherent combination that has phase and intensity modulation associated with the piston error. Each channel should individually conjugate the piston error between the two beams as previously demonstrated and this section investigates the feasibility of phasing the entire two-pass amplifier output.

The schematic diagram used for this experiment is shown in Figure 46. As with previous experiments described in this chapter, the master oscillator is a 1064 nm single-frequency NPRO laser that was preamplified, collimated, and wavefront split using two right angle prisms. The seed laser ( $\sim 450$  mW each channel) was coupled into Yb-doped LMA fibers which are pumped by a 975 nm diode laser to provide optical gain.

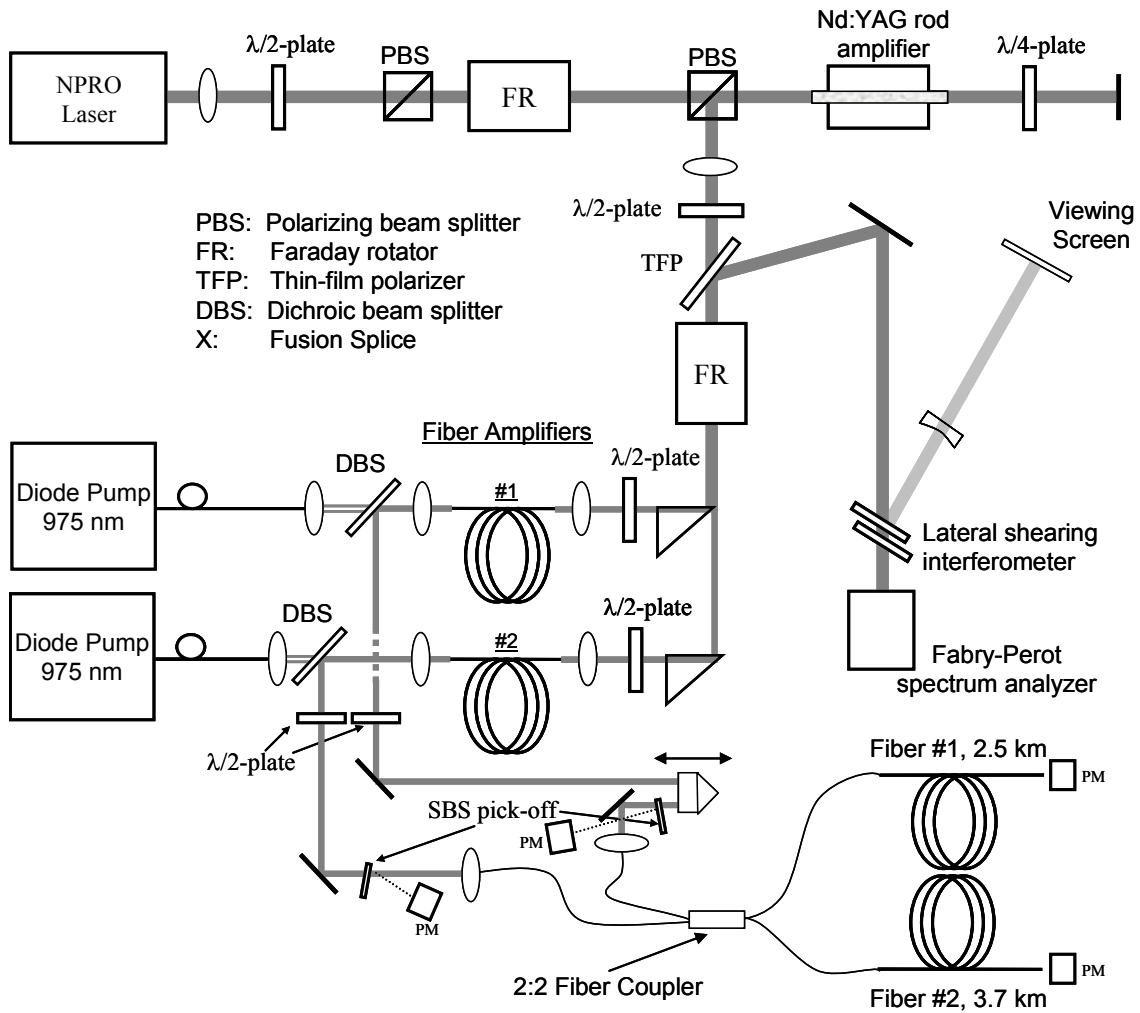


Figure 46: Experimental schematic testing SBS beam phasing for two amplified channels. A 2:2 fiber coupler is used to combine the two beams into two 50  $\mu\text{m}$  core diameter gradient index fibers.

The two outputs from the fiber amplifiers were coupled into respective ports of a 2:2 fiber coupler. The fiber coupler is designed to combine and split the power so that 50% of each input passes through each of the coupler outputs. These outputs were fused directly to two separate spools of the same 50  $\mu\text{m}$ /0.20 NA Corning gradient index multimode fiber. The lengths of the two spools were 2.5 km and 3.7 km for fibers #1 and #2, respectively.

Two initial LSI interference patterns with different fringe thickness are presented in Figure 47. Here, the beams appear to be in phase with each other as evidenced by the continuity across all three fringe zones.

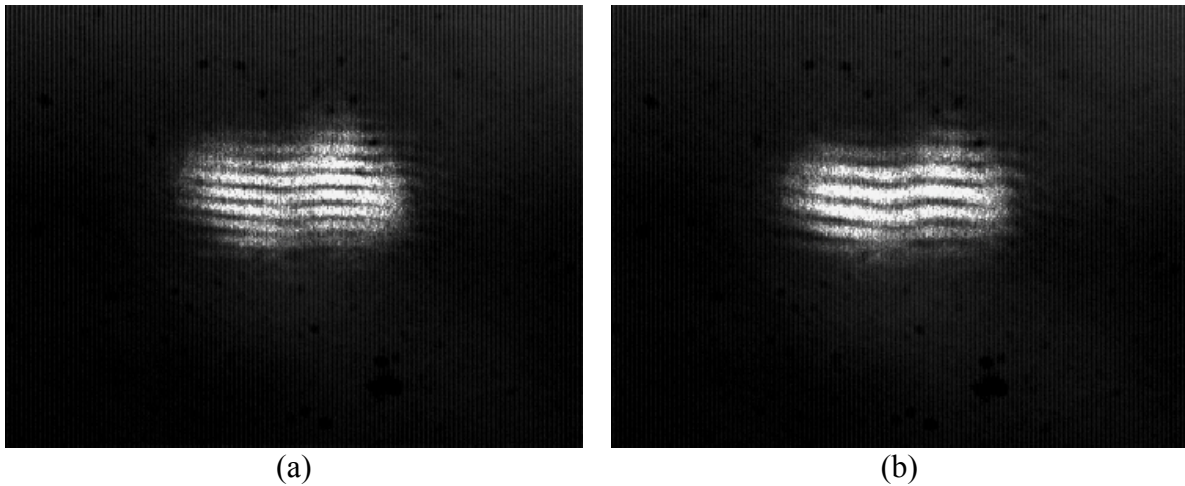


Figure 47: Lateral shearing interferometer data for two-channel amplified phasing using a 2:2 fiber coupler.

Figure 48 shows initial input-output power graphs taken in this configuration. The total power with both channels operating (a) as well as individual (b and c) two-pass amplification are provided. For this data, the total diode pump power was limited to 10 W to keep the amplifier's output below the suggested damage threshold of the fiber



couplers. As a reference, the output achieved using a 2:1 fiber coupler (Section 4.2.3) is included.

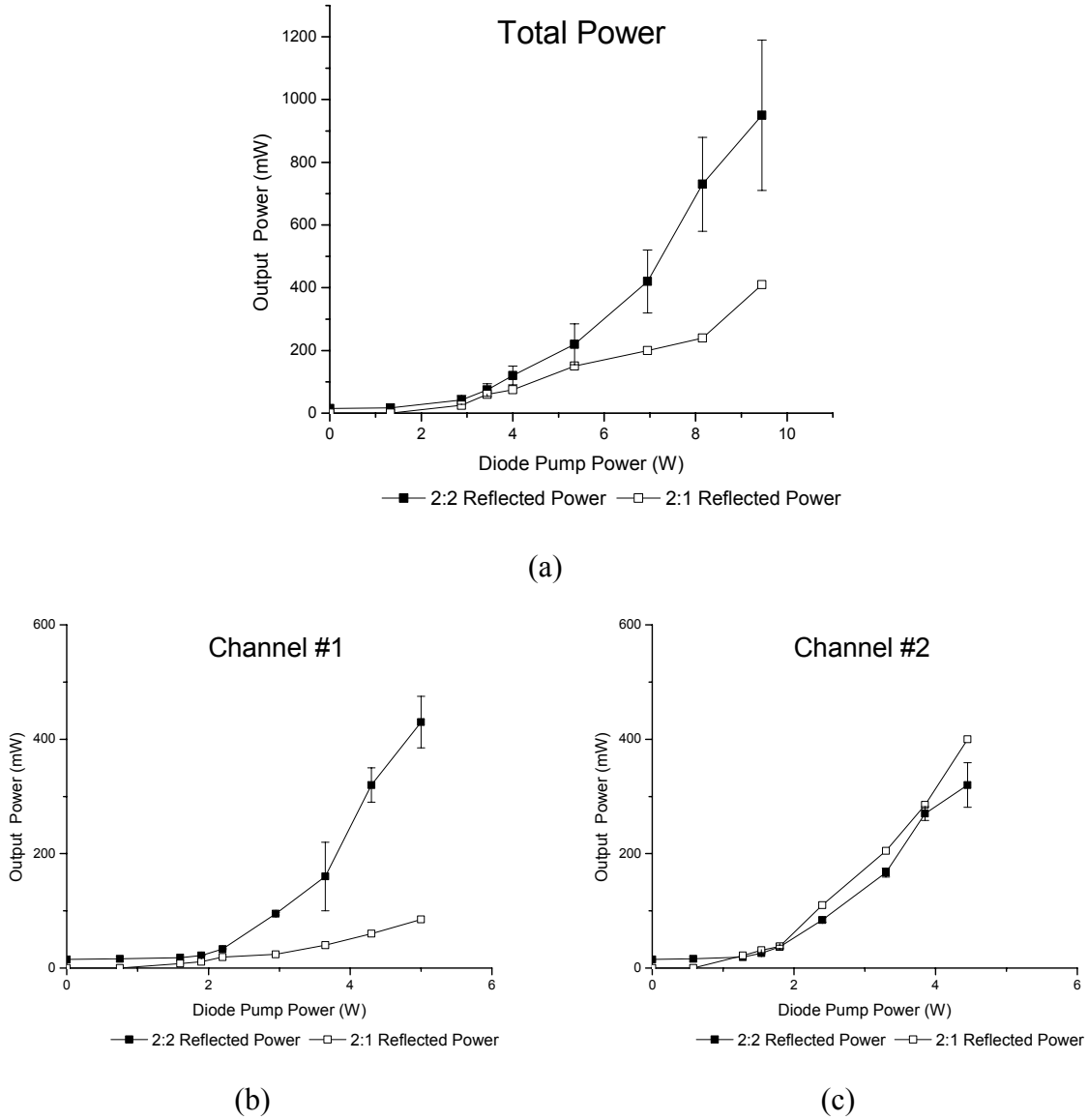


Figure 48: Input-output graphs for a two-channel fiber amplifier system using 2:2 fiber couplers. The (a) total output power and the (b and c) individual channel two-pass performance are given. Previous results obtained using 2:1 fiber couplers are included for comparison.

The improved efficiency of the 2:2 coupler is evident in the total output power of (a) and the channel #1 power of (b). As discussed previously, the 2:1 coupler output from

channel #1 was limited in that it was the crossover channel of the fiber coupler and was not as efficient at generating the Stokes beam. When using a 2:2 coupler, however, both channels have a fiber fused to the output which results in more efficient SBS production.

While the performance using the 2:2 fiber couplers improved from the previous 2:1 fiber coupler results, there remained large fluctuations in the output power as reported in earlier experiments using fiber couplers. The power instability evident in the error bars in Figure 48 is recorded in more detail in the plots of Figure 49. In these output power vs. time graphs, the power was sampled twice per second for a total of 60 seconds. The figure displays the output power fluctuations for two different diode power pump levels.

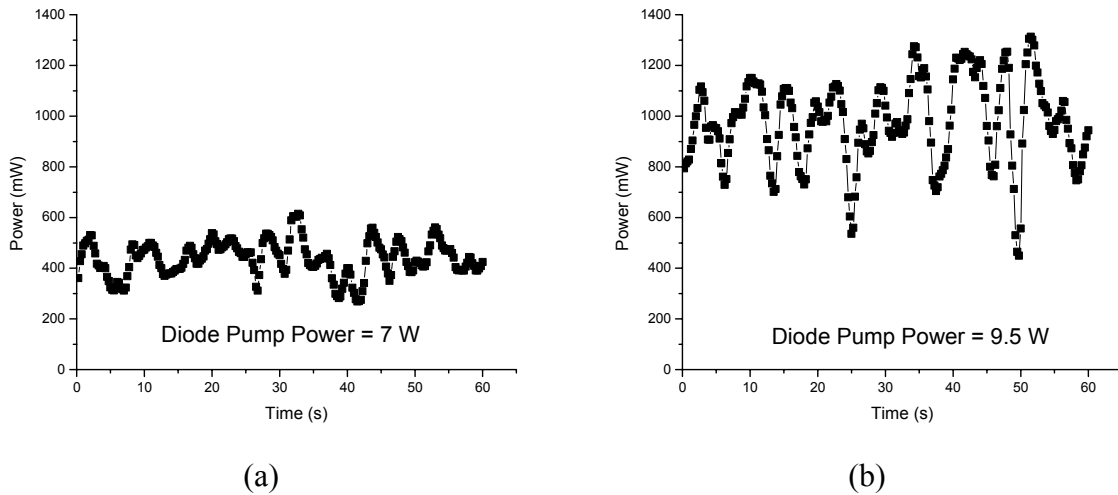


Figure 49: Graphs of output power vs. time for a diode pump power level of (a) 7 W and (b) 9.5 W.

The stability associated with using the fiber couplers is also observed as fluctuations in the LSI interference patterns. For example, Figure 50 displays an interference pattern captured a two different times. The left figure (a) is captured when the fringes are more stable and the two beams appear to be in phase by the continuity of the fringes. The right

figure (b) is taken later without making any system adjustments. In this case, the resultant fringe pattern is not as good and it is difficult to ascertain the phasing of the two beams.

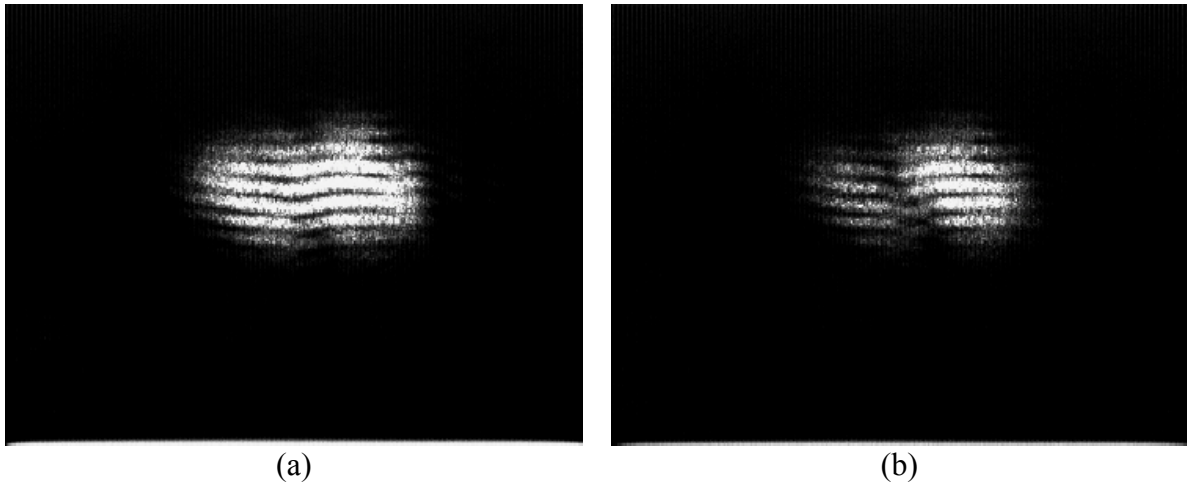


Figure 50: Lateral shearing interferometer data displaying fringe fluctuations.

Although the power instability made it more difficult to collect the data, an investigation of the residual piston error and good phasing positions as reported in Section 4.2.4 was repeated using this system configuration. As before, the corner cube of channel #1 was used to change the optical path length difference between the two channels. The LSI fringes were observed while increasing channel #1's optical path length and the periodic variation of phased fringes (continuity across the three fringe zones) with unphased fringes (lack of fringe continuity) was repeated. Figure 51 shows that as the optical path length difference increased, the fringes change from (a) phased to (b) unphased, (c) rephased, and (d) unphased again. The periodic path length difference is determined as  $\Delta_L = 19.6 \pm 0.4$  mm which leads to an SBS frequency shift of  $15.3 \pm 0.3$

GHz. The results compare well with the previous measurement presented in Section 4.2.4.

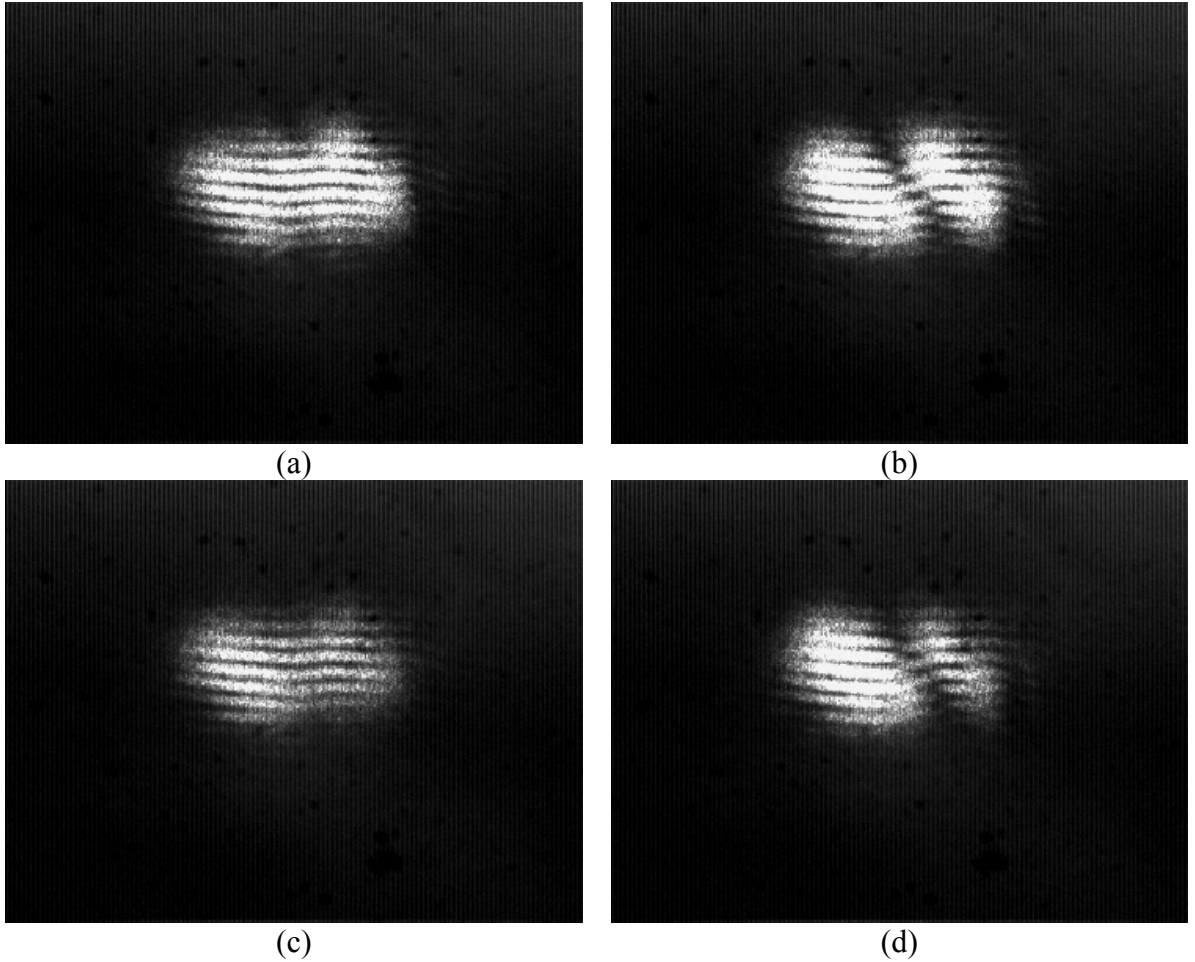


Figure 51: Lateral shearing interferometer data using 2:2 fiber couplers with amplifiers. The data shows the repetition of fringe patterns as the path length for channel 1 is increased via the optical trombone. The relative path length difference is (a) 0 mm, (b) +9.7 mm (c) +19.5 mm and (d) +29.5 mm.

In order to determine the feasibility of scaling beam phasing with fiber couplers to greater powers and more channels, it was necessary to further investigate the source of the observed instabilities. To deepen the investigation, two power meters were set up to simultaneously record power vs. time data. As shown in Figure 46, the pair of power meters synchronously recorded the transmitted power through the fibers or a fraction of

the Stokes beams which were reflected (Fresnel) from a microscope slide inserted in the beam path. Having the ability to observe the response of both channels at the same time aided in determining the source of the fiber coupler instabilities.

One primary issue in using the fiber couplers becomes apparent when simultaneously observing the transmitted power through the fiber below SBS threshold. By measuring the transmitted power below threshold, it is possible to observe the time-based splitting of the power between the two fibers. Figure 52 displays the measured transmitted power below SBS threshold when (a) both inputs of the 2:2 fiber coupler are used and (b) only one of the inputs is used.

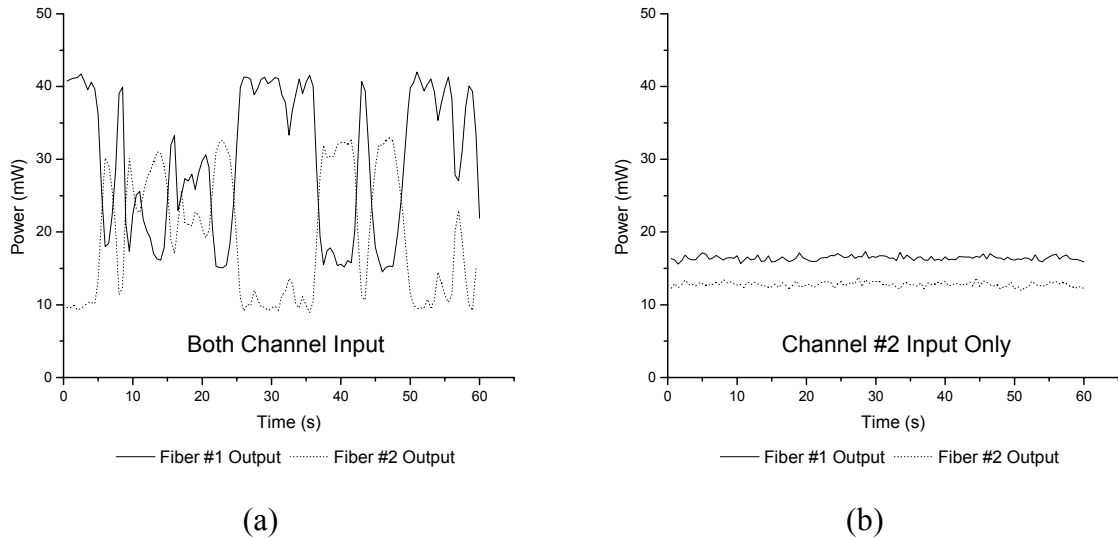


Figure 52: Transmitted power recorded simultaneously through both SBS fibers. The output dynamics when using (a) both or (b) only one of the fiber input couplers are shown.

When both beams from the fiber amplifiers are launched into the 2:2 fiber couplers, strong oscillations of the output occur as shown in (a). Instead of simply allowing 50% of the power from each beam to pass through both output fibers as desired, the fiber

coupler channels most of the power to either one output or the other. This oscillation does not occur when coupling a single input as shown in (b). It appears that as the two beams combine in the fiber coupler, the interference of the beams acts to steer the beam preferentially to one output or another. As the relative phase between the two beams changes due to air currents, temperature gradients, etc., the interference pattern changes and alters which way the majority of the beam is directed. The result is an oscillation of the fiber coupler output beam as shown in (a). The relative phase disturbances are unavoidable in the laboratory environment and one of the reasons that SBS beam phasing, which corrects for such differences, is pursued.

It is understandable that such large variation of the input power would result in the observed power instabilities of the phasing system. This is especially true at lower powers, where channeling the majority of the total input power to one fiber or the other will affect SBS threshold, etc. In this case, it is likely that the return Stokes beam would be predominately (or entirely) generated from one of the fibers. Since beams from both channels combine to generate the Stokes beam, it would still conjugate the piston error and, for a short period of time, be very similar to a single fiber experiment. The power may then switch to the other fiber and repeat the process. Overall, oscillations in output power due to changing efficiency would be likely, but phasing of the channels still possible. This hypothesis is consistent with observations reported thus far. It is hoped that as the total power for the system is increased, both channels would excite a strong Stokes beam regardless of the power channeling at the fiber coupler and stability would improve.

In support of this investigation, a portion of each Stokes beam is measured from the Fresnel reflection off a microscope slide. The powers were again recorded synchronously and the calibrated results are shown in Figure 53. In this figure, the output powers from each channel fluctuate and appear to track one another. That is, both of the powers from each Stokes channel rises and falls together. This result is consistent with the notion that one fiber at a time is predominately generating the Stokes beam. In this case, the return Stokes beam is split between the two channels so that they rise and fall together. The ‘power tracking’ of the two channels was consistently observed and Figure 53 serves as a typical representative.

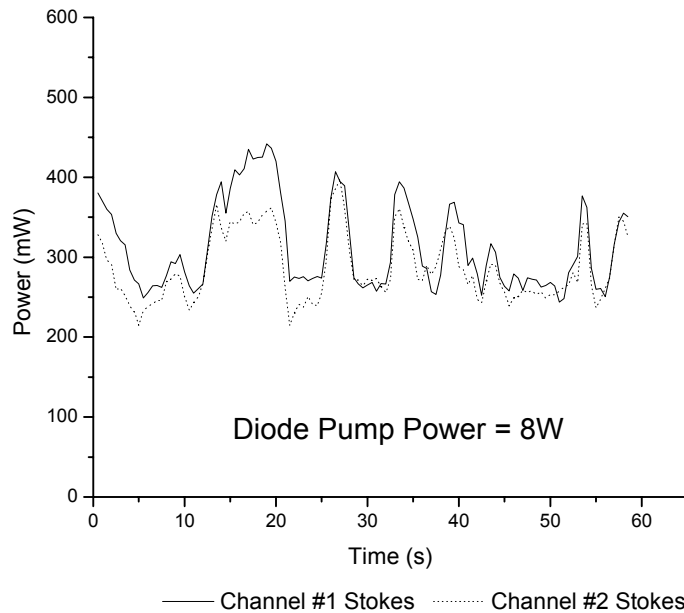


Figure 53: SBS power measured for both channels at 8W of diode pump power. The power is calibrated from the two surface Fresnel reflection of the beam pick-off.

From the discussion above, it is desirable to increase the overall power levels of the 2:2 fiber phasing system to further investigate possibilities for power scaling. Previous

power measurements (Figure 49) were kept at levels below the ‘suggested’ damage threshold from the fiber coupler manufacturer. At this point, the power was increased well beyond this suggested value to further test the abilities of the beam phasing system. During the test, no visible damage to the couplers was observed, but there appeared to be some performance degradation at the highest powers at which point the power was not increased.

Figure 54 presents the data recorded while increasing to higher power levels.

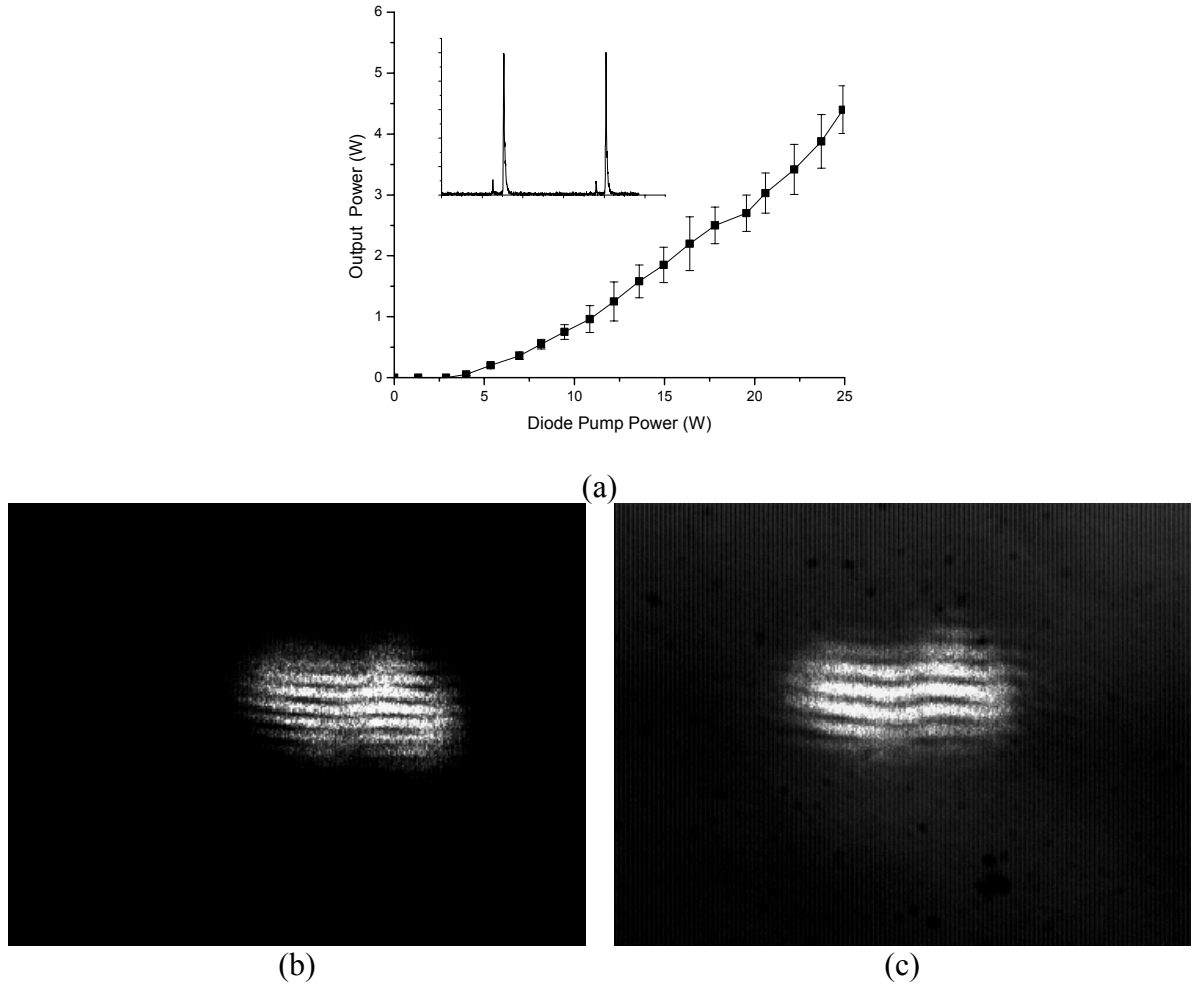


Figure 54: Input-output graphs for two-channel fiber amplifier system using 2:2 fiber couplers. The total power of the two channels demonstrating 4.4 W is shown in (a) and two LSI interference patterns for the higher power are given in (b) and (c).



Here, (a) shows the total output power from both channels and reports a maximum power of 4.4 W. The Fabry-Perot scan inset shows the Stokes (larger peaks) and pump beams recorded during the experiment. Figure 54(b and c) provides data from the LSI used to verify the beam phasing properties at higher power. Although there are still instabilities as evident from the error bars in Figure 54a and observed as LSI variation, the signal is less noisy as the power level is increased. This is best demonstrated by observing the relative error (standard deviation/average power) as the diode pump power is increased, as shown in Figure 55.

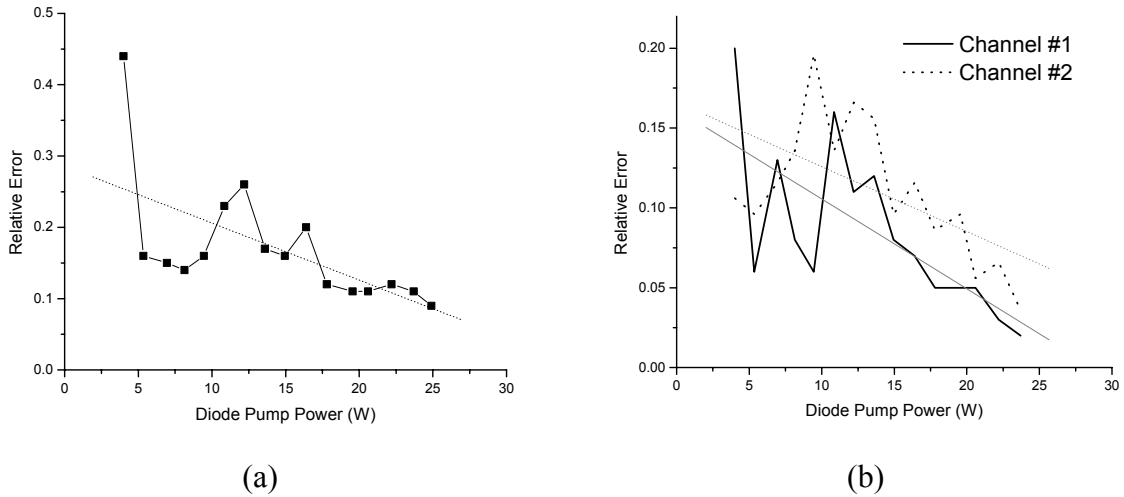


Figure 55: Relative error vs. diode pump power for (a) the total two-channel output power in the TFP leg and (b) each channel's SBS beam as collected using beam pick-offs. A linear fit is included for each of the data sets.

The first figure (a) shows the relative error collected from the total output power of both channels after the reflection from the thin film polarizer. Figure 55b provides the relative error observed from each channel's SBS beam which is collected from the beam pick-off as shown in Figure 46. Both data sets demonstrate a trend that the system noise

decreases as the power is increased. This is encouraging in respect to the previous discussion on the instabilities at lower powers. It is likely that, as desired, increasing the total system power allows both channels to generate a Stokes beam even though the 2:2 coupler is randomly channeling the percentage of power between the outputs. The total system output still fluctuates 10%, but this is reasonable and may improve even more at higher powers. As a final indication of the higher power improvement, Figure 56 presents the power vs. time from each of the SBS pick-offs. Although one channel is producing more Stokes output, the relative noise is much improved from the lower power result of Figure 53. The output power ‘tracking’ discussed above does not appear to occur in this higher power data.

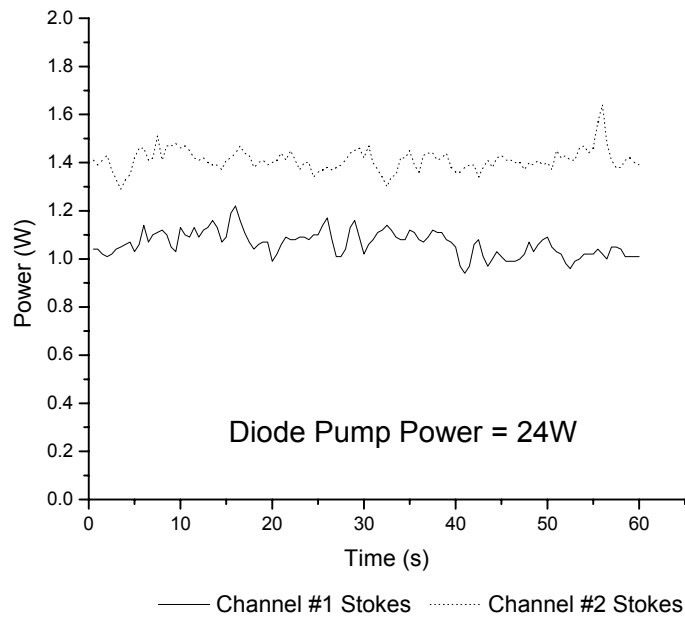


Figure 56: SBS power measured for both channels at 24 W of diode pump power. The power is calibrated from the two surface Fresnel reflection of the beam pick-off.

The work presented in this section extends SBS beam phasing exploration to include 2:2 fiber couplers. In order to scale SBS beam phasing technology to a greater number of channels and higher power, it is necessary to improve the performance available when using N:1 fiber couplers. In this case, much of the power is lost in the unused/terminated output ends. However, using an N:N coupler, such as the 2:2 data of this section, offers improved efficiency. The fiber couplers still suffer from strong channeling between the output ends resulting in instabilities at lower power. At higher power, the relative error decreases and the effect of the random coupler output channeling appears to be less significant. The output at the highest power presented in this section (4.4 W) still had some instabilities observed by the 10% relative error and as some LSI fringe fluctuation, but the general approach for beam phasing appears viable.

#### **4.2.6. Discussion**

This section investigated SBS beam phasing of a two-channel master oscillator fiber power amplifier using a long multimode fiber. A variety of experiments were performed to demonstrate the capabilities and diagnose the limitations of such an approach to power scaling. The results obtained in this work provide a framework and motivation to pursue SBS beam phasing as a feasible approach to phasing multiple channel amplifiers.

One major contribution of the work was the demonstration of piston error conjugation using a long multimode fiber. All previous work in SBS beam phasing used either an optical cell or short multimode fiber to generate a full transverse phase conjugate. While this is desirable for its ability to also correct for amplifier-induced aberrations, it is limited in that high peak powers are necessary to reach SBS threshold. Because of this,

all previous experiments were accomplished using pulsed lasers.<sup>77,84</sup> This work uses a long multimode fiber to reduce the threshold to levels obtainable using cw laser sources. This extension of SBS beam phasing to cw applications increases the potential for such a system. The SBS beam generated in a long multimode fiber does not produce a full spatial phase conjugate, but instead corresponds to the fundamental  $LP_{01}$  mode of the fiber through beam cleanup.<sup>22</sup> This work demonstrates, for the first time, that piston error conjugation necessary for SBS beam phasing is achieved using a long multimode fiber.

The piston error conjugation property of the long multimode fiber was exploited to provide the first phasing of two cw amplifier channels using an SBS fiber. A system demonstrating over 475% gain with a maximum output power of 5.3 W was developed. This result helps to progress the technology as a usable approach for laser power scaling.

This section also investigates the use of biconically fused fiber couplers to combine the inputs from multiple amplifier channels into the SBS medium. SBS beam phasing was also observed in configurations utilizing the fiber couplers. There were, however, some stability issues associated with the fiber couplers that were discussed and diagnosed in this section.

Although the long multimode fiber conjugated the piston error, it would be beneficial to reduce the fiber length to achieve full spatial phase conjugation as well. In the work of this section, the overall system efficiency was dependent on optically aligning the return Stokes beam for the second pass through the amplifier. If a spatial phase conjugate is achieved, this second pass coupling would be automatic due to the wavefront reversal of spatial phase conjugation. This should improve the overall efficiency and effectiveness of the scheme. In order to keep the SBS beam phasing accessible to cw applications, it is

necessary to examine techniques for reducing the SBS threshold so that a Stokes wave pumped by a cw laser system is generated in a short fiber ( $< 10$  m). This is one of the topics investigated in Section 4.3.

### ***4.3. SBS Beam Phasing using a Gain Fiber***

The SBS beam phasing work presented in the previous section provided the first successful phasing of a two-channel master oscillator fiber power amplifier. In the work, a long fiber was used so that the SBS threshold was reduced to allow investigation using a cw laser source. The long fiber successfully conjugated the piston phase error between the two amplifier channels and effectively phased the two-pass outputs. When using a long fiber for SBS beam phasing, the Stokes beam is generated in the  $LP_{01}$  mode and the system must be accurately aligned to couple this return beam for a second pass through the fiber amplifier and out of the system. The inability to generate a full spatial phase conjugate beam limited the performance. Expanding the work of the previous section to include a full spatial phase conjugation would improve the overall system efficiency and also allow for additional methods for increasing the number of amplifier channels.

In order to achieve spatial phase conjugation using an optical fiber, it is necessary to keep the fiber relatively short ( $< 10$  m, see Section 2.3.2). When using a short fiber, the SBS threshold is much higher (compared to previous long fiber work) and pulsed lasers have traditionally been used to achieve the necessary peak power levels. This section explores methods for reducing the SBS threshold so that a short fiber can be used to achieve full spatial phase conjugation while still allowing excitation using a cw laser source. Various techniques for reducing SBS threshold are described and experiments exploring gain fiber SBS reduction are presented.

#### 4.3.1. Background

Reducing SBS threshold is a topic that has received considerable interest in recent years. The particular interest for this research is lowering SBS threshold for optical fiber phase conjugation and amplifier phasing applications. While some work is being done to reduce SBS threshold in an optical cell configuration,<sup>87,88</sup> this discussion is limited to SBS in optical fibers.

As alluded to in the introduction of this section, the first attempt in reducing SBS threshold begins with a review of Equation 2-31 repeated here for convenience,  $P_{th} \approx 21 A_{eff} / L_{eff}$ . The SBS threshold is proportional to the effective area and inversely proportional to the length. Thus, if either the length of the medium is increased or the diameter of the core is decreased, the SBS threshold will decrease. Decreasing the fiber core diameter is not a practical approach for high power applications. One advantage of using an optical fiber is that it is easy to obtain lengths of several kilometers. For example, Cotter demonstrated SBS thresholds as low as 5 mW using a 13.2 km single-mode fiber of core diameter 9  $\mu\text{m}$ .<sup>89</sup> Threshold values in the tens of milliwatts for multimode fibers of multiple kilometers are common in the literature.<sup>22,23,90</sup> In fact, the second-order Stokes threshold (the first order Stokes acts as the pump) is reported as 273 mW for a 4.4 km, 9  $\mu\text{m}$  core multimode fiber.<sup>53</sup> One thing that should be emphasized, however, is that for very long fibers ( $\gg 10$  m), the SBS process does not generate a complete spatial phase conjugate beam. For fibers of kilometer class length, the SBS process serves to clean up the beam and produce a backward propagating Gaussian-like  $\text{LP}_{01}$  mode.<sup>22</sup> This has been discussed extensively in previous sections.

Another method used to reduce the threshold is back-seeding with another laser at the Stokes frequency. Recall that for SBS generation, the initial acoustic wave begins from thermal noise in the medium. If a laser at the Stokes frequency is back-seeded into the nonlinear medium, the wave will more quickly interfere with the incident pump beam and create the acoustic wave via electrostriction. This will serve to reduce the SBS threshold.<sup>20</sup> Along this same line, groups have also developed ‘loop’ configurations to lower the SBS threshold.<sup>22,91</sup>

In a fiber loop scheme, a portion of the back reflected Stokes wave is fed into the back end of the fiber. A simple diagram with this set-up is shown below.

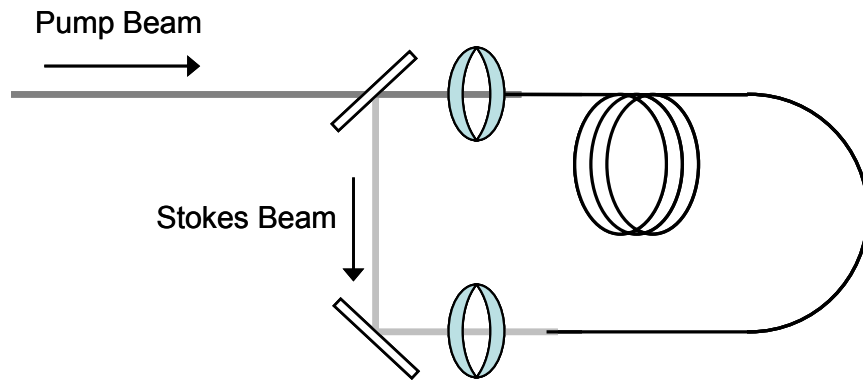


Figure 57: Fiber loop seeding configuration

The feedback provides self-seeding and the SBS Stokes signal increases. Using this technique, an SBS threshold reduction (compared to no feedback) of 26.5 mW to 19.7 mW in the cw pumped long fiber (4.4 km) case<sup>22</sup> and 130  $\mu$ J to 80  $\mu$ J in a pulsed laser short fiber (1 m) case<sup>91</sup> is reported. The laser used in the second experiment was an Nd:YAG with pulse length of  $\sim 20$  ns. This leads to a peak power threshold of  $\sim 4$  kW. While the fiber loop scheme certainly reduces the SBS threshold, the goal is to obtain a



threshold in short fibers so that a phase conjugate wave would be achievable by cw lasers in the  $< 10$  W regime.

Another method for SBS threshold reduction is using internally tapered fiber. This configuration, as demonstrated by Heuer and Menzel,<sup>92</sup> is shown in Figure 58.

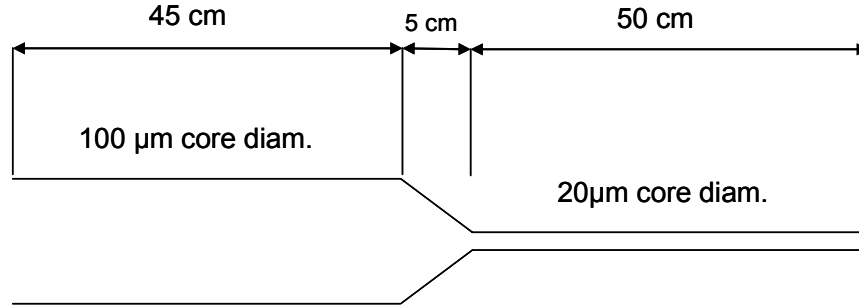


Figure 58: Tapered fiber geometry for SBS threshold reduction

Here, the smaller core has a lower SBS threshold and serves as the generator for the system. The larger outer core allows effective coupling of higher power into the fiber and amplifies the Stokes wave generated in the smaller core. For this experiment, the length of the larger core section was 45 cm long, the taper was 5 cm long, and the smaller core length was 50 cm. A SBS threshold of 15  $\mu$ J (peak power  $\sim 500$  W from Nd:YAG, 30 ns pulses) was observed. This configuration demonstrated a reflectivity of 92% and a phase conjugate fidelity larger than 95%.<sup>92</sup>

The most significant breakthrough in reduction of the SBS threshold was accomplished recently by a research group at the University of Potsdam, Germany.<sup>93,94</sup> Instead of using a standard passive fiber, a fiber amplifier was used for the SBS medium.

The gain induced by pumping with broadband diode laser light allowed for the reduction of SBS threshold. The essential components of the experiment are shown in Figure 59.

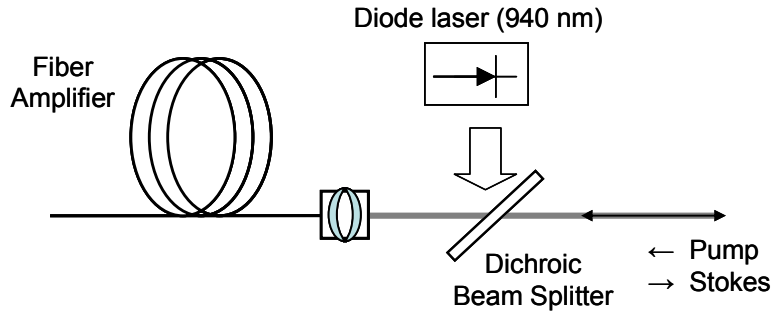


Figure 59: Basic implementation of a phase conjugate fiber amplifier

For this experiment, the active core diameter was  $47\text{ }\mu\text{m}$  and was Yb-doped with a concentration of 2200 ppm.<sup>93</sup> The group previously tried a higher doping concentration of 6500 ppm and found that the higher doping concentration produced worse reflectivity characteristics as well as a greater propensity to fiber damage.<sup>94</sup> A Q-switched Nd:YAG laser operating at 10 Hz with a variable pulse width of 30 – 100 ns was used along with two different fiber lengths. Initially a 20 ns pulse length was used with 2 m of fiber to produce a threshold of 3  $\mu\text{J}$  and SBS reflectivity greater than 100%. However, this case was not ideal because the short fiber only absorbed 11 W of the available diode power. A longer fiber (10 m) absorbed all 20 W of the available diode power resulting in an SBS threshold of 0.5  $\mu\text{J}$ , a reflectivity of 1000%, and phase conjugation fidelity  $> 90\%$  for 100 ns laser pulses.<sup>93</sup> The SBS threshold corresponds to  $\sim 5\text{ W}$  of peak power. Because of the significance of the findings in this paper, the results are summarized below in Table 8. It is the results of this paper that provided the motivation to investigate using a multimode fiber amplifier for cw SBS beam phasing.


Table 8: Summary of work by Heuer using a fiber amplifier for SBS phase conjugation

fiber	Pump pulse	Abs. diode power	R	Fidelity	Threshold
2 m	30 ns	11 W	>100%	no report	3 $\mu$ J, 100 W
10 m	100 ns	20 W	>1000%	$\sim$ 0.9	0.5 $\mu$ J, <b>5W</b>

#### 4.3.2. Ytterbium-Doped Multimode Fiber Investigation

Based upon the SBS threshold reduction results of Heuer *et al.*,<sup>93</sup> a custom, double-clad, Yb-doped multimode fiber was produced for this research. Table 9 lists the specifications for the fiber manufactured by Nufern (MM-YDF-50/400, FUD-3359). Developing this fiber led to a twofold investigation of both the SBS properties of the fiber and the performance as a multimode fiber amplifier. This section provides the detail of these two investigations.

Table 9: Specifications for Yb-doped multimode fiber

Fiber Length	55 m
Core Diameter	50 $\mu$ m
Inner Clad Diameter	400 $\mu$ m
Absorption, 915 nm	2.0 dB/m
Core NA	0.20
Cladding NA	0.46
Octagonal shape	

As shown in Table 9, the total length of the Yb-doped multimode fiber was 55 m. To determine the appropriate length of fiber to use for the experiment, several factors need to be considered. Because one part of this investigation was to examine SBS threshold using a cw source, it is desirable to keep the fiber as long as possible to reduce SBS threshold. In gain fibers, however, there is not a direct correlation. For example, the

absorption of both the diode pump power and the SBS pump (or seed that will be used so as to avoid ‘pump’ confusion) require consideration.

Figure 60 shows the Ytterbium absorption spectrum and includes a close-up of the region near the seed wavelength for this experiment, 1064 nm.<sup>70</sup>

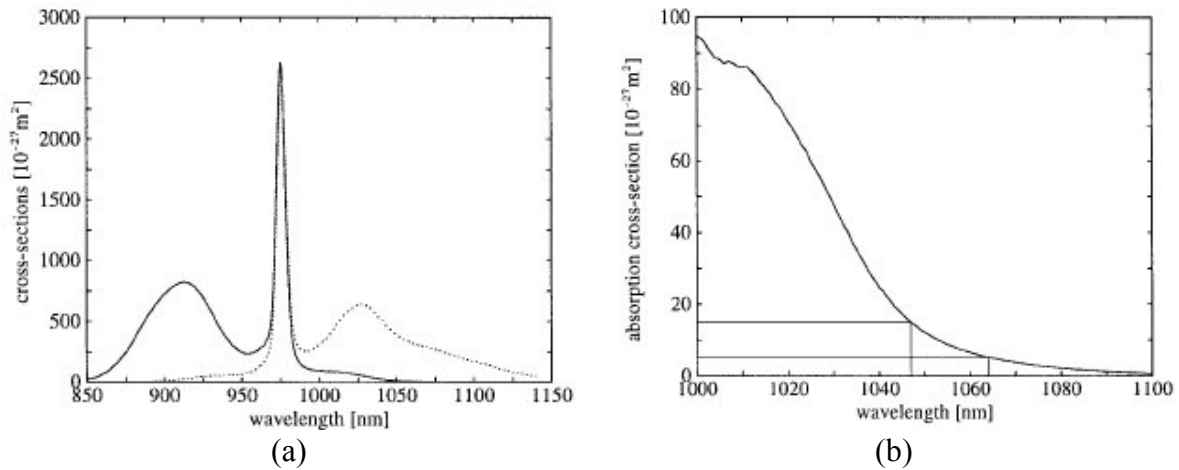


Figure 60: Ytterbium cross sections for (a) absorption (solid) and emission (dotted) and (b) absorption in the region near 1064 nm.

As evident from the graphs, the diode pump (915 nm) absorption cross section is much higher than that of the seed (1064 nm). It is important to keep in mind, however, that the specified diode pump absorption reported in Table 9 (2.0 dB/m) is the ‘effective’ core absorption of the diode light. The diode pump power is coupled into the inner cladding which is shaped to ensure that the power eventually interacts with the doped core so that it can be absorbed. The seed at 1064 nm, on the other hand, is coupled *directly* into the core of the fiber and although the cross section at this wavelength is much lower than the diode pump, significant absorption occurs. The absorption for the direct-core pumping of the 1064 nm seed is estimated to be  $\sim 1$  dB/m.

It is necessary to consider this seed absorption for regions that are not pumped by diode laser power. In this case, the seed will experience loss through absorption which will decrease the amplifier efficiency and also affect SBS threshold. Figure 61 illustrates the absorption of the diode pump power as a function of fiber length. The figure shows two cases when the diode pump power is coupled into (a) only one side or (b) both sides of the Yb-doped multimode fiber. As shown in the graph, 99% of the diode pump power is absorbed within 10 m.

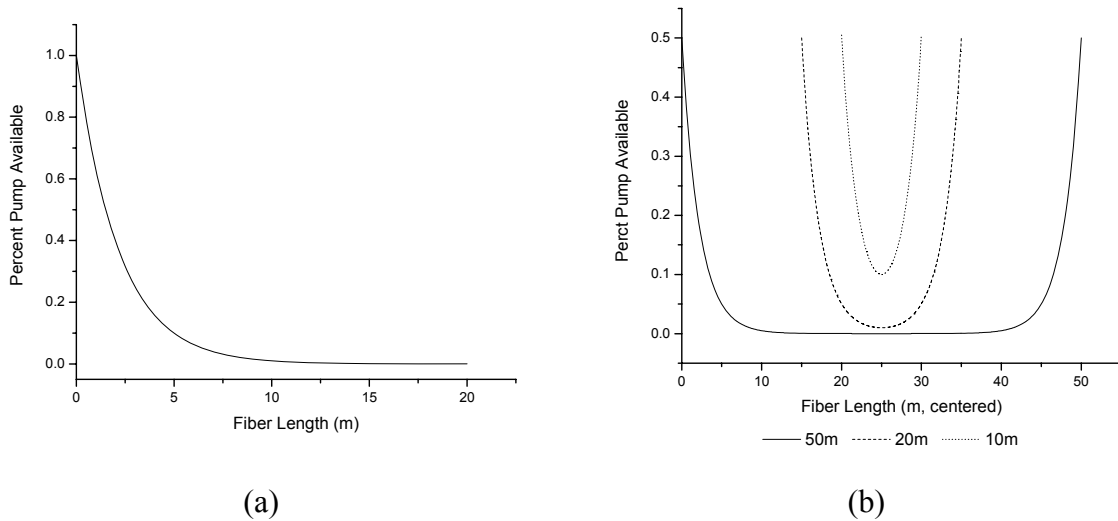


Figure 61: 915 nm diode pump absorption in Yb-doped multimode fiber. Options for coupling diode pump power into (a) only one side and (b) both sides are shown.

Three different lengths (55m, 20 m, 11.5 m) of the Yb-doped multimode fiber were explored in this work. Each of the lengths allowed for exploration of different aspects of the multimode fiber amplifier performance and SBS threshold. Results obtained with each length are presented following a description of the overall system configuration.

Figure 62 shows the system schematic used for testing all three lengths of fiber.

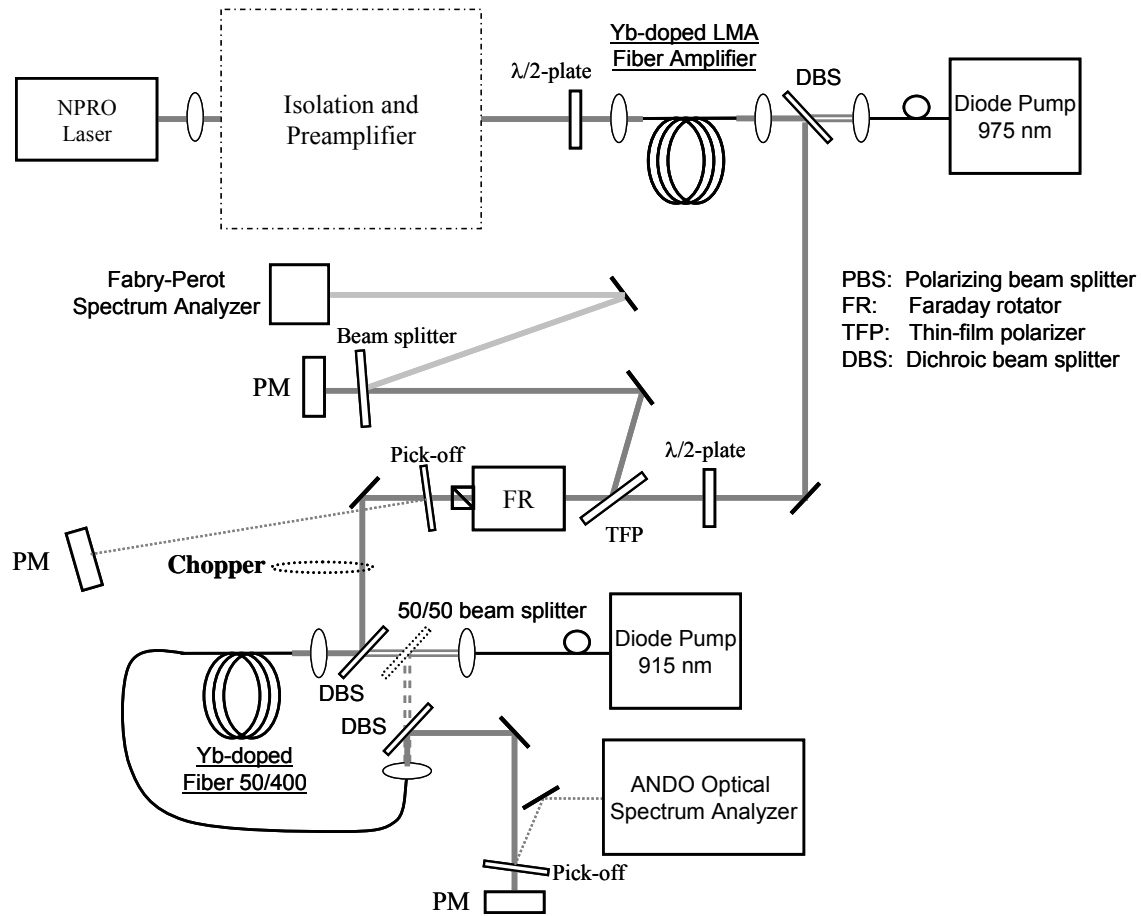


Figure 62: Schematic diagram for investigating 50  $\mu\text{m}$ , double-clad, Yb-doped fiber

A 1064 nm single-frequency NPRO laser was isolated, preamplified, and focused into a Yb-doped large mode area (LMA) fiber amplifier. The LMA fiber amplifier is pumped by a fiber-coupled 975 nm diode laser and outputs a single transverse mode as described in detail in Section 4.1. This beam from the fiber amplifier passes through a thin film polarizer (TFP), Faraday rotator, and polarizing beam splitter which serve to isolate the amplifier and to separate the return Fresnel reflection/Stokes beam. The beam pick-off shown following the Faraday rotator was also used to monitor the backwards propagating beams. Although the data that follows displays the power recorded in the leg following

the TFP, the information from this pick-off was recorded and consistently displayed identical trends. The optical chopper displayed in Figure 62 was only used for a few of the experiments and these are indicated in the discussion below. The seed was coupled into the multimode gain fiber using a 16X ( $f = 11\text{mm}$ ) aspheric lens. Initially, both ends of the fiber were cleaved normally, but oscillation was observed (see below) so the back end of the fiber was angle cleaved at  $\sim 8^\circ$  which suppressed the oscillation. The front end of the fiber was kept as a normal cleave to simplify input coupling.

The multimode Yb-doped fiber is pumped by a fiber-coupled 915 nm diode laser system. The laser system provides up to 35 W of power through its  $200\text{ }\mu\text{m}/0.2\text{ NA}$  fiber core. Figure 63 provides the input-output characteristics for this diode laser.

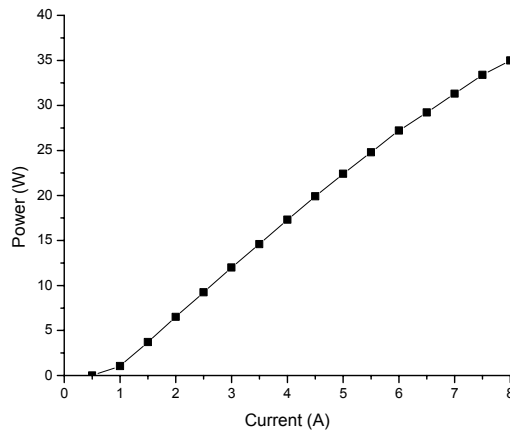


Figure 63: Current vs. output power for the Polaroid 915 nm fiber-coupled diode laser.

As shown in Figure 62, two variants for coupling the diode light into the fiber were used. The first method simply pumped the front end of the fiber via a dichroic beam splitter. The system could also be configured such that the output power of the diode laser was split using a 50/50 beam splitter. In this case, the Yb-doped multimode fiber was

pumped from both ends using two dichroic beam splitters. The experiments which used double end diode pumping are described below.

Diagnostics were used to observe both the backreflected light, which is reflected from the TFP, as well as the fiber amplifier transmitted output. The power was measured in the TFP leg and a Fabry-Perot spectrum analyzer was consistently running to detect the onset of SBS. For the transmitted fiber amplifier end, the power was measured and an ANDO optical spectrum analyzer was used to record the output spectrum.

The first fiber length tested was the full spool of fiber, 55m. The system was configured as shown in Figure 62. The Yb-doped multimode fiber was pumped by the diode laser through the front end only and the optical chopper was not used with this length. Data was collected holding the single-frequency seed input constant and increasing the diode pump power to record the amplifier performance and look for SBS threshold. The multimode fiber amplifier output and measured TFP power are presented in Figure 64a and b, respectively.

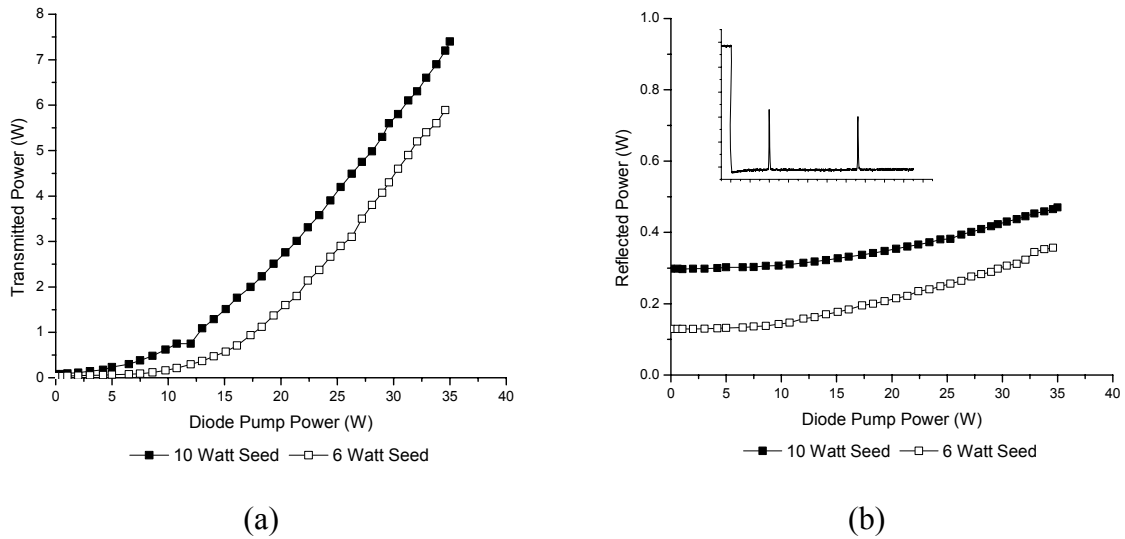


Figure 64: Data for 55m of Yb-doped multimode fiber. The (a) amplifier performance and (b) backreflected power for two different 1064 nm seed powers.



The data are presented for two different seed power levels of 6 W and 10 W. For the fiber amplifier data of (a), a maximum power output of 8 W was achieved. The primary source of the poor performance is the strong absorption of the seed beam in the unpumped regions of the fiber. Recall that the diode laser power is essentially absorbed within the first 10-20 m of the fiber so that the remaining unpumped portion of the fiber absorbs the seed and reduces the amplifier performance.

The backreflected power in Figure 64b indicates that SBS threshold was not achieved. The inset Fabry-Perot scans shows only the pump (seed) peak of the Fresnel reflection from the fiber facet. If a Stokes beam is generated, a sharp knee in the input-output curve would be observed and a strong frequency shifted Fabry-Perot peak would be visible. The slope of the slight knee visible in the two lines in Figure 64b is only  $\sim 0.7\%$  and is related to an increase in amplified spontaneous emission (ASE), not SBS.

When both ends of the 55 m fiber were normally cleaved, the Fresnel reflections from the fiber ends provided sufficient feedback to initiate oscillation. Figure 65 records this observation using the optical spectrum analyzer. The first figure (a) is taken at a seed power of 5.2W and a pump power of 6.5 W. The figure shows the residual pump beam at 915 nm, the amplified seed beam at 1064 nm, and a significant contribution from ASE. The inset figure is a comparative Yb-doped fiber ASE spectrum previously reported by Sousa *et al.*<sup>95</sup> Figure 65b shows the output spectrum with the same seed power, but with 15 W of diode pump power. In this case, an additional peak in the output spectrum is observed at 1094 nm and an increase in the power was recorded. To prevent the oscillation, as required for amplifier and SBS applications, the back end of the fiber was cleaved at  $\sim 8^\circ$ . This reduced the feedback and prevented oscillation in the remaining

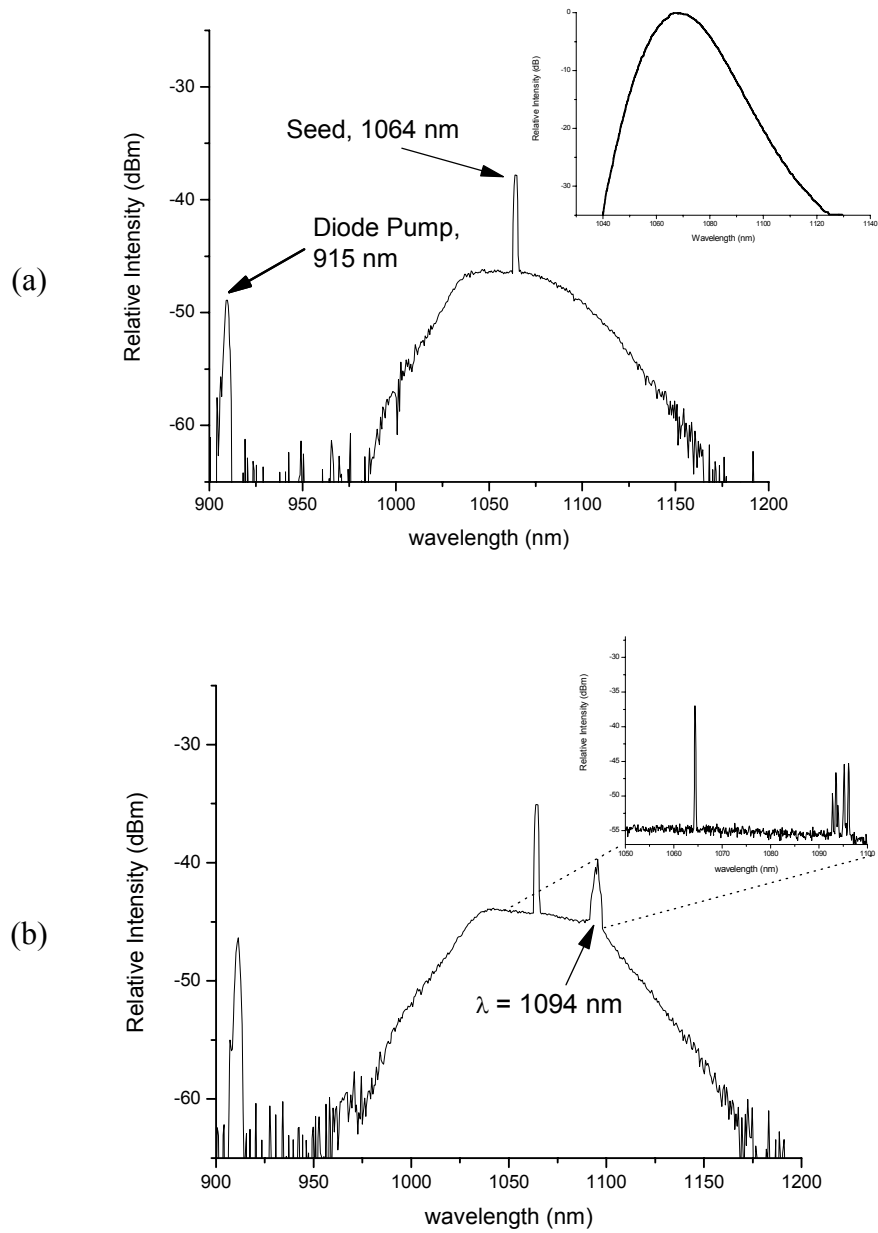


Figure 65: Output spectrum for 55 m, Yb-doped multimode fiber amplifier. The figure illustrates the necessity of angle cleaving the fiber to prevent self-oscillation.

experiments. For very high diode pump power experiments, it may be necessary to angle cleave both ends of the fiber to prevent oscillation, but the front end of the fiber was kept as a normal cleave to facilitate the seed laser coupling.

The relatively poor performance of the fiber amplifier and inability to reach SBS threshold using the full spool of gain fiber led to an exploration using a shorter fiber length, 20 m. This fiber length was used in a variety of tests including diode pumping the fiber from both ends and using an optical chopper.

Figure 66 displays the transmitted and backreflected power using a 10 W input seed and diode pumping from either one or both ends of the multimode gain fiber.

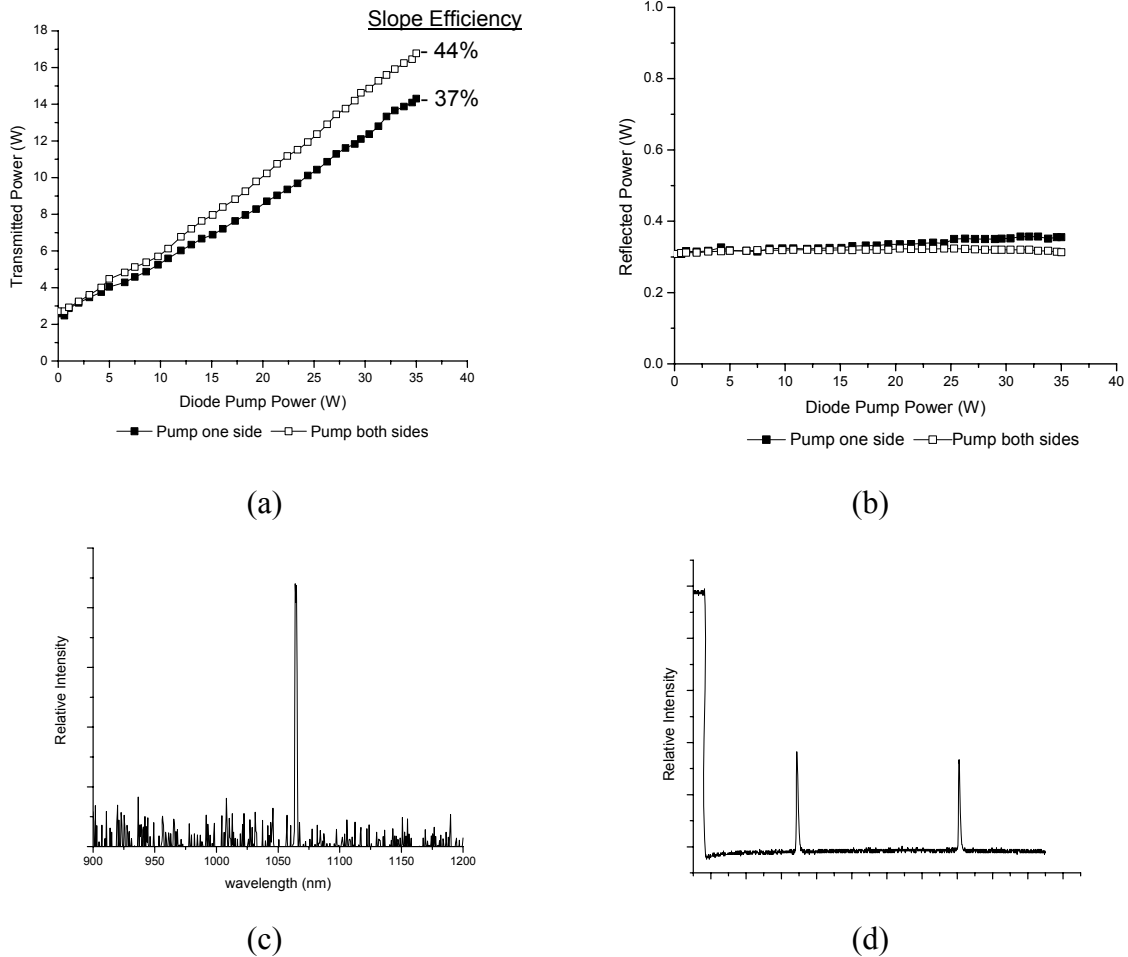


Figure 66: Data for 20 m of Yb-doped multimode fiber. The (a) amplifier performance and (b) backreflected power for front end and both end diode pumping. The fiber amplifier output spectrum and Fabry-Perot spectrum for the dual pumping are included in (c) and (d), respectively.

When the outputs from the two different diode pumping schemes are compared, it is evident that the more uniform pumping provided from both ends of the multimode fiber results in better performance. The slope efficiency for this case was 44 % vs. 37 % for front end only diode pumping. The maximum output achieved in this configuration was 16.8 W and the spectrum at this power level is shown in Figure 66c. As evident from the (b) backreflected power graph and the (d) Fabry-Perot spectral scan recorded at the highest power, a Stokes beam was not generated.

At the onset of this investigation, it was hoped that it would be possible to reach SBS threshold using a cw laser beam around 5 W which corresponds to the peak power SBS threshold observed by Heuer *et al.*<sup>93</sup> Their work for this result, however, used a pulsed laser with a 10 Hz rep rate and 100 ns pulses. This corresponds to a duty cycle (pulse length times rep rate) of  $1 \times 10^{-6}$ . In this case, the gain experienced by the short pulses is higher than the cw case due to the lessened effect of gain saturation. Specifically, the gain for a laser pulse begins at the small signal value for the leading edge of the pulse and decreases for the remainder of the pulse as the gain saturates.<sup>96</sup> In the work of Heuer *et al.*, the gain experienced by their pulsed source was sufficient to reach SBS threshold. For the cw case, the saturated gain did not amplify the input beam to the required levels to initiate a Stokes beam.

As an attempt to shorten the duty cycle and reduce the effects of gain saturation, an optical chopper (Stanford Research SR540) was used in two configurations. Table 10 gives the details of the two chopper configurations. In each case, the duty cycle is fixed by the positioning of two chopping blades and the ‘pulse’ length is controlled by the chop rate. A sample output for each duty cycle is provided in Figure 67.

Table 10: Optical chopper configuration for 20 m Yb-doped multimode fiber experiment.

Duty Cycle	Chop Rate	'Pulse' Length
50 %	2kHz - 3.5 kHz	140 $\mu$ s – 250 $\mu$ s
3 %	200 Hz - 450 Hz	70 $\mu$ s – 150 $\mu$ s

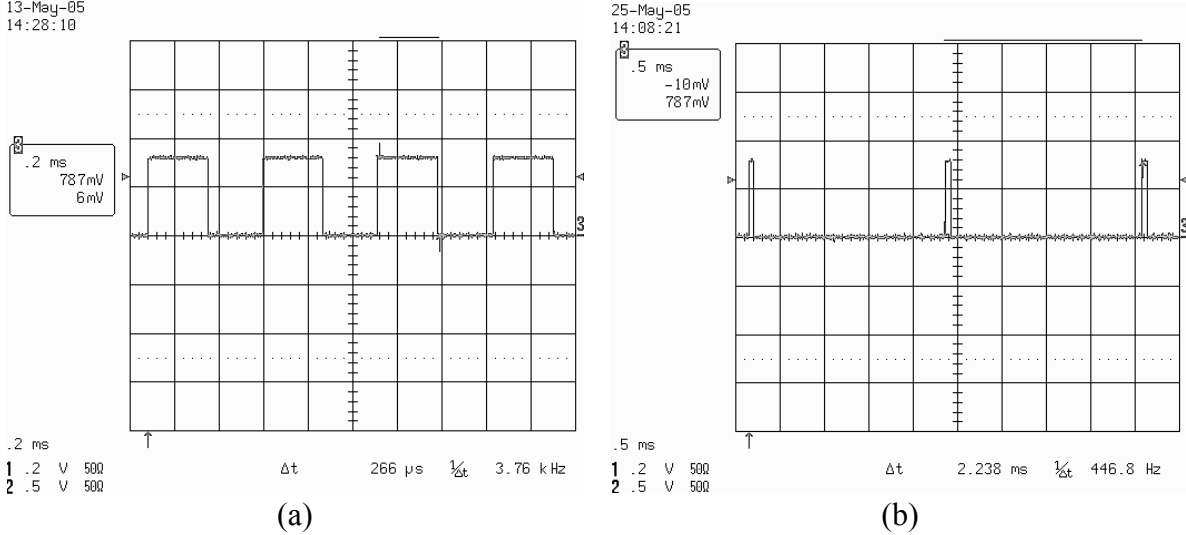
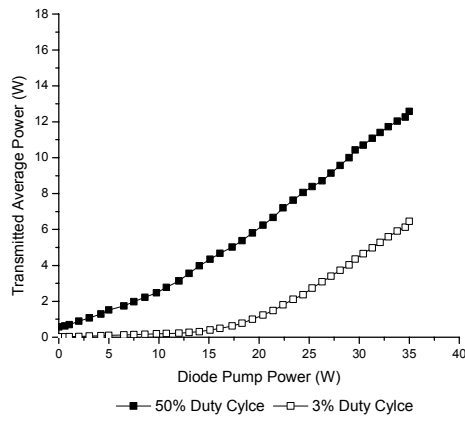
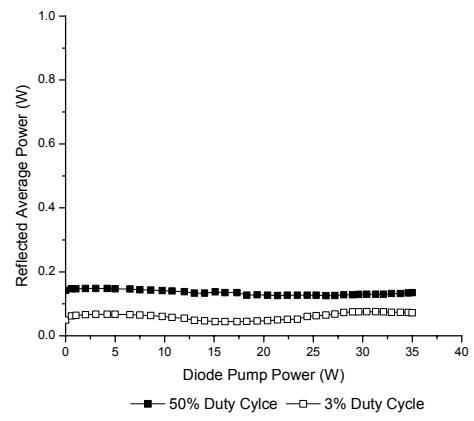


Figure 67: Duty cycle plots for chopper testing. The plots are recorded from the optical chopper output monitor and show both (a) 50% and (b) 3 % duty cycle.

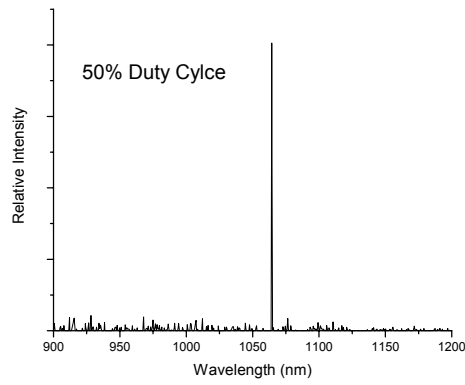
A 10 W input seed was again used in the data of Figure 68, but in this case, the input beam was mechanically chopped. For the plots, the seed power and chop frequency were kept constant while the diode power was increased. While the chop frequencies for these plots of 50% and 3% duty cycle were 2 kHz and 180 Hz, respectively, the system was tested using the full frequency range listed in Table 10. Figure 68a and b provide the average power of the fiber amplifier output and backreflected power. The output spectrum and Fabry-Perot result for each chop frequency is also included in the figure. It was possible to monitor the backreflected signal with the Fabry-Perot by observing the output when a scan effectively captured a ‘pulse’ from the chopper.



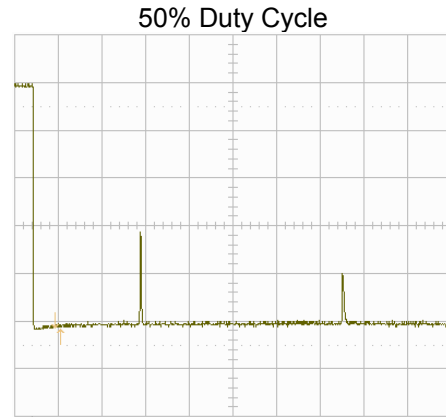
(a)



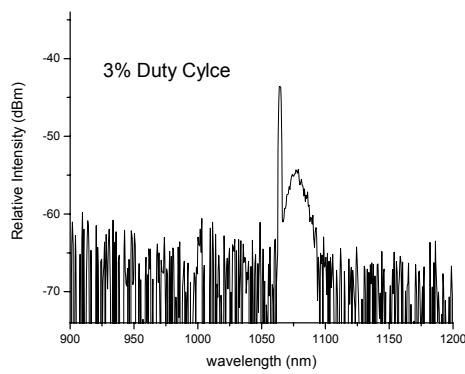
(b)



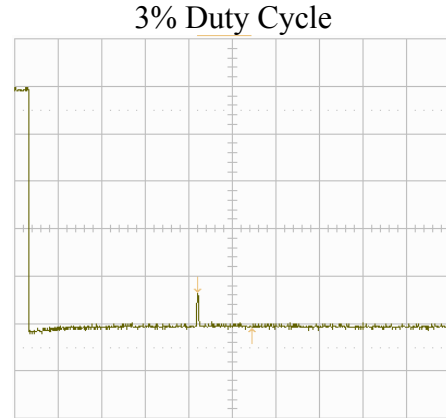
(c)



(d)



(e)



(f)

Figure 68: Data for 20 m of Yb-doped multimode fiber using an optical chopper. The (a) amplifier performance, (b) backreflected power, output spectrum, and Fabry-Perot scan for duty cycles of (c,d) 50% and (e,f) 3% are recorded.

Using the mechanical chopper allowed testing with a duty as low as 3% and a pulse length as short as 70  $\mu$ s, but both values are orders of magnitude away from that demonstrated by Heuer *et. al.*<sup>93</sup> and the reduced gain from the saturated amplifier was not sufficient to reach SBS threshold.

The initial two fiber lengths of 55 m and 20 m were used in a hope that the longer medium would facilitate the initiation of a Stokes beam in the fiber. Although SBS threshold was not achieved in the experiments, both lengths were tested as a multimode fiber amplifier. The final fiber test length was 11.5 m. Because the fiber was designed such that this length absorbed > 99% of the 915 nm diode pump light, the test provided an optimized configuration for the multimode fiber amplifier and a final attempt to reach SBS threshold.

The 11.5 m length fiber was tested by diode pumping only the front end. Diode pumping from both ends was avoided to protect the fiber coupled diode laser from unabsorbed light coupling back into the laser. Figure 69 shows the fiber amplifier performance and measured backreflected power when using a 10 W single-frequency seed. The fiber amplifier achieved a maximum power output of 19.8 W with a slope efficiency of 49%. The output spectrum at the maximum power is provided in (c) of the figure. As evident from the recorded backreflected power (b) and the Fabry-Perot spectrum analyzer scan (d), SBS threshold was not achieved.

Because fiber lengths in the 10-12 m range are optimal for pump absorption, a few additional experiments were performed to test the characteristics of the multimode fiber amplifier. Specifically, three different seed powers were used to compare their performance. Seed powers of 0.5 W, 1.0 W, and 10 W were tested. For each

measurement, the seed power was held constant and the diode pump power was increased while recording the power output. Figure 70 compares the results of this test.

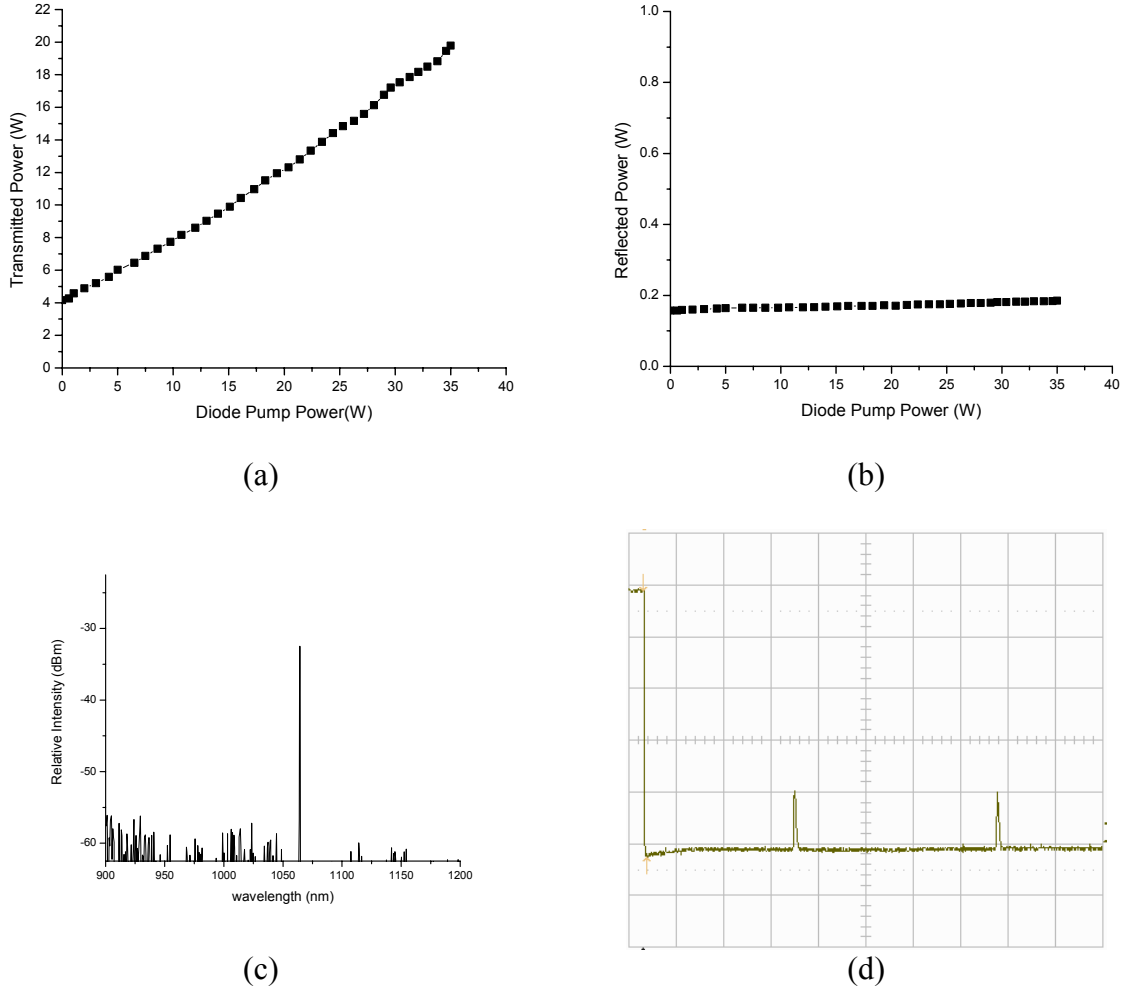
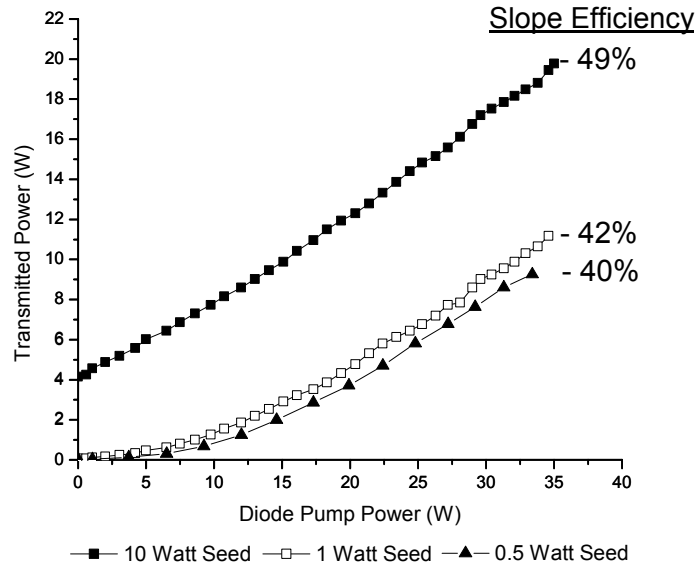


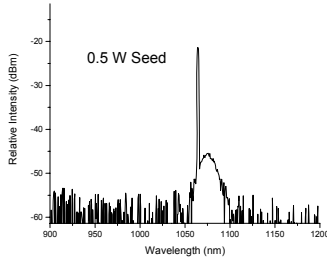
Figure 69: Data for 11.5 m of Yb-doped multimode fiber. The (a) amplifier performance, (b) backreflected power, (c) output spectrum, and (d) Fabry-Perot scan are recorded.

The figure shows the transmitted output power for the three 1064 nm seed powers. As one may expect, the highest seed power corresponds to a highest output power and best slope efficiency. At lower seed powers, Figure 70 b and c show an increase in amplified spontaneous emission.

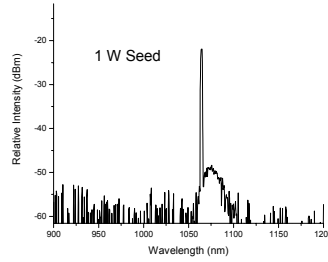




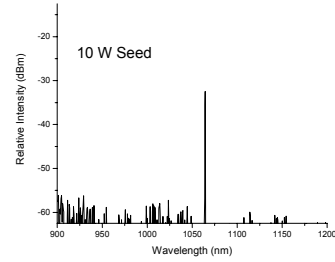
(a)



(b)



(c)



(d)

Figure 70: Data for 11.5 m of Yb-doped multimode fiber with three different 1064 nm seed powers. The (a) amplifier performance and output spectrum are provided for seed powers of (b) 0.5 W (c) 1.0 W and (d) 10.0 W.

As a final test, the diode pump power was held constant at 26 W, the 1064 nm seed was varied, and the effect on output powers were recorded in Figure 71. As shown in the graph, increasing the seed power linearly increases the output power. The experiment also confirmed the increased amplified spontaneous emission at lower seed powers which was observed in Figure 70. The effect was observed in the backreflected power as shown in Figure 71b. The power dip in the graph is a result of increased ASE at the lowest seed

powers. This change in ASE contribution was also observed using the spectrum analyzer. At the higher seed powers, the ASE is reduced as presented in Figure 70d. The ASE also increases if the input seed alignment is purposely misaligned so that only a fraction of the power is coupled into the core of the multimode fiber.

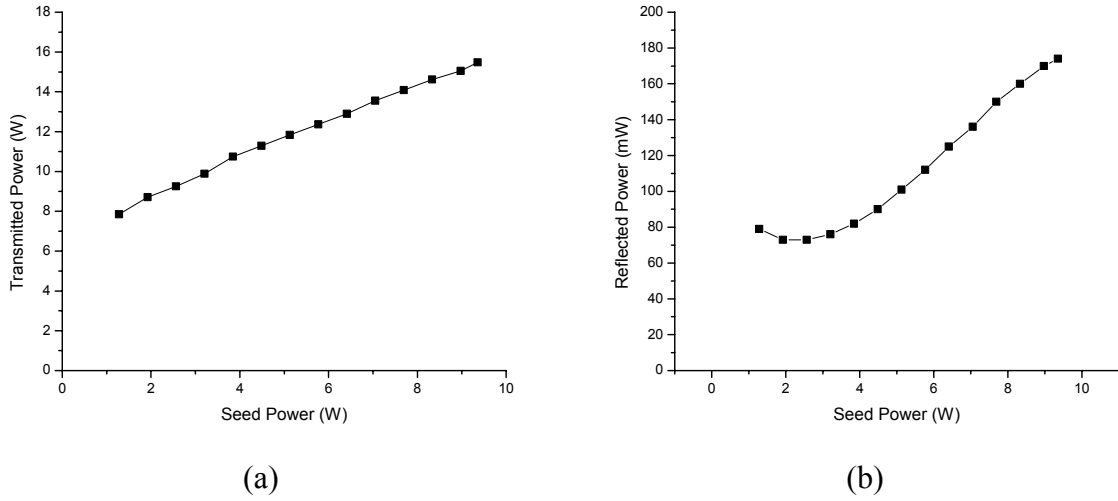


Figure 71: Data for 11.5 m of Yb-doped multimode fiber varying seed power while keeping diode pump power constant at  $P_{\text{pump}} = 26$  W. The (a) amplifier performance and (b) backwards propagating power are presented.

The experiments using 11.5 m of fiber served as the final test length of the multimode gain fiber. The next section tabulates some of the results and includes a discussion on reaching SBS threshold using optical gain fiber.

### 4.3.3. Discussion

The work presented in this section detailed the investigation of a Yb-doped multimode gain fiber. The intent of the work was twofold; the first goal was to test and

characterize the performance of the custom-designed fiber as a single-frequency amplifier. The second objective was to test the system for SBS threshold and verify generation of an SBS Stokes wave using the fiber.

The results of the fiber amplifier tests are included in the different investigations of the fiber lengths presented above. To summarize amplifier results for the three lengths tested, Figure 72 shows the front-end pumped performance of the different lengths with a 1064 nm seed power of 10W. The best performance was achieved using an 11.5 m length of the gain fiber. With this fiber, 19.8 W of single-frequency output power was achieved with a 49% slope efficiency.

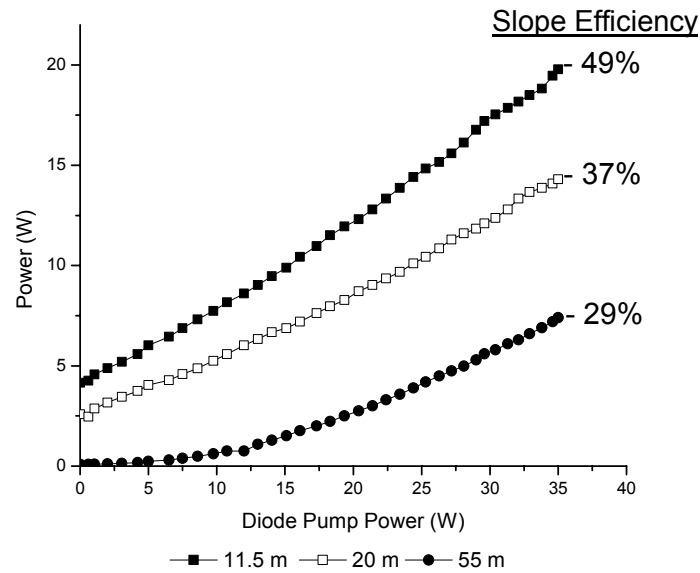


Figure 72: Yb-doped multimode fiber amplifier performance comparison for three fiber lengths: 11.5 m, 20 m, and 55 m.

The work in this section also investigated the effects of dual-side diode pumping, changing seed power, and seed chopping on amplifier performance. The results of this work provide a baseline for future experiments utilizing multimode fiber amplifiers.

The other main aspect of this section was investigating SBS threshold for the gain fiber. From the discussion of Section 4.2, it is desirable to use a short multimode fiber for SBS beam phasing. The spatial phase conjugate achieved when using a short multimode fiber is desirable to increase the SBS beam phasing efficiency as well as to allow new coupling methods for extending the work to more channels. For this work, SBS threshold was not observed in the experiments.

The motivation for pursuing gain fiber based SBS threshold reduction stemmed from the work of Heuer *et. al.* in which they achieved SBS threshold using a 10 Hz Q-switched laser with 100 ns pulses (duty cycle  $1 \times 10^{-6}$ ).<sup>93</sup> The threshold in this work corresponded to a peak power of 5 W and it was hoped that it would be possible to generate a Stokes beam with a similar amount of cw power. The cw diode pumping and low pulse duty cycle of the Heuer experiment provided enough gain to the short pulses to generate a Stokes beam. Although a greater peak power was tested for the cw case ( $\sim 10$ W), the reduced gain from the saturated amplifier was insufficient to reach SBS threshold.

The inability to generate a Stokes beam with a Yb-doped gain fiber corresponds to results published during this investigation.<sup>72,73,97</sup> The most notable of the publications is a paper demonstrating 264 W of single-frequency, single-mode, cw output power from 6.5 m of LMA, 25  $\mu\text{m}$  core diameter, Yb-doped fiber. SBS was not observed in this experiment and the limiting factor was available diode pump power.<sup>73</sup> The same group later used 9 m of 43  $\mu\text{m}$  Yb-doped fiber for a single-frequency amplifier and achieved over 500 W before reaching SBS threshold. The amplifier output in this experiment was no longer diffraction limited but had a measured  $M^2$  of 1.6.<sup>97</sup> For both experiments, the

SBS threshold is much higher than predicted by the simplest models.<sup>21</sup> A few different explanations are offered for the significant increase in SBS threshold.

Jeong, *et. al.* suggests that the increase in SBS threshold is a result of a decrease of the Brillouin gain due to the composition of the fiber or broadening of the Brillouin gain due to strain and temperature gradients in the fiber. They suggest that the most significant contribution is a strong temperature gradient that reduces the SBS gain by a broadening process.<sup>73</sup> To further understand the temperature broadening process an analytical model was developed.<sup>98</sup> Some details of the model are now discussed so as to apply the results to our investigation using the 50  $\mu\text{m}$  gain fiber.

The analytical model developed by Kovalev *et al.*<sup>98</sup> is based on previous work investigating thermal distribution in double cladding gain fibers<sup>99,100</sup> and the effect of a thermal gradient on Brillouin gain distribution.<sup>101,102</sup> For double clad diode-pumped fiber, the most significant temperature effect is the variation along the length of the fiber (as opposed to radial effects).<sup>99,100</sup> The change in temperature along the length of a fiber is given by<sup>98</sup>

$$\Delta T(x) = \frac{\alpha_p \eta P_p(x) a^2}{2\pi b^3 h}, \quad (4-2)$$

where  $\alpha_p$  is the pump absorption coefficient,  $a$  is the core radius, and  $b$  is the inner cladding radius. The fraction of pump power converted to heat,  $\eta$ , is approximated as  $\eta \cong (\lambda_{seed} - \lambda_{diode}) / \lambda_{seed}$ . For the model, single-end pumping is used where the diode laser is coupled into the back end of a fiber length,  $L$ . In this case, the pump power along the fiber is given by  $P_p(x) = P_L(L)e^{-\alpha_p(L-x)}$ . In Equation 4-2,  $h$  is the convective

coefficient. Values near 1 W/m<sup>2</sup>K are used in previous models and the results are presented as a function of this value.<sup>98</sup>

The exponential gain term for the Stokes signal (i.e.  $I_s(0) = I_s(L)e^{G_t}$ ),  $G_t$ , is given by the sum of the exponential laser ( $G_L$ ) and SBS gain ( $G_B$ ).<sup>98</sup> Table 11 presents the symbols along with values used by Kovalev *et al.*<sup>98</sup> in modeling the 264 W single-frequency result of Jeong *et al.*<sup>73</sup> The table also shows values used to extend the model to the fiber used in this dissertation effort.

$$G_t = G_L + G_B \quad (4-3)$$

$$G_L = \ln \left[ 1 + \frac{\gamma P_p(L) P_{st}}{\alpha_p P_s(0)} (1 - e^{\alpha_p L}) \right] \quad (4-4)$$

$$G_B = \frac{g_B}{4S} \int_0^L \frac{[P_s(0) + (\gamma / \alpha_p) P_p(L) P_{st} e^{-\alpha_p L} (e^{\alpha_p x} - 1)] \Gamma_B [\Gamma_B + C_\delta \Delta T(x)]}{[(\Gamma_B + C_\delta \Delta T(x))^2 / 4 + (C_f (\Delta T(L) - \Delta T(x)) - \Delta f)^2]} dx \quad (4-5)$$

Figure 73 shows the total Stokes gain vs. pump power for the 264 W single-frequency which was demonstrated by Jeong<sup>73</sup> and modeled by Kovalev.<sup>98</sup> A few different values for  $h$  are provided, but a value of  $\leq 1$  is expected.<sup>98</sup>

In the experiment, a total diode pump power of 390 W was used to generate the 264 W output.<sup>73</sup> Figure 73 shows that for convective values of less than 2, the exponential Stokes gain is below the SBS threshold value  $G_{th} = 20$ .<sup>98</sup> This is consistent with the experimental results of Jeong *et al.*<sup>73</sup> In fact, Kovalev predicts that a pump power of 1850 W may be used for this fiber amplifier without initiating a Stokes beam.<sup>98</sup>

Table 11: Summary of symbols used in temperature broadened Brillouin gain

Symbol	Definition	264 W experiment	50/400 $\mu\text{m}$ of this work
$\gamma$	pump to gain conversion coefficient	calculated	calculated
$\alpha_p$	pump absorption coefficient	2 dB/m	2 dB/m
$P_{St}$	saturation power	0.05 W	0.05 W
$P_s(0)$	seed input power	3 W	10 W
$L$	fiber length	6.5 m	11.5 m
$S$	core area	$5 \times 10^{-10} \text{ m}^2$	$20 \times 10^{-10} \text{ m}^2$
$g_B$	SBS gain coefficient	$4 \times 10^{-11} \text{ m/W}$	$4 \times 10^{-11} \text{ m/W}$
$\Gamma_B$	SBS gain bandwidth	40 MHz	40 MHz
$C_\delta$	Brillouin frequency temperature coefficient	-0.2 MHz/K	-0.2 MHz/K
$C_f$	Brillouin bandwidth temperature coefficient	2 MHz/K	2 MHz/K
$\Delta f$	detuning of Stokes emission from theoretical SBS shift at $x = L$	calculated	calculated
$a$	fiber core radius	12.5 $\mu\text{m}$	25 $\mu\text{m}$
$b$	fiber cladding radius	190 $\mu\text{m}$	200 $\mu\text{m}$
$h$	convective coefficient	various	various

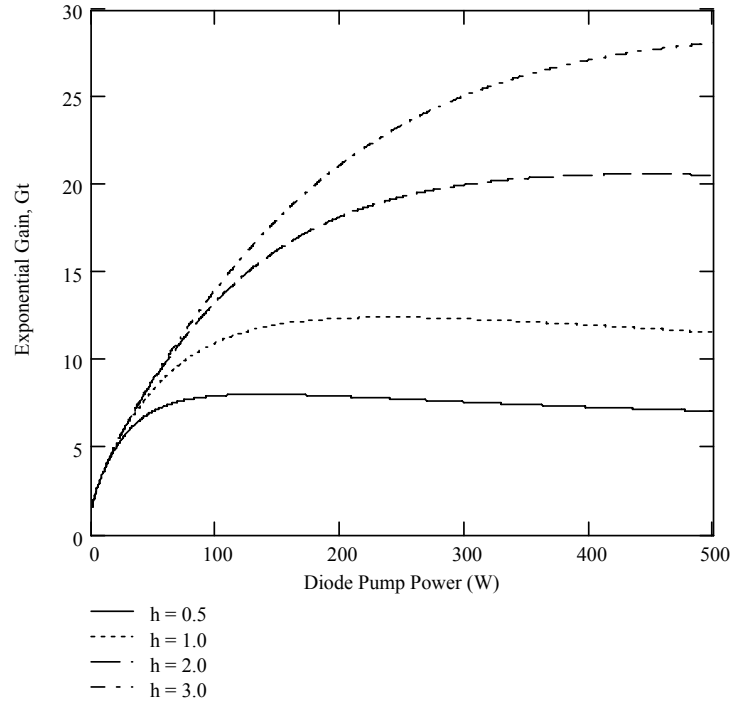


Figure 73: Total exponential Stokes gain ( $G_t$ ) vs. diode pump power for 264 W single-frequency amplifier. A few different value for the convective coefficient are shown.

The same model was used to investigate the inability to achieve SBS threshold discussed previously in this section. As shown in Table 11, the fiber length is slightly longer (11.5 m vs. 6.5m), but the larger fiber core area,  $S$ , suggests less chance of reaching SBS threshold. This is verified in the model results shown in Figure 74.

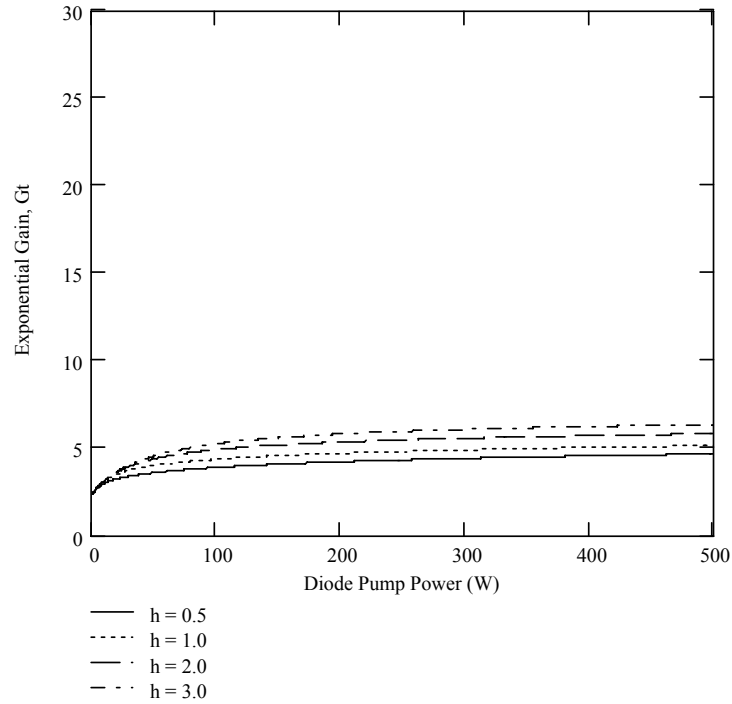


Figure 74: Total exponential Stokes gain ( $G_t$ ) vs. diode pump power for the Yb-doped multimode fiber presented in this section. A few different value for the convective coefficient are shown.

In this case, none of the convective values approach the necessary SBS threshold value of  $G_{th} = 20$ . In fact, with a 10 W seed, it does not appear that this fiber will reach SBS threshold. As the pump power increases, the temperature gradient along the fiber correspondingly increases and makes achieving SBS threshold difficult, if not impossible.

While the increase of SBS threshold due to temperature gradients in gain fibers was not helpful for generating a short, cw-pumped fiber phase conjugator, the result is quite



promising for laser power scaling in general. The most prominent beam phasing techniques (including SBS beam phasing) require a single-frequency source. As discussed in Section 4.1, achieving high power single frequency radiation is not trivial and has been the focus of many investigations. The increase of SBS threshold due to the gradient temperature effect may allow for single frequency amplifiers greater than 1 kW,<sup>97</sup> which would be a significant step to developing very high power laser arrays.

## 5 Conclusions

The objective of this dissertation effort was exploring methods for laser beam brightness scaling using stimulated Brillouin scattering in optical fibers. For this work, two techniques were explored for combining and phasing multiple laser beam channels. The first method exploited beam cleanup and combining using a uniquely designed beam combining system. The second method investigated the use of SBS piston error conjugation in optical fibers to phase the output of double-pass multiple channel amplifier system. This chapter first presents the significant contributions of both techniques followed by recommendations for future work.

### 5.1. *Significant Contributions*

The first method investigated for laser brightness scaling was based upon beam cleanup and combining in long multimode fibers. Previous work has accomplished beam cleanup and two-channel combining using optical fibers with a core diameter up to 50  $\mu\text{m}$ .<sup>54</sup> This work furthered the technique for power scaling by demonstrating beam cleanup in two larger diameter fibers, 62.5  $\mu\text{m}$  and 100  $\mu\text{m}$ . Using larger fibers facilitates coupling a larger number of beams and the increased end-facet surface area distributes the input intensity to allow higher power levels. For multiple-channel beam combining, a technique for efficiently coupling the Stokes beam was designed and tested. The SBS beam combiner provided the first successful demonstration of pump to Stokes power conversion from four-channel SBS beam combination.

This dissertation work also demonstrated, for the first time, phasing of a two-channel cw master oscillator power amplifier using piston phase conjugation in an optical fiber. As part of this effort, a series of different configurations investigated the phasing properties using a long multimode fiber. First, beam phasing was demonstrated using a passive two-channel double-pass geometry. This work was followed by experiments using fiber amplifiers in each of the channels. These experiments demonstrated up to 475% gain with over 5 W of phased output power. This output power level advocates consideration as a viable method for laser power scaling. Specifically, the successful phasing demonstration of two cw amplifier beams with fiber-based piston error conjugation greatly enhances the prospects for phasing of multiple laser amplifiers without complex servo-loop control.

## ***5.2. Recommendations for Future Work***

Laser brightness scaling using SBS properties in optical fibers remains an area for continued development. The investigations as part of this work have fostered the technologies toward the end goal of a fieldable high power laser system, but work remains to be done. Suggestions for future work using a multiple channel SBS beam combiner and SBS beam phasing are discussed below.

### **5.2.1. Multiple Channel SBS Beam Combiner**

As mentioned in Section 3.3, one primary limitation for the four-beam SBS ‘Gatlin gun’ beam combiner experiments was the amount of available power. At the time of the experiment, the maximum available single-frequency power was 2 W. This limited the

ability to firmly establish the operational efficiency of the beam combining experiment. Since the time of the experiment, the necessary Yb-doped gain fiber and fiber-coupled diode lasers were purchased to build single-frequency fiber amplifiers. As demonstrated in Section 4.1 the fiber amplifiers are capable of amplifying a 500 mW seed power to over 13 W while maintaining a diffraction-limited output. This increase in available power should provide insight into the scalability of the beam combining system. Work is currently in progress using the increased single-frequency power to further test the system.<sup>103</sup>

Another difficulty associated with the SBS beam combiner was the need to keep the collimated output of the multiple channel beams parallel with one another. The major contribution to this problem was the poor alignment of the GRIN lens used to collimate the output of the fiber pigtails. Future applications will require strict tolerance for the optical alignment of the output coupling lenses. Also, great care is needed to keep the beams parallel while assembling the fiber pigtail collimators. It is necessary to use shrink-free epoxy and to ensure that the mounting system securely holds the fibers during the curing process. Although vendors were solicited to build a complete, parallel-beam SBS beam combiner as described in Section 3.3, the suppliers were not willing to commit to the required specifications

Scaling to a larger optical fiber will also facilitate coupling the light into the fiber. As with the 62.5  $\mu\text{m}$  and 100  $\mu\text{m}$  fibers used in this work, it will first be necessary to test larger gradient index fibers for SBS beam cleanup. The AFIT nonlinear research group is currently purchasing a 200  $\mu\text{m}$  gradient-index fiber to continue this investigation as well as other beam cleanup experiments.

### 5.2.2. SBS Beam Phasing

Two of the major directions for extending fiber-based SBS beam phasing are shortening the fiber to achieve full spatial phase conjugation and developing coupling geometries for increasing the number of amplifier channels. A few suggestions for each of the topics are presently discussed.

Chapter 4 discussed SBS beam phasing properties using a long multimode fiber as well as the advantage of switching to a short fiber. For example, the long fiber work was dependent on the optical alignment of the Stokes beam for a second pass through the fiber amplifiers. It is likely that the Stokes beam is not completely coupled for the second pass, resulting in a lower system efficiency. If a short fiber ( $< 10$  m) is used for the experiment, a more complete spatial phase conjugation is achieved and the second-pass beam will couple more efficiently due to the wavefront reversal property of phase conjugation.

One difficulty when using a short fiber is that the SBS threshold is much higher and more difficult to obtain using a cw source. A few options for reducing SBS threshold will be discussed shortly, but as the single-frequency output from high power fiber amplifiers continues to increase, it may be possible to generate an SBS beam in a standard silicon-based fiber. Equation 2-31 provides an estimation of the SBS threshold. Using the same fiber parameters listed in Table 2, Figure 75 presents the SBS threshold vs. length for fibers with core diameters of 50  $\mu\text{m}$ , 100  $\mu\text{m}$ , and 200  $\mu\text{m}$ . The estimated SBS thresholds for the three core sizes at 10 m are 36 W, 140 W, and 560 W, respectively.

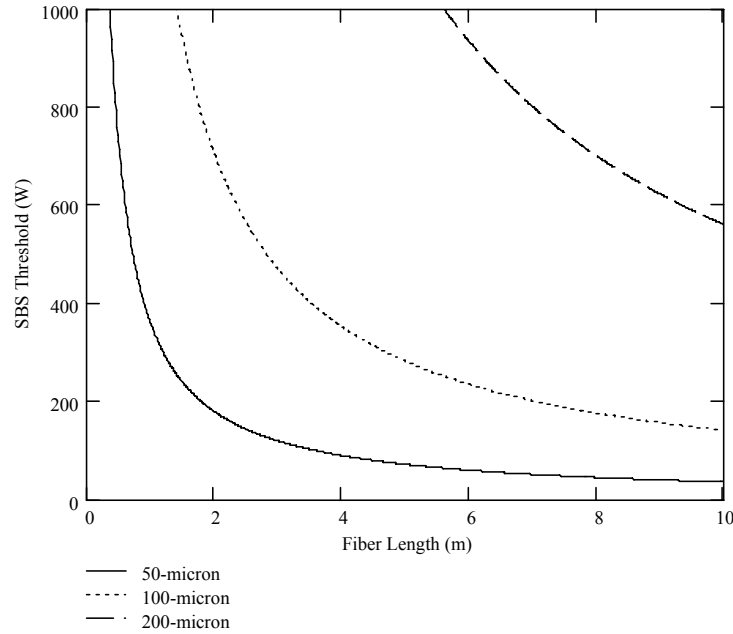


Figure 75: SBS threshold for 50  $\mu\text{m}$ , 100  $\mu\text{m}$ , and 200  $\mu\text{m}$  fibers.

Currently, the maximum diffraction-limited output from single-frequency fiber amplifiers is 264 W<sup>73</sup> and over 500 W has been demonstrated with an  $M^2$  of 1.6.<sup>97</sup> With power projected to continue to grow over 1 kW,<sup>97,98</sup> the SBS thresholds shown in Figure 75 indicate that it may be possible to use 10 m or less of a standard silica fiber as the SBS medium.

The difficulty and expense of obtaining very high power amplifiers will still make it necessary to pursue lower power alternatives. For these investigations, it will be desirable to reduce the SBS threshold for short fiber lengths. This work investigated using a Yb-doped multimode gain fiber pumped by a 915 nm diode laser to reduce the SBS threshold. A Stokes beam was not generated with the available seed and diode power. From the discussion of Section 4.3.3, the broadening of the SBS gain due to a strong temperature gradient along the length of the fiber indicates it will not be simple to

implement this technique for cw SBS threshold reduction. One option that may be pursued is manufacturing a fiber that is designed to absorb the diode pump light in a longer length of fiber (greater than 10 m as reported in 4.3). In this case, the longer length may help to reduce SBS threshold without the negative effect of seed absorption in unpumped regions of the fiber. Due to the high cost associated with manufacturing a custom fiber and the uncertainty of the effectiveness of cw SBS threshold in gain fibers, this approach is not recommended as a first option.

One technique for SBS threshold reduction that holds great promise and has not yet been explored is using tellurite-based ( $\text{TeO}_2$ ) optical fibers. A recent investigation reported ‘ultrahigh-gain’ using a  $\text{TeO}_2$  crystal.<sup>104</sup> In this work, a 4.0 cm commercially available  $\text{TeO}_2$  crystal was used to generate a SBS phase conjugate mirror. The reported steady-state SBS gain in this paper is  $100 \times 10^{-11} \text{ m/W}$ , which is more than 20 times greater than silica. If similar SBS gain can be achieved in a tellurite-based optical fiber, the SBS threshold will be significantly reduced. Figure 76 shows a similar graph to Figure 75 except that the Brillouin gain used is  $100 \times 10^{-11} \text{ m/W}$ . As evident from comparing the two graphs, the SBS threshold of the latter is considerably reduced. In this case, the estimated SBS thresholds for a 10 meter length of fiber are 2 W, 7 W, and 28 W, for the 50  $\mu\text{m}$ , 100  $\mu\text{m}$ , and 200  $\mu\text{m}$  fibers, respectively. SBS thresholds at this power level would allow an investigation of short-fiber SBS beam phasing with lower power single-frequency sources.

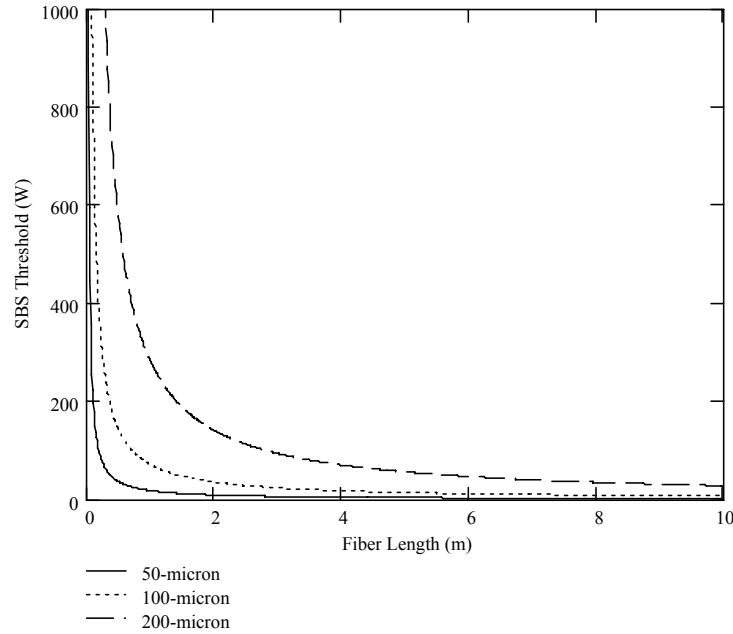


Figure 76: Potential SBS threshold in for 50  $\mu\text{m}$ , 100  $\mu\text{m}$ , and 200  $\mu\text{m}$  using tellurite-based fibers.

Wang *et. al.* first proposed tellurite glass as a candidate for fiber devices.<sup>105</sup> Their work has led to the development of a number of rare-earth doped fiber lasers and amplifiers.<sup>106,107,108</sup> Specifically, Erbium-doped tellurite-based fiber amplifiers have become popular for telecom amplification near 1500 nm.<sup>107,109</sup> Tellurite glasses have also been quite successful as Raman amplifiers<sup>110,111</sup> demonstrating over 90 times higher Raman gain than silica-based devices.<sup>111,112</sup> It appears that stimulated Brillouin scattering in tellurite fibers has not yet been investigated.

One issue that may be a concern in developing tellurite fibers for SBS applications is the attenuation in the fibers. Wang *et. al.* modeled the intrinsic loss of tellurite glass fiber and predicts a minimum loss of  $3.5 \times 10^{-3}$  dB/km at 3020 nm and a higher value, 0.29 dB/km at 1064 nm. Unfortunately, their best loss achieved in a manufactured fiber was



0.9 dB/m at 1350 nm.<sup>106</sup> The group suggests the high loss is attributed to material impurities and contamination during the manufacturing process.

Later work has used very pure TeO<sub>2</sub> and achieved background losses of 20.4 dB/km at 1560 nm<sup>110</sup> and 54 dB/km at 1200 nm.<sup>113</sup> The fiber loss becomes most significant for long fiber SBS investigations. For example, the SBS threshold given in Equation 2-31 is dependent on the effective length,  $L_{eff} = [1 - \exp(-\alpha L)]/\alpha$ , where  $\alpha$  is the loss term (converted from dB/km to 1/km).<sup>21</sup> A fiber attenuation of 20 dB/km reduces the effective length of a 10 m and 1000 m fiber to 9.8 m and 215 m, respectively. Hopefully a supplier will be able to manufacture a tellurite fiber with relatively low loss at the wavelength of interest (currently 1064 nm).

Investigating tellurite-based fiber for SBS applications may provide a means for significantly reducing the SBS threshold. This will be beneficial as it will allow a shorter fiber to be used for SBS phasing applications with less power required to reach threshold. Testing tellurite fibers for SBS applications will likely require manufacturing a custom fiber and it will be necessary to carefully consider the specifications for specific aspects of interest such as the fiber attenuation.

Another topic for future investigation is developing a method for coupling an increased number of channels for SBS beam phasing. One method for scaling to increased channels is using biconically fused fiber couplers as described in Section 4.2. An investigation of phasing two channels using 2:2 fiber couplers was presented and future work may increase the investigation to a higher number of channels using 4:4, 8:8, etc.

One issue to address in future fiber coupler experiments is the power handling capabilities. The units used in this work were commercially available telecom products that were not intended for high power. The manufacturer suggested a maximum total input power of 3 W. While the units were tested slightly over 10 W, a more robust fiber coupler is required for future high-power testing. Fortunately, higher power fiber components are in development at ITF Optical technologies,<sup>114</sup> which may allow scaling to more channels as well as increased power per channel.

It may also be interesting to pursue the design of a custom N:1 fiber beam combiner. As discussed in Section 4.2, the conventional telecom N:1 biconically fused coupler is simply an N:N coupler with the extra end(s) terminated. New fusing techniques have developed N:1 multimode fiber combiners capable of transmitting over 90% of the power from seven input channels into a single multimode output fiber.<sup>115</sup> Figure 77 shows a schematic representation of such a device along with an actual picture of the cleaved end facets for a 7:1 fiber bundle.<sup>116</sup>

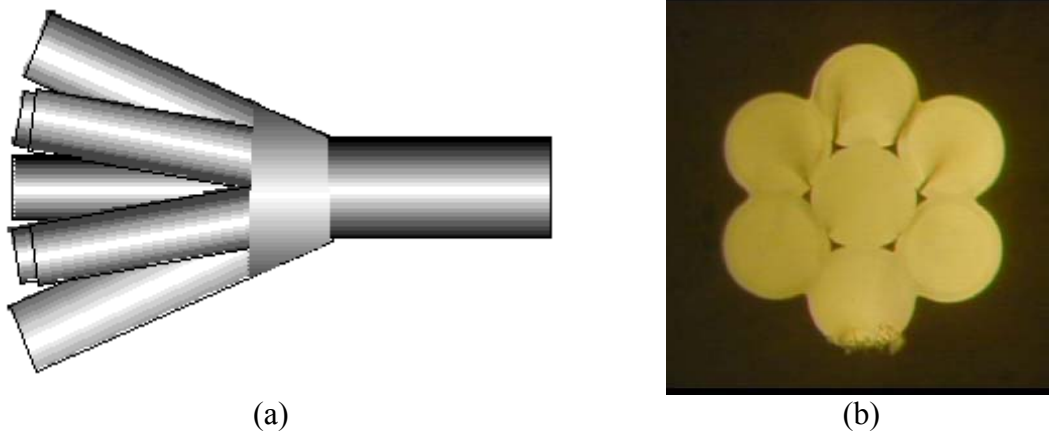


Figure 77: 7:1 multimode fiber combiner. A (a) schematic representation of the device is shown along with (b) an actual picture of the cleaved end facets.

The commercially available devices of this type are created to combine multiple diode pump beams into a gain fiber. Because of this, they are designed to minimize (isolate) any power that is traveling in the backwards direction.<sup>115</sup> This is not conducive to the SBS beam phasing experiments which require high bidirectional transmission. ITF optical incorporated speculates that they can produce a device capable of high transmission in both directions.<sup>114</sup> Such a device requires an original design in which case the cost may be significant. If it is possible to obtain an N:1 coupler with efficient transmission in both directions, an SBS phasing scheme such as shown in Figure 78 is possible. Such a configuration is very attractive for its simplicity for scaling and implementation.

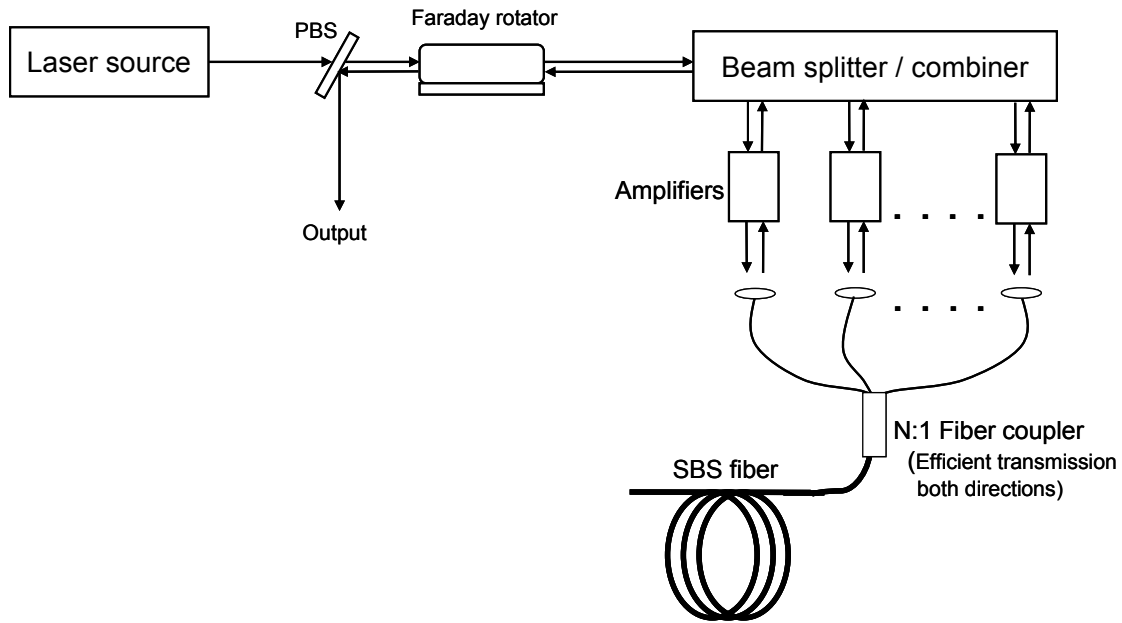


Figure 78: SBS beam phasing diagram using a N:1 bidirectional fiber coupler

If it is possible to develop short fiber SBS beam phasing with high phase conjugate fidelity, the wavefront reversal properties of phase conjugation may allow for additional coupling geometries. Figure 79 portrays an example of such a geometry.

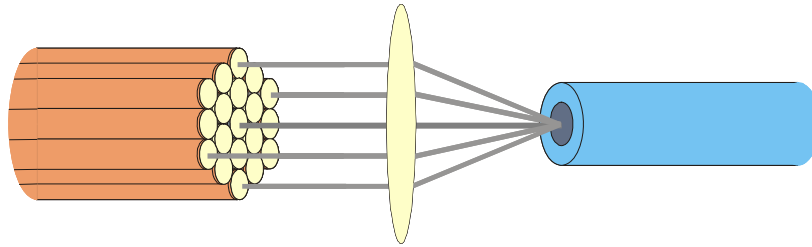


Figure 79: Multiple channel SBS beam phasing using a fiber bundle

The device is similar to the ‘Gatlin gun’ SBS beam combiner discussed in Chapter 3.<sup>54</sup> In this case, however, there is no center hole and the outputs of each channel’s fiber amplifier are collimated and bundled together. The beams are then focused into an SBS fiber where they all contribute to generate the Stokes beam. If the Stokes beam is a high fidelity phase conjugate, the beams will backtrack along their original path and couple into the amplifiers for a second pass. After the second pass along each channel’s optical path, the piston error is corrected and the beams are phased as described in Chapter 4.

There are a wide variety of implementations and techniques that can be explored in future work. The results achieved in this dissertation provide the motivation and confidence to continue investigations using SBS in optical fibers to scale laser power using a multiple channel approach.

## Appendix A: Glossary of Symbols

$x$	scalar
$\mathbf{v}$	vector
$v_i$	component of $\mathbf{v}$ in the direction of the $i^{\text{th}}$ Cartesian coordinate
$T^{(n)}$	$n+1$ rank tensor
$T^{(n)}_{ijkl}$	component of $T^{(n)}$ where $i, j, k, l$ are labels for the Cartesian coordinate axis. (each label take on $x, y$ , and $z$ )

$a$	fiber core radius
$A_{\text{eff}}$	effective area of the fiber
$A_i$	Field amplitude
$\mathbf{B}$	magnetic induction
$b$	inner cladding radius
$c$	velocity of light in a vacuum
$C_f$	Brillouin bandwidth temperature coefficient
$C_\delta$	Brillouin frequency temperature coefficient
$\mathbf{D}$	electric displacement
$d_{\text{coll}}$	diameter of pigtail collimator fiber (SBS beam combiner chapter 3)
$d_h$	diameter of hole in SBS beam combiner (SBS beam combiner chapter 3)
$d_{\text{offset}}$	focusing offset from non parallel beams (SBS beam combiner chapter 3)
$d_s$	focused diameter of SBS beam combiner beams (chapter 3)
$d_{\text{SBS}}$	diameter of SBS fiber (SBS beam combiner chapter 3)
$\mathbf{E}$	electric field
$f_{\text{coll}}$	focal length of GRIN collimation lens (SBS beam combiner chapter 3)
$f_{\text{SBS}}$	focal length of SBS fiber focusing lens (SBS beam combiner chapter 3)
$g_B$	Brillouin gain factor
$G_L$	exponential laser gain coefficient
$G_B$	SBS exponential gain coefficient
$G_t$	total exponential Stokes gain coefficient ( $I_s(0) = I_s(L)e^{G_t}$ )
$G_{\text{th}}$	total exponential Stokes gain coefficient required to reach SBS threshold
$\mathbf{H}$	magnetic field
$h$	convective coefficient
$\mathbf{J}$	current density
$\mathbf{k}$	Wave vector
$k_0$	free space propagation constant
$k_B$	acoustic propagation constant
$L$	fiber length
$L_{\text{chief}}$	off-axis distance of pigtail collimator (SBS beam combiner chapter 3)
$L_{\text{eff}}$	effective length of fiber

$M^2$	beam quality parameter
$n$	index of refraction
NA	Numerical aperture of the fiber
$NA_{coll}$	numerical aperture of pigtail collimator (SBS beam combiner chapter 3)
$\mathbf{P}$	polarization vector
$\mathbf{P}_{NL}$	nonlinear component of the polarization vector
$P_s(0)$	seed input power
$P_{St}$	saturation power
$P_{th}$	SBS threshold power
$r_0$	allowable non-phase-conjugated fraction of Stokes beam
$S$	fiber core area
$V$	Normalized frequency parameter
$v_a$	acoustic wave velocity
$Z_R$	Rayleigh range
$\alpha$	optical loss term
$\alpha_p$	pump absorption coefficient
$\gamma$	pump to gain conversion coefficient
$\Gamma'$	acoustic damping parameter
$\Gamma_B$	Brillouin linewidth
$\delta$	residual piston error
$\Delta_B$	SBS shift in wavenumber
$\Delta f$	detuning of Stokes emission from theoretical SBS shift at $x = L$
$\Delta_L$	path length difference
$\Delta T(x)$	temperature change along length of fiber
$\Delta\epsilon$	change in permittivity
$\Delta\theta_{chief}$	entrance angle of off-axis marginal ray (SBS beam combiner chapter 3)
$\Delta\rho$	incremental change in mass density
$\epsilon$	permittivity
$\epsilon_0$	free space permittivity
$\eta$	fraction of pump power transferred to heat
$\theta_{chief}$	entrance angle of off-axis chief ray (SBS beam combiner chapter 3)
$\theta_{div}$	divergence angle
$\theta_{max}$	Maximum entrance angle from off-axis SBS beam combiner (chapter 3)
$\theta_{off}$	angle offset of non parallel beams (SBS beam combiner chapter 3)
$\Lambda$	acoustic wavelength
$\lambda$	optical wavelength
$\mu$	permeability
$\mu_0$	free space permeability
$\rho_0$	average mass density
$\rho_c$	charge density
$\tau_p$	phonon lifetime
$\nu_B$	Brillouin acoustic wave frequency (Hz)
$\chi(\mathbf{E})$	field dependent susceptibility of the material
$\chi^{(n)}$	nth order susceptibility tensor

$\Omega$	frequency of driven acoustic wave in the SBS process
$\omega$	frequency of optical wave
$\omega_0$	Gaussian spot size
$\Omega_B$	Brillouin acoustic wave frequency (rad/sec)
$\omega_{f0}$	fiber mode field radius
$\omega_{SBS}$	collimated SBS waist size (SBS beam combiner chapter 3)

## Bibliography

1. Verdeyen, Joseph T., *Laser Electronics*, 3<sup>rd</sup> ed., Upper Saddle River, New Jersey, Prentice Hall, 1995.
2. Schwartz, William C., "Solid-state lasers point to the future in military applications," *Laser Focus*, **27**, 1991.
3. Wall, Robert, "Waging war precisely," *Aviation Week and Space Technology*, **158**, 2003.
4. Muller, Clifford, H. III, *Department of Defense High Power Laser Program Guidance*, Funding number PE63605F, Phillips Research Laboratory, Kirtland AFB, 1994 (ADA282915).
5. Wirsig, Gerald W., *The Airborne Laser and the Future of Theater Missile Defense*, Air Command and Staff College, Maxwell AFB, AL, 1997 (ADA397885).
6. "Airborne Laser: System description," <http://www.airbornelaser.com/description/>, Dec 2003.
7. "Advanced Tactical Laser: Advanced Concept Demonstration," The Boeing Company: Missile Defense Systems, Seal Beach, CA, 2003 (atl\_actd\_c130\_ms).
8. Andrews, L.C. and Phillips, R. L., *Laser Beam Propagation through Random Media*, Bellingham, WA, SPIE-The International Society of Optical Engineering, 1998.
9. "Directed Energy Weapons: Something for a Star Wars Sequel?" *Journal of Electronic Defense*, **20**, 37, 1997.
10. Stafford, D. Shane, and Mark. J. Kushner, "Global modeling of singlet-delta-oxygen production in glow discharges with application to oxygen-iodine lasers," Department of Chemical and Biomolecular Engineering, University of Illinois at Urbana-Champaign, <http://uigelz.ece.uiuc.edu/Projects/ECOIL/ecoil.html>, 2003.
11. Carroll, David L. and Wayne C. Colomon, "ElectriCOIL: an advanced chemical iodine laser concept", *Proceedings of the XIII International Symposium on Gas Flow and Chemical Lasers and High Power Lasers Conference*, Florence, Italy, 18-22 Sept 2000.
12. Carroll, David C., J. Verdeyen, D. M. King, J. W. Zimmerman, J. K. Laystrom, B. S. Woodard, G. F. Benavides, K. Kittell, D. S. Stafford, M. J. Kushner, and W. C. Solomon, "Continuous-wave laser oscillation on the 1315 nm transition of atomic



- iodine pumped by  $O_2(a^1\Delta)$  produced by electric discharge,” *Appl. Phys. Lett.*, **86**, 111104, 2005.
13. Lange, Mathew A., “Kinetics of the electric discharge pumped oxygen-iodine laser,” *Sixth Annual Directed Energy Symposium*, Albuquerque, NM, 20-24 Oct 2003.
  14. Garcia, J. Rich, “Air Force is developing a solid-state laser,” *Air Force Research Laboratory News*, Jan 2003.
  15. Rockwell, David A., “A review of phase-conjugate solid-state lasers,” *IEEE J. Quantum Electron.*, **24**, 1124-1140, 1988.
  16. Moyer, Richard H., M. Valley, and M. C. Cimolino, “Beam combination through stimulated Brillouin scattering,” *J. Opt. Soc. Am. B*, **5**, 2473-2489, 1988.
  17. Rockwell, D. A., and C. R. Giuliano, “Coherent coupling of laser gain media using phase conjugation,” *Opt. Lett.*, **11**, 147-149, 1986.
  18. Becht, Hubert, “Experimental investigations on phase locking of two Nd:YAG laser beams by stimulated Brillouin scattering,” *J Opt. Soc. Am. B*, **15**, 1678-1684, 1998.
  19. Basov, N. G., V. F. Efimkov, I. G. Zubarev, A. V. Kotov, A. B. Mironov, S. I. Mikhaïlov, and M. G. Smirnov, “Influence of certain radiation parameters on wavefront reversal of a pump wave in a Brillouin mirror,” *Sov. J. Quantum Electron.*, **9**, 455-458, 1979.
  20. Boyd, Robert W., *Nonlinear Optics*, San Diego, Academic Press, 1992.
  21. Agrawal, Govind. P., *Nonlinear Fiber Optics*, 3<sup>rd</sup> ed., San Diego, Academic Press, 2001.
  22. Rodgers, B. C., T. H. Russell, and W. B. Roh, “Laser beam combining and cleanup by stimulated Brillouin scattering in a multimode optical fiber,” *Opt. Lett.*, **24**, 1124-1126, 1999.
  23. Russell, T. H., W. B. Roh, and J. R. Marciante, “Incoherent beam combining using stimulated Brillouin scattering in multimode fibers,” *Opt. Exp.*, **8**, 246-254, 2001.
  24. Kuzin, E. A., M. P. Petrov, and B. E. Davydenko, “Phase conjugation in optical fibre,” *Opt. and Quant. Elect.*, **17**, 393-397, 1985.
  25. Risse, E., O. Mehl, T. Riesbeck, A. Mocofanescu, and H. J. Eichler, “Continuously pumped all-solid-state laser systems with fiber phase conjugate mirror,” *Proc. of SPIE*, **4184**, 179-182, 2001.

26. Zahn, Marcus, *Electromagnetic Field Theory: a Problem Solving Approach*, Malabar, Florida, Krieger Publishing Company, 1987.
27. Butcher, P. and D. Cotter, *The Elements of Nonlinear Optics*, Cambridge, Great Britain, Cambridge University Press, 1990.
28. He, Guang S. and Song H. Liu, *Physics of Nonlinear Optics*, Singapore, World Scientific Publishing Co., 1999.
29. Fisher, Robert A. (editor), *Optical Phase Conjugation*, New York, Academic Press, Inc., 1983.
30. Yariv, A., and P. Yeh, *Optical Waves in Crystals*, Hoboken, New Jersey, John Wiley Sons, Inc., 2003.
31. Shen, Y. R., *The Principles of Nonlinear Optics*, New York, John Wiley & Sons, 1984.
32. Brignon, Arnaud and Jean Pierre Huignard, *Phase Conjugate Laser Optics*, Hoboken, New Jersey, John Wiley & Sons, 2004.
33. Pannell, C. N., P. St. J Russell, and T. P. Newson, "Stimulated Brillouin scattering in optical fibers: the effects of optical amplification," *J. Opt. Soc. Am. B*, 10, 684-690, 1993.
34. Buck, John A., *Fundamentals of Optical Fibers*, New York, John Wiley & Sons, Inc., 1995.
35. Smith, R. G., "Optical power handling capacity of low loss optical fibers as determined by stimulated Raman and Brillouin scattering", *App. Opt.*, 11, 2489-2494, 1972.
36. Willis, Shawn, *Phasing a Dual Optical Path System Using an Optical Fiber and a Phase Conjugate Mirror*, MS Thesis, AFIT/GAP/ENP/03-06, School of Engineering, Air Force Institute of Technology, Wright-Patterson AFB, 2003 (ADA412678).
37. Gower, M. and D. Proch, *Optical Phase Conjugation*, New York, Springer-Verlag, 1994.
38. Pepper, D. M., "Nonlinear optical phase conjugation," *Opt. Eng.*, 21, 156-183, 1982.
39. Zel'dovich, B. Y., N. F. Pilipetsky, and V. V. Shkunov, *Principles of Phase Conjugation*, New York, Springer-Verlag, 1985.

40. Zel'dovich, B. A., V. I. Popovichev, V.V. Ragul'skii, and F. S. Faizullov, "Connection between the wave fronts of the reflected and exciting light in stimulated Mandel'shtam-Brillouin scattering," *JETP Lett.*, **15**, 109-112, 1972.
41. Hellwarth, R. W., "Phase conjugation by stimulated backscattering," ch. 7, *Optical Phase Conjugation*, R. Fisher ed., New York, Academic Press, Inc., 1983.
42. Eichler, H. J., J. Kunde, and B. Liu, "Quartz fibre phase conjugators with high fidelity and reflectivity," *Opt. Comm.* **139**, 327-334, 1997.
43. Pashinin, V., V. Sturm, V. Tumorin, and R. Noll, "Stimulated Brillouin scattering of Q-switched laser pulses in large core optical fibres," *Opt. and Laser Tech.*, **33**, 617-622, 2001.
44. Zel'dovich, B. Y., and V. V. Shkunov, "Wavefront reproduction in stimulated Raman scattering," *Sov. J. Quant. Elect.*, **7**, 610-615, 1977.
45. Lehmberg, R. H., and K. A. Holder, "Numerical study of optical ray retracing in laser-plasma backscatter," *Phys. Rev.* **22**, 2156-2170, 1980.
46. Lehmberg, R. H., "Numerical study of phase conjugation in stimulated backscatter with pump depletion," *Opt. Comm.*, **43**, 369-374, 1982.
47. Lehmberg, R. H., "Numerical study of phase conjugation in stimulated Brillouin scattering from and optical waveguide," *J. Opt. Soc. Am.* **73**, 558-566, 1983.
48. Hu, P. H., J. A. Goldstone, and S. S. Ma, "Theoretical study of phase conjugation in stimulated Brillouin scattering," *J. Opt. Soc. Am. B*, **6**, 1813-1822, 1989.
49. Bruesselbach, H., "Beam cleanup using stimulated Brillouin scattering in multimode fibers," *Conf. of Las. and Elec. Opt.*, **11**, 424, 1993.
50. Murray, J. T., W. L. Austin, and R. Powell, "Intracavity Raman conversion and Raman beam cleanup", *Opt. Mater.*, **11**, 353-371, 1999.
51. Papoulis, A., *Probability, Random Variables, and Stochastic Processes*, New York, McGraw-Hill, 1965.
52. Baek, S. H., and W. B. Roh, "Single-mode Raman fiber laser based on a multimode fiber," *Opt. Lett.*, **29**, 1-3, 2004.
53. Russell, T. H. and W. B. Roh, "Threshold of second-order stimulated Brillouin scattering in optical fiber," *J. Opt. Soc. Am. B.*, **19**, 2341-2345, 2002.
54. Russell, T., *Laser Intensity Scaling Through Stimulated Scattering in Optical Fibers*, PhD Dissertation, AFIT/DS/ENP/02-03, School of Engineering, Air Force Institute of Technology, Wright-Patterson AFB, 2002 (ADA398033).

55. Kane, Thomas, and R. Byer, Monolithic, "Unidirectional single-mode Nd:YAG ring laser", *Opt. Lett.*, **10**, 65-67, 1985.
56. Imai, M. and E. H. Hara, "Excitation of fundamental and low-order modes of optical fiber waveguides by Gaussian beams. 1: Tilted beams," *Appl. Opt.*, **13**, 1893-1899, 1974.
57. Saijonmaa, J., A. B. Sharma, and S. J. Halme, "Selective excitation of parabolic-index optical fibers by Gaussian beams," *App. Opt.*, **19**, 2442-2452, 1980.
58. Karásek, M., "Selective excitation of multimode fibers," *Archiv für Elektronik und Übertragungstechnik Electronics and Communications*, **40**, 113-116, 1986.
59. Raab, F., "Overview of LIGO instrumentation," *Proc. of SPIE*, **5500**, 11-24, 2004.
60. Bienfang, J. C., C. A. Denman, B. W. Grime, P. D. Hillman, G. T Moore, and J. M. Telle, "20 W of continuous-wave sodium D<sub>2</sub> resonance radiation from sum-frequency with injection-locked lasers," *Opt. Lett.*, **28**, 1-3, 2003.
61. Anderegg, J., S. Brosan, M. Weber, H. Komine, and M. Wickham, "8-watt coherently phased 4-element fiber array," *Proc. of SPIE*, **4974**, 1-6, 2003.
62. Freitag, I., A. Tünnermann, and H. Welling, "Power scaling of diode-pumped monolithic Nd:YAG lasers to output powers of several watts," *Opt. Comm.*, **115**, 511-515, 1995.
63. Wiechmann, W., T. J. Kane, D. Haserot, F. Adams, G. Truong, and J. Kmetec, "20-W diode-pumped single-frequency Nd:YAG MOPA for the Laser Interferometer Gravitational Observatory," *Proc. of CLEO*, paper CthP2, 2003.
64. Shailendhar, S., S. Sinha, A. Sridharan, and R. Byer, "100 W single frequency, diffraction-limited Nd:YAG MOPA for LIGO," *Proc. of CLEO*, paper CthPDB12, 1-6 June 2003.
65. Freitag, I., D. Golla, S. Knoke, W. Schöne, H. Zellmer, A. Tünnermann, and H. Welling, "Amplitude and frequency stability of a diode-pumped Nd:YAG laser operating at a single-frequency continuous-wave output power of 20W," *Opt. Lett.*, **20**, 462-464, 1995.
66. Teehan, R. F., J. C. Bienfang, and C. Denman, "Power scaling and frequency stabilization of injection-locked Nd:YAG rod laser," *Appl. Opt.*, **39**, 3076-3084, 2000.
67. Takeno, K., T. Ozeki, S. Moriwaki, and N. Mio, "100 W, single-frequency operation of an injection-locked Nd:YAG laser," *Opt. Lett.*, **30**, 2110-2112, 2005.

68. Koplow, J., D. Kliner, and L. Goldberg, "Single-mode operation of a coiled multimode fiber amplifier," *Opt. Lett.*, **25**, 442-444, 2000.
69. Liu, C., A. Galvanauskas, B. Ehlers, and S. Heinemann, "KW-power fiber lasers with single-transverse mode output using standard 20- $\mu$ m core Yb-doped fibers," *Proc. of Solid State Diode and Las. Tech. Rev.*, Albuquerque, NM, June 2004.
70. Paschotta, R., J. Nilsson, A. Tropper, and D. Hanna, "Ytterbium-doped fiber amplifiers," *IEEE Jour. of Quant. Elect.*, **33**, 1049-1056, 1997.
71. Höfer, S., A. Liem, J. Limpert, H. Zellmer, A. Tünnermann, S. Unger, S. Jetschke, H.-R. Müller, and I. Freitag, "Single frequency master-oscillator fiber amplifier system emitting 20 W of power," *Opt. Lett.*, **26**, 1326-1328, 2001.
72. Liem, A., J. Limpert, H. Zellmer, and A. Tünnermann, "100-W single-frequency master-oscillator fiber power amplifier," *Opt. Lett.*, **28**, 1537-1539, 2003.
73. Jeong, Y., J. Nilsson, J. Sahu, D. Soh, C. Alegria, P. Dupriez, A. Codemard, D. Payne, R. Horley, L. Hickey, L. Wanzcyk, C. Chryssou, J. Alvarez-Chavez, and P. Turner, "Single-frequency, single-mode, plane-polarized, Ytterbium-doped fiber master oscillator power amplifier source with 264 W of output power," *Opt. Lett.*, **30**, 459-461, 2005.
74. Coherent, Auburn Division, "ModeMaster PC-M<sup>2</sup> beam propagation analyzer," Product literature, 2005.
75. Augst, S. J., T. Y. Fan, and A. Sanchez, "Coherent beam combining and phase noise measurements of ytterbium fiber amplifiers," *Opt. Lett.*, **29**, 474-476, 2004.
76. Höfer, S., H. Zellmer, J. Ruske, and R. Tünnermann, "Coherent beam combining of fiber amplifiers," *Proc. of CLEO*, 635, 22-27 June 2003.
77. Moyer, Richard., "Beam combination with stimulated Brillouin scattering: A Review," *Proc. of SPIE*, **1000**, 25-32, 1988.
78. Basov, N. G., I. G. Zubarev, A. B. Mironov, and S. I. Mikhaïlov, and A. Y. Okulov, "Laser interferometry with wavefront-reversing mirrors," *Sov. Phys. JETP*, **52**, 847-851, 1980.
79. Valley, M., G. Lombardi, and R. Aprahamian, "Beam combination by stimulated scattering," *J. Opt. Soc. Am. B.*, **3**, 1492-1497, 1986.
80. Carroll, D. L., R. Johnson, S. Pfiefer, and R. Moyer, "Experimental investigations of stimulated Brillouin scattering beam combination," *J. Opt. Soc. Am. B.*, **9**, 2214-2224, 1992.

81. Falk, J., M. Kanefsky, and P. Suni, "Limits in the efficiency of beam combination by stimulated Brillouin scattering," *Opt. Lett.* **13**, 39-41, 1988.
82. Chu, Rajjun, X. Hua, R. Mehringer, P. Suni, M. Kanefsky, and J. Falk, "A statistical description of stimulated Brillouin scattering beam combination efficiency," *IEEE J. Quant. Electr.*, **28**, 1582-1592, 1992.
83. Sternklar, S. D. Chomsky, S. Jackel, and A. Zigler, "Misalignment sensitivity of beam combination by stimulated Brillouin scattering," *Opt. Lett.*, **15**, 469-470, 1990.
84. Willis, Shawn and W. Roh, "Beam phasing properties of optical fiber as a phase conjugate mirror," *Conf. Proc. LEOS*, **1**, 105-106, 2003.
85. "Canstar Fiber Optic Couplers," Product Catalog of FCI, [www.fciconnect.com](http://www.fciconnect.com), 2005.
86. Well, Penn "Fused-fiber developments offer passive foundation for optical splicing," *Lightwave*, March 2000.
87. Dunigna, M. T., B. J. Feldman, and W. T. Whitney, "Threshold reduction for stimulated Brillouin scattering using a multipass Herriott cell", *J. Opt. Soc. Am. B*, **9**, 548-559, 1992.
88. Kim, H. S., S. Kim, D. Ko, G. Lim, B. H. Cha, and J. Lee, "Threshold reduction of stimulated Brillouin scattering by the enhanced stokes noise initiation", *App. Phys. Lett.*, **74**, 1358-1360, 1999.
89. Cotter, D., "Observation of stimulated Brillouin scattering in low-loss Silica fibre at 1.3  $\mu\text{m}$ ," *Elect. Lett.* **18**, 495-496, 1982.
90. Harrison, R. G., V. Kovalev, W. Lu, and D. Yu, "SBS self-phase conjugation of cw Nd:YAG laser in an optical fibre," *Opt. Comm.*, **163**, 208-211, 1999.
91. Hänish, C., A. Heuer, and R. Menzel, "Threshold reduction of stimulated Brillouin scattering (SBS) using fiber loop schemes," *Appl. Phys. B.*, **73**, 851-854, 2001.
92. Heuer, A. and R. Menzel, "Phase-conjugation stimulated Brillouin scattering mirror for low powers and reflectivities above 90% in an internally tapered optical fiber," *Opt. Lett.*, **23**, 834-836, 1998.
93. Heuer, A., C. Hänisch, and R. Menzel, "Low-power phase conjugation based on stimulated Brillouin scattering in fiber amplifiers," *Opt. Lett.*, **28**, 34-36, 2003.
94. Heuer, A., C. Hänisch, and R. Menzel, "New concept for low threshold optical phase conjugation via SBS in a fiber amplifier," *Proc. of SPIE*, **4972**, 151-157, 2003.

95. Sousa, J. M., J. Nilsson, C. C. Renaud, J. A. Alvarez-Chavez, A. B. Grudinin, and J. D. Minelly, "Broad-band diode-pumped ytterbium-doped fiber amplifiers with 34-dBm output power," *IEEE Photon. Tech. Lett.*, **11**, 1999.
96. Siegman, A. E., *Lasers*, Mill Valley, California, University Science Books, 1986.
97. Payne, D. N., Y. Jeong, J. Nilsson, J. K. Sahu, D. B. S. Soh, C. Alegria, P. Dupriez, C. A. Codemard, V. N. Philippov, and V. Hernandez, "Kilowatt-class single-frequency fiber sources," *Proc. of SPIE*, **5709**, 133-141, 2005.
98. Kovalev, V. I., R. G. Harrison, J. Nilsson, Y. Jeong, V. Hernades-Solis, and J. K. Sahu. "Analytical modeling of Brillouin gain in rare-earth doped amplifiers with high-power single-frequency signals," *Proc. of SPIE*, **5709**, 142-146, 2005.
99. Wang, Y., C. Xu, and H. Pong, "Thermal effects in kilowatt fiber lasers," *IEEE Photon. Tech. Lett.*, **16**, 63-65, 2004.
100. Brown, David C., "Thermal, stress, and thermo-optic effects in high average power double-clad silica fiber lasers," *IEEE J. of Quant. Electron.*, **37**, 207-217, 2001.
101. Imai, Y., and N. Shimada, "Dependence of stimulated Brillouin scattering on temperature distributions in polarization maintaining fibers," *IEEE Photon. Tech. Lett.*, **5**, 1335-1337, 1993.
102. Mao, X. P., R. W. Tkach, A. R. Chraplyvy, R. M. Jopson, and R. M. Derosier, "Stimulated Brillouin threshold dependence on fiber type uniformity," *IEEE Photon. Tech Lett.*, **4**, 66-69, 1992.
103. Brown, Kirk, *Multiple Channel SBS Beam Combining*, MS Thesis, AFIT/GAP/ENP/06, School of Engineering, Air Force Institute of Technology, Wright-Patterson AFB, *in progress*.
104. Dubinskii, M. and L. D. Merkle, "Ultrahigh-gain bulk solid-state stimulated Brillouin scattering phase conjugation material," *Opt. Lett.*, **29**, 992-994, 2004.
105. Wang, J. S., E. M. Vogel, E. Snitzer, "Tellurite glass: a new candidate for fiber devices," *Opt. Mater.* **3**, 187-203, 1994.
106. Wang, J. S., D. P. Machewirth, F. Wu, E. Snitzer, and E. M. Vogel, "Neodymium-doped tellurite single-mode fiber laser," *Opt. Lett.*, **19**, 1448-1449, 1994.
107. Mori, A., T. Sakamoto, K. Kobayashi, K. Oikawa, K. Hoshino, T. Kanamori, Y. Ohishi, and M. Shimizu, "1.58- $\mu$ m broad-band erbium-doped tellurite fiber amplifier," *J. Lightwave Tech.*, **20**, 794-799, 2002.

108. Taylor, E. R. M., L. N. Ng, J. Nilsson, R. Caponi, A. Pagano, M. Potenza, and B. Sordo, "Thulium-doped tellurite fiber amplifier," *IEEE Phot. Tech. Lett.* **16**, 777-779, 2004.
109. Ohishi, Y., A. Mori, M. Yamada, H. Ono, Y. Nishida, and K. Oikawa, "Gain characteristics of tellurite-based erbium-doped fiber amplifiers for 1.5- $\mu$ m broadband amplification," *Opt. Lett.*, **23**, 274-276, 1998.
110. Mori, A., H. Masuda, K. Shikano, and M. Shimizu, "Ultra-wide band tellurite-based fiber Raman amplifier," *J. Lightwave Tech*, **21**, 1300-1306, 2003.
111. Murugan, G. S., T. Suzuki, and Y. Ohishi, "Tellurite glasses for ultrabroadband Raman amplifiers," *Appl. Phys. Lett.*, **86**, 161109, 2005.
112. Plotnichenko, V. G., V. O. Sokolov, V. V. Koltashev, E. M. Dianov, I. A. Grishin, and M. F. Churbanov, "Raman band intensities of tellurite glasses," *Opt. Lett.*, **10**, 1156-1158, 2005.
113. Mori, A., K. Kobayashi, M. Yamada, T. Kanamori, K. Oikawa, Y. Nishida, and Y. Ohishi, "Low noise broadband tellurite-based  $Er^{3+}$ -doped fibre amplifiers," *Elect. Lett.*, **34**, 887-888, 1998.
114. Holehouse, Nigel, Senior Director of Sales and Marketing, ITF Optical Technologies, Inc., [www.itfoptical.com](http://www.itfoptical.com), Personal Communication, 8 June 2005.
115. ITF Optical Technologies, Inc., "High-power components: 7 x 1 multimode combiners," Product literature, [www.itfoptical.com](http://www.itfoptical.com), 4 Oct 2005.
116. Gonthier, Francois, "Fiber coupled pumping concepts for double-clad fibers," *CLEO Europe*, Munich, Germany, 12-17 June, 2005.



<b>REPORT DOCUMENTATION PAGE</b>				Form Approved OMB No. 074-0188	
<p>The public reporting burden for this collection of information is estimated to average 1 hour per response, including the time for reviewing instructions, searching existing data sources, gathering and maintaining the data needed, and completing and reviewing the collection of information. Send comments regarding this burden estimate or any other aspect of the collection of information, including suggestions for reducing this burden to Department of Defense, Washington Headquarters Services, Directorate for Information Operations and Reports (0704-0188), 1215 Jefferson Davis Highway, Suite 1204, Arlington, VA 22202-4302. Respondents should be aware that notwithstanding any other provision of law, no person shall be subject to a penalty for failing to comply with a collection of information if it does not display a currently valid OMB control number.</p> <p><b>PLEASE DO NOT RETURN YOUR FORM TO THE ABOVE ADDRESS.</b></p>					
<b>1. REPORT DATE (DD-MM-YYYY)</b> 12-22-2005		<b>2. REPORT TYPE</b> Doctoral Dissertation		<b>3. DATES COVERED (From – To)</b> Sep 2002 – Dec 2005	
<b>4. TITLE AND SUBTITLE</b>  Multiple Channel Laser Beam Combination and Phasing Using Stimulated Brillouin Scattering in Optical Fibers				<b>5a. CONTRACT NUMBER</b>	
				<b>5b. GRANT NUMBER</b>	
				<b>5c. PROGRAM ELEMENT NUMBER</b>	
<b>6. AUTHOR(S)</b>  Grime, Brent W., Captain, USAF				<b>5d. PROJECT NUMBER</b> NAFRL056209093	
				<b>5e. TASK NUMBER</b>	
				<b>5f. WORK UNIT NUMBER</b>	
<b>7. PERFORMING ORGANIZATION NAMES(S) AND ADDRESS(S)</b> Air Force Institute of Technology Graduate School of Engineering and Management (AFIT/EN) 2950 Hobson Way WPAFB OH 45433-7765				<b>8. PERFORMING ORGANIZATION REPORT NUMBER</b>  AFIT/DS/ENP/06-1	
<b>9. SPONSORING/MONITORING AGENCY NAME(S) AND ADDRESS(ES)</b> AFRL/DELO ATTN: Rick Berdine 3550 Aberdeen Ave SE Kirtland AFB, NM 87117-5776 505-853-4342				<b>10. SPONSOR/MONITOR'S ACRONYM(S)</b>	
				<b>11. SPONSOR/MONITOR'S REPORT NUMBER(S)</b>	
<b>12. DISTRIBUTION/AVAILABILITY STATEMENT</b> APPROVED FOR PUBLIC RELEASE; DISTRIBUTION UNLIMITED.					
<b>13. SUPPLEMENTARY NOTES</b>					
<b>14. ABSTRACT</b> Brightness scaling lasers using stimulated Brillouin scattering (SBS) in optical fibers is explored. A multiple-channel amplifier approach is used to increase the total power of a laser system while avoiding a significant burden on a single channel. The work explores two approaches utilizing both SBS beam cleanup and SBS piston error conjugation. A unique beam combiner that takes advantage of the SBS beam cleanup properties of a long, gradient-index multimode fiber was designed and tested. The beam combiner was developed to combine multiple-channel laser beams simultaneously with high input and output coupling efficiency. The design for the SBS beam combiner is presented along with experimental demonstration of multiple-channel beam combining using the technique. Using SBS piston error conjugation to phase multiple-channel two-pass amplifiers is also explored. Various system configurations were investigated to demonstrate SBS beam phasing of both passive, unamplified channels and active channels containing fiber amplifiers. Beam phasing of the channels was successfully demonstrated with enough gain and power to merit consideration as a viable approach to multiple-channel laser power scaling. Methods for improving efficiency and scaling to include a greater number of channels were also tested.					
<b>15. SUBJECT TERMS</b> Laser Arrays, Coherent Beam Combination, Laser Amplifiers, Phase Conjugation, Brillouin Scattering, Stokes Radiation, Lasers, Fiber Optics, Nonlinear Optics					
<b>16. SECURITY CLASSIFICATION OF:</b>			<b>17. LIMITATION OF ABSTRACT</b>  UU	<b>18. NUMBER OF PAGES</b> 176	<b>19a. NAME OF RESPONSIBLE PERSON</b> Won B. Roh, AFIT/ENP
<b>REPORT</b> U	<b>ABSTRACT</b> U	<b>c. THIS PAGE</b> U			<b>19b. TELEPHONE NUMBER (Include area code)</b> (937) 255-6565, ext 4509; e-mail: Won.Roh@afit.edu

**Standard Form 298 (Rev: 8-98)**

Prescribed by ANSI Std. Z39-18